The Institute of Paper Chemistry

Appleton, Wisconsin

Doctor's Dissertation

Creeping Flow of Fluids Through Assemblages of Elliptic Cylinders and its Application to the Permeability of Fiber Mats

George Ronald Brown

June, 1975

CREEPING FLOW OF FLUIDS THROUGH ASSEMBLAGES
OF ELLIPTIC CYLINDERS AND ITS APPLICATION
TO THE PERMEABILITY OF FIBER MATS

A thesis submitted by

George Ronald Brown

B.S. 1969, North Carolina State University

M.S. 1971, Lawrence University

in partial fulfillment of the requirements
of The Institute of Paper Chemistry
for the degree of Doctor of Philosophy
from Lawrence University,
Appleton, Wisconsin

June, 1975

TABLE OF CONTENTS

SUMMARY

An analysis of the slow permeation of fluids through assemblages of elliptic cylinders based upon a cell flow model is developed and applied to flow through mats of noncircular synthetic fibers. The aim of the investigation was to determine what effect fiber cross-sectional shape has on the resistance to flow through a fiber mat. An elliptic cylinder was chosen as a fiber model because the shape of the elliptic cross section can be varied from circular to nearly flat with a mathematical description of the contour easily specified by using confocal elliptic coordinates.

The cell used as a model of the porous space consists of two confocal elliptic cylinders, the inner one representing the solid fiber and the outer one a virtual surface within the fluid. The virtual boundary is positioned such that the cell porosity equals the mat porosity. The no-slip condition is assumed on the solid cylinder, while zero vorticity is stated as a condition on the fluid surface in the manner of the analysis by Kuwabara for circular cylinders.

The creeping motion equations are applied to flow through the model cell, and solutions are determined for flow parallel to the central fiber axis, flow perpendicular to the central axis and to the minor cross-sectional axis, and flow perpendicular to the central axis and to the major cross-sectional axis. A novel approximate method for solving Poisson equation problems using a polynomial form is successfully utilized and shown to be reasonably accurate. Using the Kozeny factor from the Kozeny-Carman theory as an indicator of relative resistance to flow through the assemblage, expressions for each flow direction are developed as functions of porosity and cross-sectional axis ratio. Several mat structures are considered and composite mat Kozeny factors are estimated. These composite Kozeny factors are compared to experimental data for noncircular fiber mats and to previous analyses.

The principal conclusion is that the flow resistance for an isotropic mat of fibers is not greatly affected by the fiber cross-sectional shape until a fairly flat axis ratio is used. For example, at porosity 0.90 the Kozeny factor for a mat of circular fibers is very close to that for fibers of axis ratio 0.10; at porosity 0.75, going from circular fibers to an axis ratio of 0.30 causes a change of only ten percent in the mat Kozeny factor.

The contact area between fibers in a mat is considered as a means for correcting the surface area of the porous mat for that area not passed by the fluid. Although valid, this correction is seen to be insignificant for the fiber mats of interest to this work. The contact area estimate is developed from the theory of two isotropic elastic bodies in contact and relates the contact area to the fiber elastic properties as well as to mat characteristics.

INTRODUCTION AND HISTORICAL REVIEW

The flow of fluids through fiber mats is of importance in many processes, including the filtration of air with high porosity synthetic fiber filters, water filtration with fiber mats formed from fiber slurries, and water removal on a paper machine forming section. The large majority of existing studies which have explored the basic relationships guiding such flow have been empirical or semiempirical in approach. Few analyses from a theoretical standpoint have contributed significantly because of the extreme difficulties in defining the structure and properties of the porous mat of fibers. Some analytical studies of regular arrays of fiberlike cylinders have been completed, but these are of little practical importance to the abovementioned processes where the fiber assemblage is not well ordered. The effect of fiber character-istics, such as fiber cross-sectional shape, deformability, etc., on the flow behavior has not been clearly determined either.

Obviously, the subject of fluid flow through fiber mats needs considerable attention from investigators before widely applicable, well defined relation-ships are obtained. This thesis attempts to contribute to this area by applying the fundamental principles of hydrodynamics to a model of the porous space in order to determine the effect of fiber shape on flow resistance.

Neither experiment nor analysis should be overlooked in studies in this area. Both are essential for further insight into the governing relationships. Because of the complexity of the flow in a fiber assemblage, empirical studies often appear to provide a faster means for resolving questions than an analytical approach does. But the results from such empiricism are limited to the specific set of conditions employed in the study, while an analytical approach

based upon valid reasoning can relate the variables of interest over a wide range of conditions. New theories, however, certainly need verification by experimental measurement before confidence in them is obtained and they are accepted as sound. The approach in this thesis is primarily theoretical, but laboratory data are compared with the analytical results in an effort to demonstrate the usefulness of the theory.

FUNDAMENTAL RELATIONSHIPS

Porous media possess numerous and varied physical forms, but all are characterized by the fact that the apparent volume of the material is greater than the true solid volume because of "pores" or void spaces present within the structure. The properties of a porous medium are highly dependent upon the ratio of void space to solid volume, as well as on the manner in which the void space is distributed within the medium. In most cases the "pores" are randomly interconnected so that fluids can permeate the structure in all directions.

A thick mat of fibers is the porous medium of interest to this work. The characteristics of a fiber mat depend greatly on what type of fibers are in it and how the mat was formed. No fiber mat of practical importance has a regular, ordered structure. As a result, it is very difficult to describe in exact terms the porous structure of a mat, which would be desirable for hydrodynamic analysis.

The basic principles of hydrodynamics, i.e., the differential equations of the conservation relationships, describe the motion of fluids in any geometric system. But mathematical solutions for only a very few flow cases involving fairly simple geometries have been obtained. This is because more

complicated flow problems present extreme difficulties in specifying the most
suitable coordinate system for equations and their boundary conditions, a
step necessary for rigorous solutions. For these reasons, most of the studies
to date on flow through porous media have utilized empirical or semiempirical
approaches.

DARCY'S EQUATION

The fundamental relationship describing slow, steady-state, isothermal
flow of an incompressible fluid through a homogeneous porous medium is the
equation of Darcy (1),

$$U = Q/A = K_o \, \Delta p/L = -K_o \, dp/dx, \tag{1}$$

where U = superficial velocity

    Q = volumetric flow rate

    A = cross-sectional area of porous medium presented to flow

    Δp = pressure drop across the medium

    L = thickness of the medium

    K_o = proportionality factor

  dp/dx = pressure gradient

The Darcy equation simply states that the flow rate is directly proportional
to the pressure drop. It is applicable for laminar flow where inertial effects
are negligible and where the resistance to flow, as expressed by $1/K_o$, is due
entirely to the viscous drag of the fluid. Also, the fluid must be nonreactive
with the porous structure.

The proportionality factor, K_o, combines the structural properties of
the porous medium and the characteristics of the permeating fluid. The fluid

properties are separated from those of the medium by the commonly accepted Scheidegger (2) relationship

$$K_o = K/\mu, \qquad (2)$$

where μ is the dynamic viscosity of the fluid and $\underline{K}$ is termed the permeability coefficient, which is dependent only on the porous structure and not on the fluid properties. The dimension of $\underline{K}$ is that of length squared. The Darcy equation becomes

$$U = - (K/\mu) \; dp/dx. \qquad (3)$$

Darcy's law was empirically determined in 1856, but recently a theoretical basis for it has been demonstrated. Irmay (3) showed that the equation was valid on a macroscopic scale by obtaining a space average of the microscopic flow obeying the creeping flow form of the Navier-Stokes equation. A theoretical derivation of Darcy's law was presented by Whittaker (4), who applied the conservation principles to the flow in an anisotropic porous medium and derived the Darcy equation.

KOZENY-CARMAN THEORY

Since the permeability coefficient is structure dependent, efforts have been made to relate $\underline{K}$ to the properties of the porous medium by assuming a model of the structure. One of the more widely known theories of this type is represented by the Kozeny-Carman equation (5), a semiempirical relationship based upon the assumption that the medium is analogous to a system of parallel capillary channels. The size of the channels is represented by the hydraulic radius, $\underline{m}$, defined as the ratio of cross-sectional area to wetted perimeter. In a porous medium of porosity ε (volumetric void fraction), the

hydraulic radius is the ratio of ε to the specific surface, S_o (surface area per unit volume of the medium). The Kozeny-Carman equation is

$$K = \varepsilon m^2/k = \varepsilon^3/(kS_o^2) \tag{4}$$

with k referred to as the Kozeny factor. Originally k was termed the Kozeny constant but later work has demonstrated its variability with medium properties. Carman (5) suggests that the Kozeny factor is the product of a pore shape factor and the square of a tortuosity factor, with a value between 4 and 6 for most porous beds. The specific surface of the medium, S_o, is converted to specific surface based on particle volume, S_v (area per unit volume of solid fraction), assuming point contact between particles, by

$$S_o = S_v(1-\varepsilon). \tag{5}$$

Thus the permeability coefficient is

$$K = \varepsilon^3/[kS_v^2(1-\varepsilon)^2], \tag{6}$$

and the Darcy equation is

$$U = - (dp/dx) \, \varepsilon^3/[\mu kS_v^2(1-\varepsilon)^2]. \tag{7}$$

For porous mats with constant porosity, specific surface, viscosity, and flow rate, a higher value of the Kozeny factor means that a greater pressure gradient is required. Because of this, k can be used as a relative measure of the resistance to flow through a porous sample and can serve as a basis for comparing similar mats.

Other approaches to flow through porous media exist, but the purpose of this discussion is not to critically review the area. The monographs by

Scheidegger (2), Davies (6), and Carman (7) cover the subject in considerably more detail. Bliesner (8) also reviews the prior work.

FLOW THROUGH FIBER MATS

The permeation of fluids through mats of fibers is a special type of flow through porous media. The general considerations presented above are applicable to fibrous mats. In this section studies concerned primarily with fiber assemblages, rather than any porous medium, will be discussed. A recent review of fiber mat permeation is given by Han (9). The Darcy equation combined with the Kozeny-Carman equation, Equation (7), will be used as the basic relationship for flow through fiber mats. The primary concern will be the elucidation of the Kozeny factor in terms of mat and fiber properties.

CIRCULAR FIBERS

Because of the availability of synthetic fibers of circular cross section and because of the simpler analysis of flow past such fibers, the flow through beds of circular fibers has received much attention.

Empirical Approaches

For beds of fibers used for air filters over the porosity range 0.70 to 0.994, Davies (10) demonstrated the dependence of Kozeny factor on bed porosity and expressed his findings by the equation

$$k = k_1 \varepsilon^3 (1-\varepsilon)^{-1/2} [1 + k_2 (1-\varepsilon)^3], \qquad (8)$$

where k_1 and k_2 have values of 4.0 and 56, respectively.

Ingmanson and associates (11) performed water permeability experiments with mats of nylon and glass fibers of circular cross section oriented principally

in the plane normal to flow. Their measurements yielded the values 3.5 and

57 for k_1 and k_2, respectively. The difference between these values and those

of Davies probably results from fiber orientation effects, since Davies'

fibers are believed to have had more alignment parallel to flow.

Carroll (12) has presented a three-parameter correlation of Kozeny factor

and porosity for beds of cylindrical synthetic fibers which fits the data

below a porosity of 0.80 better than does the more widely used Davies-

Ingmanson equation. The Carroll relationship is*

$$k = 5.0 + \exp[14(\epsilon - 0.80)]. \qquad (9)$$

One drawback to this equation is the failure to approach infinity as the

porosity goes to unity. Both the Davies-Ingmanson and Carroll equations are

plotted in Fig. 1.

Theoretical Approaches

The choice of a regular array of circular cylinders enables analytical

solutions to the hydrodynamic flow equations to be obtained as one way to

study the flow past fiberlike objects. Emersleben (13) solved the Navier-

Stokes equation for the problem of flow parallel to a square array of infinitely

long parallel circular cylinders of equal radii. This analytical solution

yields a rigorous permeability equation based on fundamental principles which

can be compared with the Kozeny-Carman equation. Because of the mathematics

of the analysis, Emersleben's equation applies well above a porosity of 0.80,

but becomes poorer as the porosity is reduced. At a porosity of 0.90,

Emersleben obtained a Kozeny factor of 6.3, while at 0.80 his k was 3.5.

---

*The exponential operation is indicated by "exp": $\exp(x) = e^x$.
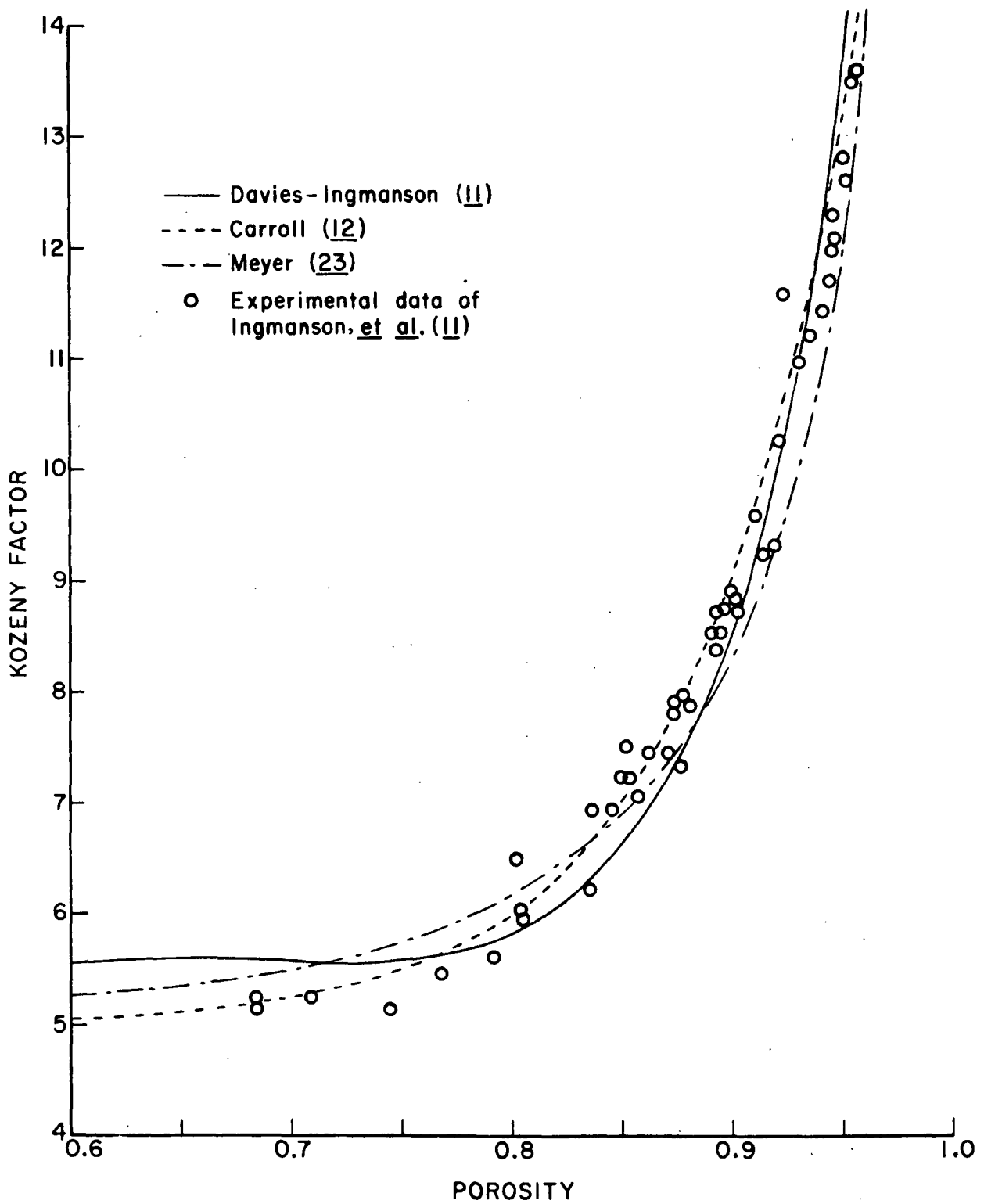
Figure 1. Correlations of Kozeny Factors for Mats of Circular Synthetic Fibers

A similar flow problem was considered by Sparrow and Loeffler (<u>14</u>), with laminar flow parallel to the cylinders arranged in square and equilateral triangular arrays. The square array case is the same as that of Emersleben. The analytical solution by Sparrow and Loeffler was obtained using series expressions, and has the advantage of being applicable at porosities below 0.80. At $\varepsilon = 0.50$, they found a Kozeny factor of 3.5 for the equilateral array and 2.9 for the square array.

A comparison of these two approaches for regular arrays is given by Happel and Brenner (<u>15</u>), while Carman (<u>7</u>) discusses Emersleben's analysis in detail.

Hasimoto (<u>16</u>) solved the two-dimensional problem of flow perpendicular to the longitudinal axes of an infinite square array of circular cylinders by obtaining periodic fundamental solutions of the Stokes equations of motion with the aid of Fourier series. Converting his drag force expression to Kozeny factor yields

$$k = \varepsilon^3/\{(1-\varepsilon)[\frac{1}{2} \ln(\pi/1-\varepsilon) - 1.3105 + (1-\varepsilon) + (1-\varepsilon)^2/\pi^2]\}. \quad (10)$$

Values from this analysis are compared in Table II with another approach. Results of this method are valid only for square arrays at porosities above 0.80.

A real fiber mat is an irregular assemblage of fibers. Even with some preferred fiber orientation, the actual structure is too complex to be easily described mathematically. Nevertheless, analytical applications of the basic hydrodynamic principles to irregular fiber assemblages have been completed. One method by which this is done is the cell model technique. In this method, the fiber bed is considered to be composed of a great number of

individual cells, each consisting of a fiber segment surrounded by a fluid
envelope bounded by a virtual fluid surface. For the analysis, an average
cell is assumed with the quantity of fluid in the cell sufficient to make
the cell porosity equal the bed porosity. Boundary conditions are specified
on the solid surface and the virtual fluid surface. The fluid boundary has
a shape similar to that of the particle in the cell, for example, a cylinder
concentric with the solid cylindrical fiber. The cell model technique has
been successfully applied to beds of spheres (17-19) as well as to assemblages
of cylinders (18,20).

Two separate but similar analyses of flow through arrays of circular
cylinders using the cell model method were published in 1959 by Kuwabara (18)
and Happel (20). The difference between the two is in the choice of boundary
conditions.

In the Happel analysis the cell model consisted of two concentric cylin-
ders, the inner one representing the solid surface and the outer one the virtual
fluid surface. Boundary conditions were specified for the solid cylinder
moving within the fluid, with the no-slip condition identified on the solid
surface and the conditions of zero normal velocity and zero shear stress
assumed on the fluid boundary. Two flow problems were treated: flow parallel
to the cylinder and flow perpendicular to the cylinder. In the parallel case,
Happel applied the complete Navier-Stokes equation, obtaining as the differential
equation to be solved

$$(1/r) \ d(r \ dv/dr)/dr = (1/\mu) \ dp/dx, \tag{11}$$

where r is the radius and v the velocity in the x-direction, using the
conditions

$$v = 0 \quad \text{on } r = a \text{ (solid cylinder)}$$
$$dv/dr = 0 \quad \text{on } r = b \text{ (virtual cylinder in fluid)}. \tag{12}$$

The solution for $\underline{v}$ was

$$v = - (1/4\mu)(dp/dx)[(a^2 - r^2) + 2b^2 \ln(r/a)]. \tag{13}$$

By integrating $\underline{v}$ over the entire annular region between the cylinders, the flow rate $\underline{Q}$ is obtained. From the Darcy equation, the permeability coefficient was found to be

$$K = [4a^2b^2 - a^4 - 3b^4 + 4b^4 \ln(b/a)]/(8b^2). \tag{14}$$

Applying the Kozeny-Carman theory, Equation (4), with the hydraulic radius, $\underline{m}$, defined as

$$m = (b^2 - a^2)/(2a), \tag{15}$$

the Kozeny factor for parallel flow, $\underline{k}_{(\underline{p})}$, was obtained, as follows:

$$k_{(p)} = 2\varepsilon^3/\{(1-\varepsilon)[2\ln(1/1-\varepsilon) - 3 + 4(1-\varepsilon) - (1-\varepsilon)^2]\}. \tag{16}$$

Table I compares values for the parallel Kozeny factors from the analyses of Happel, Sparrow and Loeffler, and Emersleben. For high porosities, the Happel result is equivalent to the findings of Sparrow and Loeffler for regular arrays, which demonstrates the success of the cell model approach in describing parallel flow past arrays of circular cylinders.

TABLE I

COMPARISON OF KOZENY FACTORS FOR PARALLEL FLOW PAST
REGULAR ARRAYS OF CIRCULAR CYLINDERS

Analysis	Porosity		
	0.90	0.80	0.50
Square array:			
Emersleben	6.3	3.5	--
Sparrow and Loeffler	7.3	5.0	2.9
Happel	7.3	5.2	3.7
Equilateral triangular array:			
Sparrow and Loeffler	7.3	5.2	3.5
Happel	7.3	5.2	3.7

The analysis by Happel for the perpendicular flow case was based on the creeping flow equations, obtained by omitting the inertia terms from the Navier-Stokes equation. Using cylindrical coordinates and introducing the stream function, ψ, defined by

$$v_r = (1/r)\, \partial\psi/\partial\theta \text{ and } v_\theta = -\partial\psi/\partial r \tag{17}$$

the creeping motion equations in two dimensions reduce to the biharmonic equation

$$\nabla^4\psi = 0 \tag{18}$$

with the boundary conditions as follows:

$$
\left.
\begin{aligned}
v_r &= U\cos\theta \\
v_\theta &= -U\sin\theta
\end{aligned}
\right\} \text{ on } r=a \text{ (no-slip)}
$$

$$v_r = 0 \text{ on } r=b \text{ (zero normal velocity)}$$

$$\partial v_\theta/\partial r + (1/r)\partial v_r/\partial\theta - v_\theta/r = 0 \text{ on } r=b \text{ (zero shear stress)} \tag{19}$$

These are stated for the cylinder moving in the fluid. A solution for this is

$$\psi = \sin \theta [Cr^3/8 + Dr(\ln r - \tfrac{1}{2})/2 + Er + F/r] \tag{20}$$

in which the factors $\underline{C}$, $\underline{D}$, $\underline{E}$, and $\underline{F}$ are determined from the boundary conditions. The drag on the solid cylinder is

$$F = 2 \pi \mu D \tag{21}$$

and $\underline{D}$ was found to be

$$D = - 2U/[\ln(b/a) + a^4/(a^4 + b^4) - \tfrac{1}{2}]. \tag{22}$$

If the cylinder is stationary, the drag on a cell is related to the pressure drop by

$$F/(\pi b^2) = dp/dx. \tag{23}$$

Equation (23) may be compared with the Darcy equation to determine the permeability coefficient $\underline{K}$:

$$K = (b^2/4)[\ln(b/a) - \tfrac{1}{2}(b^4 - a^4)/(b^4 + a^4)]. \tag{24}$$

Converting to the Kozeny factor for transverse flow, $\underline{k}_{(t)}$, with $\nu = (1-\varepsilon)$,

$$k_{(t)} = 2(1-\nu)^3/\{\nu[- \ln \nu - (1-\nu^2)/(1+\nu^2)]\}. \tag{25}$$

The effect of porosity on $\underline{k}_{(\underline{p})}$ and $\underline{k}_{(\underline{t})}$ from Happel's analysis is demonstrated in Fig. 2.

The analysis by Kuwabara is like that of Happel except that zero vorticity was assumed on the virtual fluid surface instead of zero shear stress as a boundary condition. Kuwabara only considered the perpendicular flow problem, but in the parallel flow case both the zero vorticity and the zero shear stress conditions yield mathematically identical conditions. For perpendicular flow, Kuwabara's solution was
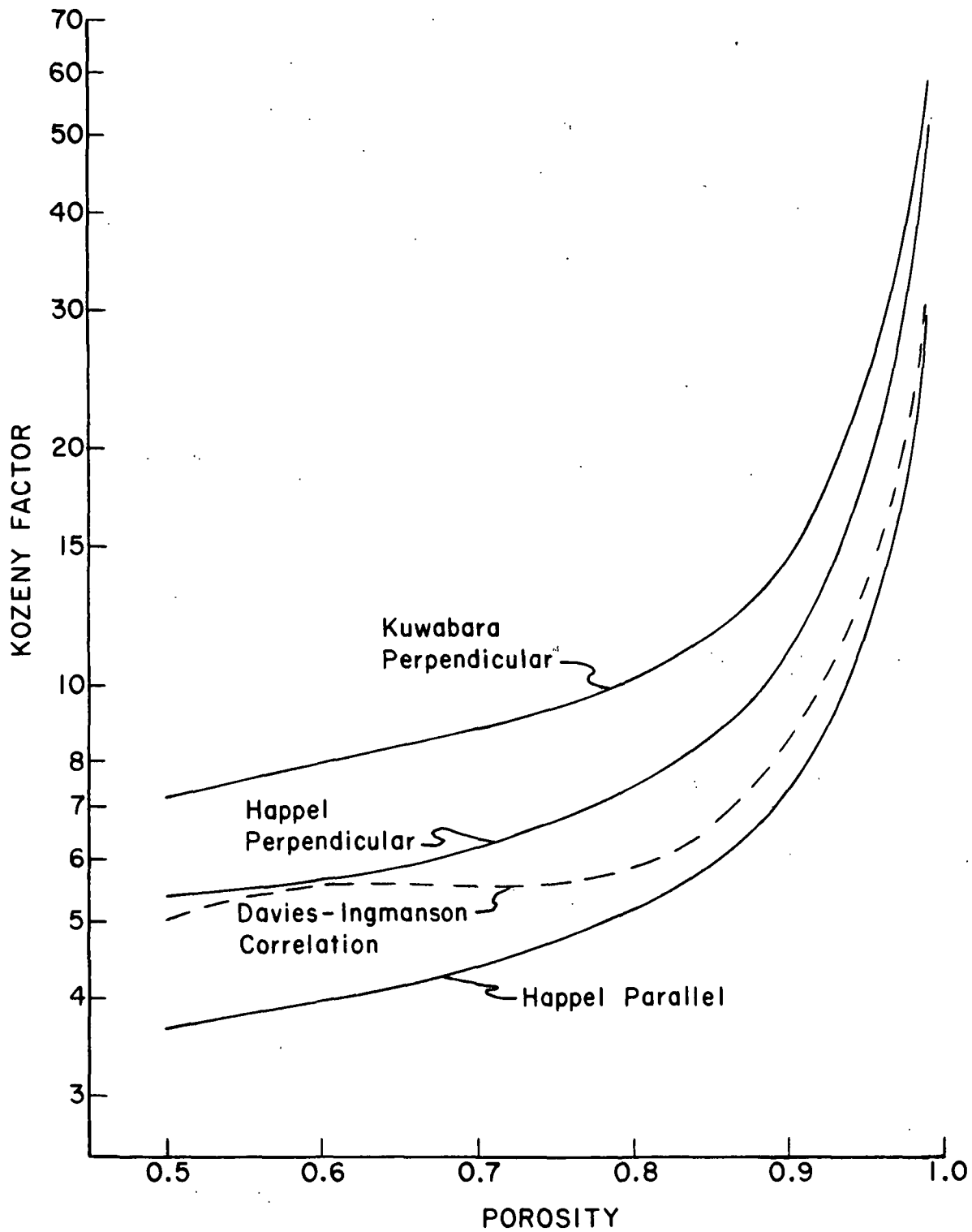
Figure 2. Circular Cell Model Kozeny Factors

$$\psi = (A/r + Br + Cr \ln r + Dr^3) \sin \theta. \tag{26}$$

The resulting Kozeny factor for the Kuwabara analysis is

$$k_{(t)} = 4\varepsilon^3/\{(1-\varepsilon)[2 \ln(1/1-\varepsilon) - 3 + 4(1-\varepsilon) - (1-\varepsilon)^2]\}. \tag{27}$$

This relationship is plotted in Fig. 2 along with the Happel results. The results are similar, but the Kuwabara equation predicts higher values for the Kozeny factor. Surprisingly, the Kuwabara transverse flow Kozeny factor is exactly twice Happel's parallel flow Kozeny factor.

The flow patterns obtained in the Happel and Kuwabara analyses are similar. Streamlines (curves of constant stream function) for perpendicular flow through the cell at a porosity of 0.75 are demonstrated in Fig. 3. Near the solid surface the streamlines are very close. As the outer surface is approached the two begin to differ, but not by much.

The question of which condition, zero vorticity or zero shear stress, is more valid has not been clearly settled. Happel and Brenner suggest that the Happel model is more physically reasonable since the Kuwabara model cell exchanges energy with neighboring cells, whereas the zero shear stress model does not. For flow past spheres, the model of Happel agrees better with experimental data; but for assemblages of cylinders, the Kuwabara approach fits the observed behavior better (21).

Kirsch and Fuchs (21) investigated the pressure drop in models of fibrous filters composed of parallel rows of circular cylinders oriented perpendicular to the flow direction and compared the experimental data to the models of Kuwabara and Happel. A conclusion from this study was that the Kuwabara analysis fits the data well down to a porosity near 0.73, while the Happel analysis underestimates the pressure drop over the porosity range considered.
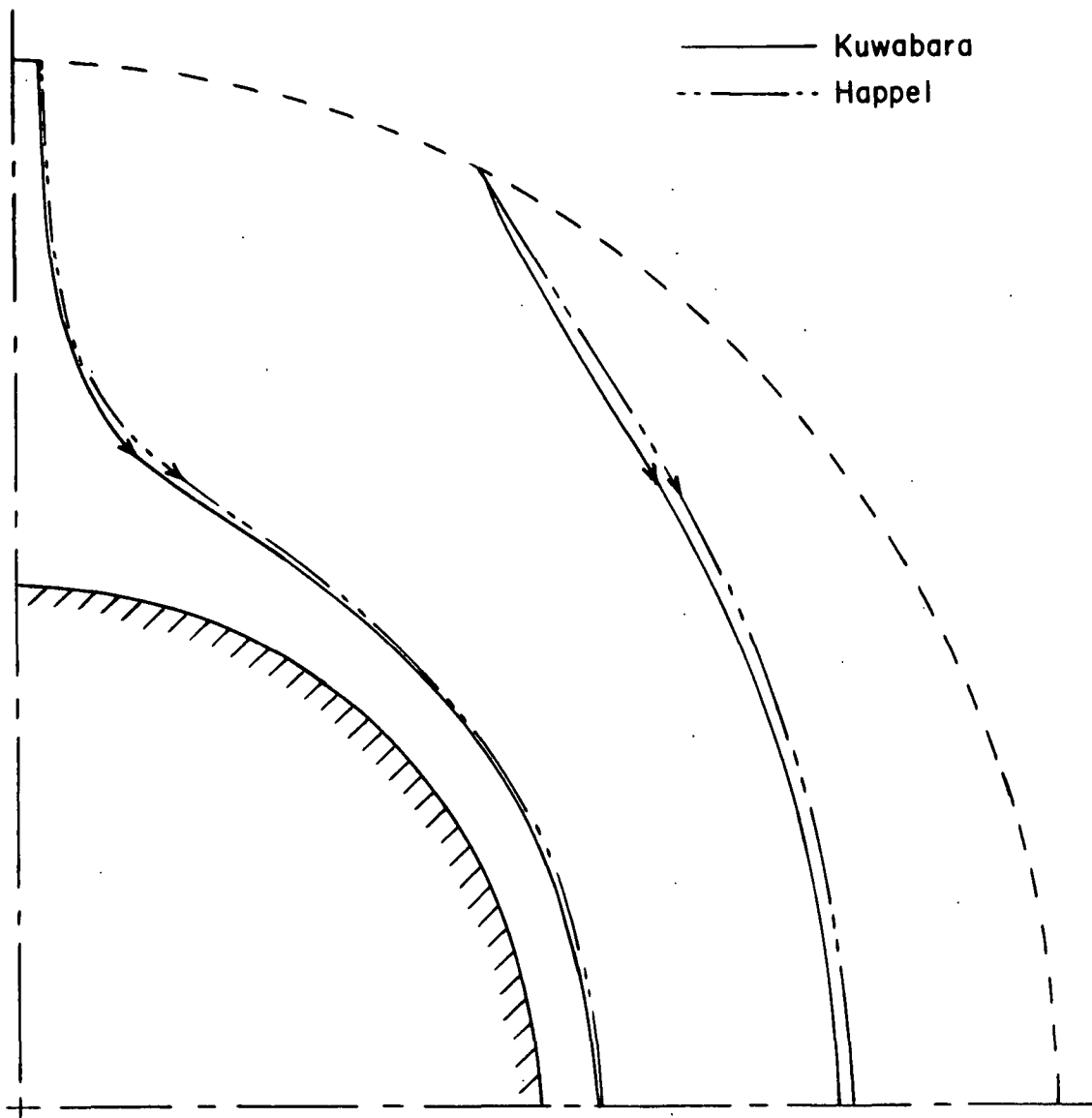
Figure 3. Comparison of Streamlines for Perpendicular Flow in
Circular Cell from Analyses of Kuwabara and
Happel at Porosity 0.75

In another study of perpendicular flow past a system of parallel cylinders, Kirsch and Fuchs (22) experimentally observed the flow patterns around the cylinders and compared the results to the streamlines predicted by the Happel and Kuwabara analyses. Again, the zero vorticity model agreed with the observations better than the zero shear stress model did.

The cell model analyses for perpendicular flow agree well with the results obtained by Hasimoto for perpendicular flow through a square array of circular cylinders, although the agreement worsens below a porosity of 0.80. Table II summarizes a few Kozeny factors from these approaches. Kuwabara's zero vorticity model is closer to the Hasimoto values than is Happel's zero shear stress model for porosities above 0.80, suggesting that the choice of zero vorticity as an outer boundary condition may be more acceptable for arrays of circular cylinders, at least at higher porosities.

TABLE II

KOZENY FACTORS FOR PERPENDICULAR FLOW THROUGH
ARRAYS OF CIRCULAR CYLINDERS

Porosity	Square Array Hasimoto	Cell Models	
		Kuwabara	Happel
0.99	61.6	62.1	53.8
0.90	14.2	14.6	11.0
0.80	9.46	10.2	7.46
0.70	6.61	8.80	6.19

A comparison of the curves in Fig. 1 and 2 shows that the empirical correlations of Davies-Ingmanson and Carroll fall between the parallel and perpendicular Kozeny factor curves from the cell model analyses. This observation supports the validity of the cell concept as applied to fiber mats. Meyer (23) suggested that the two directional values be mixed by employing a weighting function, $\underline{w}(\epsilon)$, in the following manner:

$$1/k = w(\varepsilon)/k_{(p)} + [1 - w(\varepsilon)]/k_{(t)}. \tag{28}$$

A real fiber mat has fiber segments oriented at various angles to the flow direction. The flow velocity and drag vectors can be resolved into components both parallel and perpendicular to the fiber segment, thereby providing a basis for the weighting method. Combining the directional values in this manner yields a porosity-dependent correlation for the Kozeny factor based upon the analytical results. The weighting factor chosen by Meyer was

$$w(\varepsilon) = 1.6 \ (\varepsilon - 0.5). \tag{29}$$

The Kozeny factor curve using this approach fits the experimental data as well as the Davies-Ingmanson correlation, as seen in Fig. 1. The weighting technique demonstrates that rigorous analysis of idealized cases can be useful and complementary to empirical observations.

In addition to the application of the cell model approach to the permeability of fiber mats, it has been employed by Fuchs and Stechkina (24) as the basis for a theory of aerosol filtration using fibrous filters and by Pich (25) who extended the theory to include slip flow at the fiber surface.

The cell method used by Happel and Kuwabara has attracted the attention of investigators recently who are interested in extending the results beyond the creeping flow region to higher Reynolds numbers. LeClair and Hamielec (26) used the cell model concepts of Happel and Kuwabara for flow through assemblages of circular cylinders, solving the Navier-Stokes equation by finite difference methods to cover the ranges of Reynolds number from 0.1 to 500 and of porosity from 0.4 to 1.0. El-Kaissy and Homsy (27) performed a similar analysis in extending the cell model results to intermediate particle Reynolds numbers by a regular perturbation technique.

Approaches other than treating regular arrays of cylinders or looking at the flow in a model cell have been presented by various researchers.

Iberall (28) utilized a drag theory approach in considering the permeability of glass wool and similar highly porous media. The cell model method is one form of a drag theory, but Iberall's analysis preceded the cell analyses. By assuming the porous medium to consist of randomly distributed uniform circular cylinders, Iberall proposed that the permeability is related to the drag force on individual elements. With the fibers oriented randomly, the pressure drops for each of the three orthogonal directions past an element were merely added together to give the overall pressure drop. For flow parallel to a fiber element, the equation for drag force derived by Emersleben was used. For perpendicular flow, Lamb's solution of Oseen's equations (29) was used. The result of Iberall for a random assemblage of cylinders in terms of the Kozeny factor is

$$k = (1/3)\epsilon^2(1-\epsilon)^{-1}(2 - \ln Re)/(4 - \ln Re) \qquad (30)$$

and is applicable for flow up to a particle Reynolds number (Re) of about 1.0. When Iberall studied experimental data, he found that the above result was valid if different constants were used. In his paper, Iberall compares the hydraulic radius theories, such as the Kozeny-Carman analysis, with the drag theories, concluding that neither is good for the entire porosity range of interest. The hydraulic radius method works best at lower porosities, while the drag theory is best at higher porosities where interference from other particles is minimized.

A recent analysis by Spielman and Goren (30) applies a model different from the cell approaches to flow through fibrous media. The technique is the

one proposed by Brinkman (31) originally for swarms of spheres. The model assumes that a particle within the porous medium is subjected to a damping force due to the effect of surrounding objects in addition to the viscous and pressure forces. The damping force is linearly proportional to velocity and is treated analytically by adding the Darcy term to the creeping motion equation. The Brinkman model becomes invalid at low porosities because a simple damping term cannot then adequately account for the numerous inter-actions among the particles. Neither does the model hold for very high porosities where the behavior can be treated as flow past isolated cylinders. Spielman and Goren considered four orientation distributions expected in fiber mats, as follows: all fibers in planes perpendicular to the flow but random in those planes; all fibers parallel to flow; all fibers in planes parallel to flow but random in those planes; and, fibers randomly oriented. For the first case above, the predicted pressure drop was compared to the estimates from the cell model analyses of Happel and Kuwabara for perpendicular flow, and the empirical analysis of Davies. For porosities above 0.9, the present model predicts pressure drops below the values from both the cell models and is close to Davies' results. This model estimates higher resis-tances than the Happel and Kuwabara models below porosities of 0.87 and 0.79, respectively. The Spielman and Goren model shows a stronger dependence on porosity than any of the other three studies.

A different approach to flow through fibrous beds was employed by Kyan, Wasan, and Kintner (32), who developed a pore model to account for the high pressure drop despite high porosities. They base their model on two assump-tions which explain the higher than expected pressure drops. First, they propose that a portion of the void space within the medium is occupied by stagnant fluid so that the flow occurs in only a fraction of the void volume.

Second, they suggest that the deflection of individual fibers within the mat as a result of the flow absorbs energy, thereby increasing the actual pressure drop. The resulting model is complicated and involves several parameters dependent on mat and fiber properties.

Another pore model was used by Clarenburg and Piekaar (33) in developing a theory for the pressure drop across fibrous filters. Their model is based on geometrical considerations. An equation for the pressure drop is the result of the analysis, but it is an involved function of filter, fiber, and flow characteristics, and its applicability to real fiber mats is questionable.

NONCIRCULAR FIBERS

Many natural fibers and some commercially available synthetic fibers have cross-sectional shapes that deviate considerably from a circular shape. Fibers such as wood and cotton possess numerous cross-sectional shapes because of the hollow center, or lumen, which can collapse under pressure. Since the permeability of wood fiber mats is of importance to the paper industry, the question of what effect fiber shape has on the flow resistance through a fiber mat has arisen. The application of the results of studies with circular fibers to the permeation of mats of noncircular fibers is of questionable value pending further analysis. Consequently, some investigators have studied the permeability of fiber mats made from noncircular fibers.

Empirical Approaches

Several experimental programs have been conducted in which the permeability of wood fiber mats was the principal concern. For a discussion of these, refer to the reviews by Meyer (34) and Han and coworkers (35). With wood fibers, the permeability measurements are complicated not only because

of their irregular shape but also because they swell in water dependent upon the compressive stress. This makes estimates of specific volume and specific surface difficult to obtain.

One study (36) of the cross-sectional shape of wet wood fibers which had been freeze-dried so that the lumens would not collapse indicated that the ratios of largest to smallest diameters were generally below 3.5 to 1. After drying, the lumen collapses and the ratio can increase to near 10 to 1.

An investigation of the factors affecting air permeation of plugs of textile fibers was reported by Lord (37). Using a number of different natural fibers, the Kozeny factors were determined experimentally. Lord's findings confirm the strong dependence of Kozeny factor on porosity. The possibility of an effect of fiber cross-sectional shape on the Kozeny factor was suggested, but no definitive conclusion was obtained.

Bliesner (8) investigated the permeability of thick mats of wood pulp fibers. In interpreting his data, he proposed that the collapse of the fibers under pressure partially explained his findings. Since he was using the Kozeny-Carman analysis, he became concerned about the effect of fiber shape on the value of the Kozeny factor, k. In an attempt to determine if k were indeed changing as the fibers changed shape, Bliesner performed water permeability measurements with beds of synthetic fibers of three different cross-sectional shapes. One set of fibers was 15-denier nylon with a circular cross section (axis ratio = ratio of minor to major axes of cross section = 1.0). Another set was prepared from the circular fibers by softening in a hot water bath and then passing the monofilament strands through the steel rolls of a rolling mill, a procedure which yielded an approximately elliptic cross section

of axis ratio 0.344. The third set was 10-denier orlon with a flattened, "dog-bone" cross section of axis ratio 0.242. From the flow rate and pressure drop data, the permeability coefficient, $\underline{K}$, was computed; the experimental Kozeny factor was then found by using the Kozeny-Carman equation. The results, which are plotted in Fig. 4, indicate no obvious conclusion about the effect of fiber shape on Kozeny factor. Bliesner reasoned that the flatter noncircular fibers could overlap more easily than round ones, thereby excluding more surface area from the permeating fluid as a result of interfiber contact. To account for this, he corrected his data and found a significant dependence on fiber shape, as seen from the corrected curves in Fig. 4. His contact area analysis, based on the fiber network model of Onogi and Sasaguri ($\underline{38}$), produced estimates of interfiber contact for the orlon fiber of axis ratio 0.242 at 0.70 porosity of 23% of the total surface area. Since Bliesner was not primarily interested in this question, he did not pursue the matter further.

As a result of the findings of Bliesner, Labrecque ($\underline{39}$) proceeded to investigate further the effect of fiber shape on mat permeability. A synthetic fiber manufacturer produced four experimental batches of nylon 6 monofilaments of approximately elliptic cross sections. After drawing and cutting the fibers, the axis ratios were 1.00, 0.379, 0.243, and 0.213. Labrecque encountered some experimental problems in his early efforts to form mats at room temperature because the fibers tended to curl and prevent good mat formation. To overcome this problem, he resorted to a procedure in which he first dispersed the fibers in absolute ethanol at near -50°C, then formed the mat from the cold, dilute fiber slurry. After mat formation, the temperature was increased to about 5°C, the ethanol was displaced with distilled water, and the apparatus was then warmed to room temperature and the permeability measurements were begun.
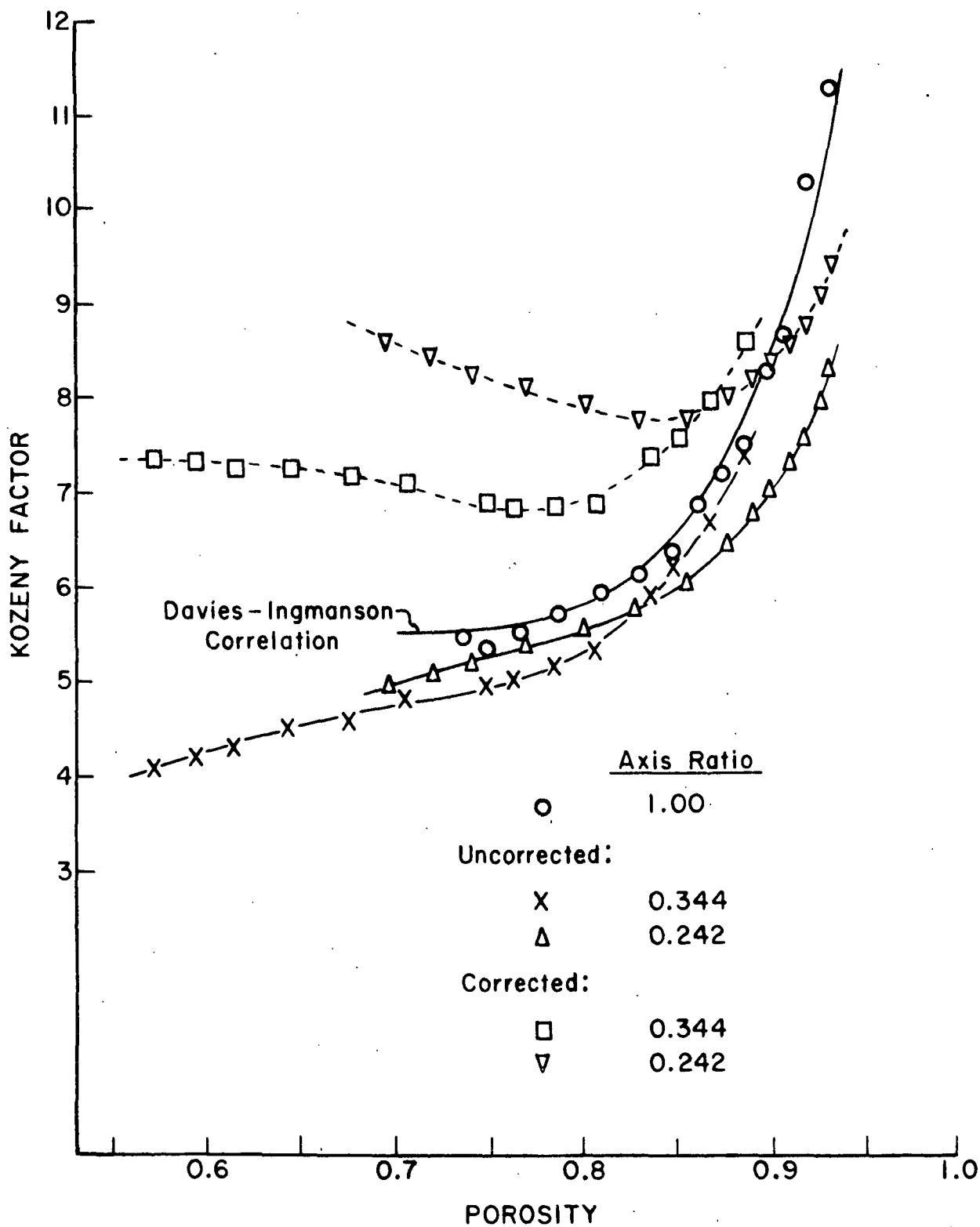
Figure 4. Bliesner's Experimental Kozeny Factors for Noncircular Synthetic Fiber Mats

The Kozeny factors calculated from these experimental tests have been analyzed by a curvilinear regression analysis, as summarized in Appendix I; the regression curves for Labrecque's experimental data are plotted in Fig. 5. At a porosity below 0.70, the circular fiber values deviate significantly from similar previous measurements by others, as seen by comparison with the Carroll correlation. The elliptic fiber data also show a trend similar to the unexpected circular fiber values. Because of the lack of agreement for the round fibers at lower porosities, the data obtained by Labrecque are of questionable validity. The correction for interfiber contact was also used by Labrecque, modifying the Bliesner approach with some refinements and corrections of errors. The area excluded from the fluid was estimated to be about 9% for the fiber of axis ratio 0.243 at porosity 0.70, as compared to the Bliesner estimate of 23% under similar conditions. Labrecque also estimated the surface area available to the fluid by a light scattering procedure.

Theoretical Approaches

Very few theoretical analyses have been reported in which noncircular fibers were the object of consideration. The choice of an elliptic cylinder as a model of a noncircular fiber can be treated mathematically without excessive difficulties, and by changing the axis ratio of the elliptic cross section, the fiber cross-sectional shape can be varied from very nearly round to almost flat.

Because of the success of the cell models of Happel and Kuwabara in describing the flow through assemblages of circular cylinders, and more practically through fiber mats, Meyer (23) began to extend the cell model analysis to the case of elliptic cylinders. The problem of parallel flow along the cylinder was solved by an approximate method. The perpendicular flow problem for an elliptic cylinder cell model was also set up.
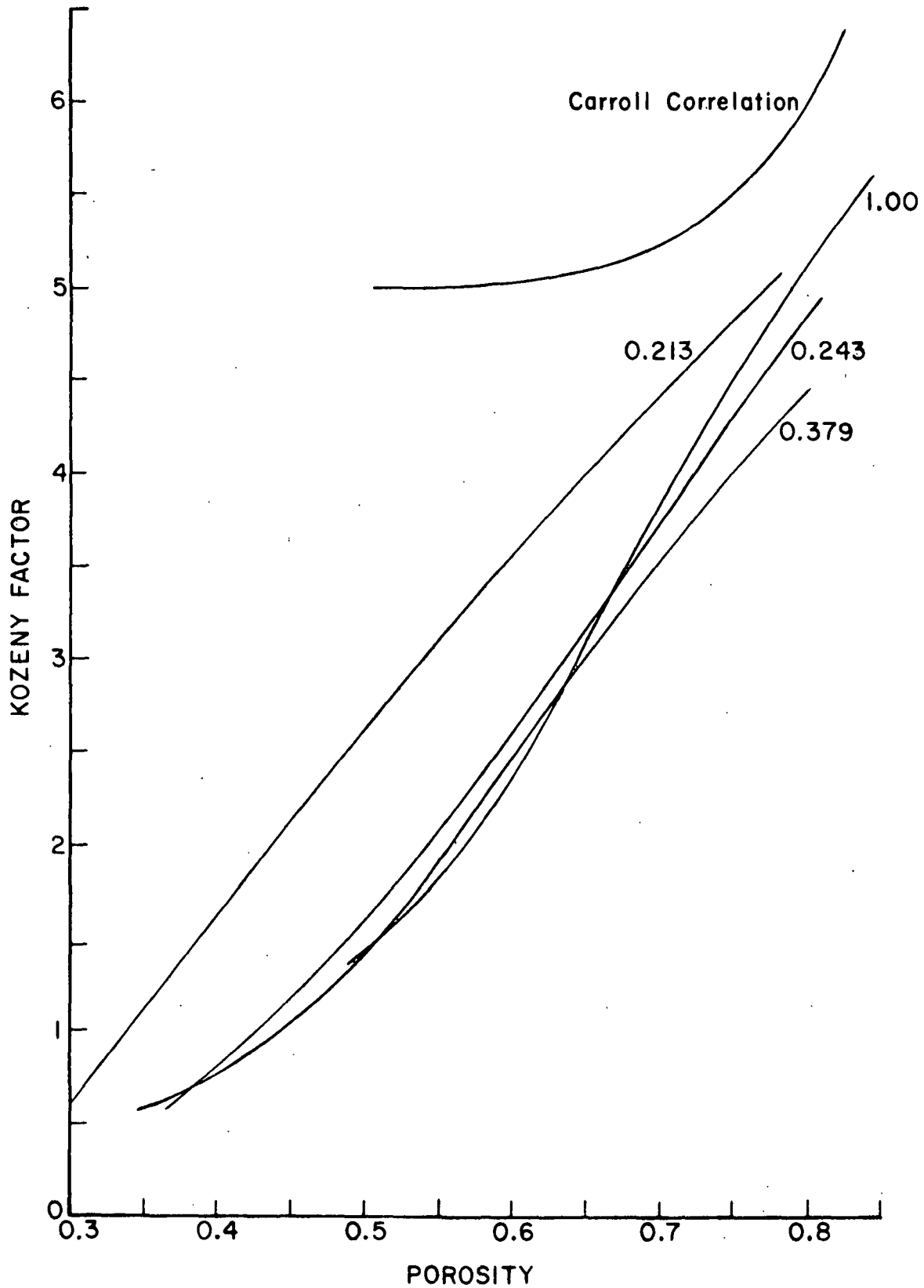
Figure 5. Regression Curves of Labrecque's Experimental Data
Not Corrected for Interfiber Contact Area

Recently Masliyah and Epstein (40-42) published the results of an analysis
of perpendicular flow past arrays of elliptic cylinders based on the cell
models. They put the complete steady-state Navier-Stokes equation in a finite
difference form and solved it using a relaxation scheme at a few combinations
of axis ratio, porosity, and Reynolds number. Results for creeping flow were
obtained by choosing a small Reynolds number. They covered the porosity range
0.4 to 1.0 for axis ratios 1.0, 0.9, 0.5, and 0.2, and considered flow along
both the minor and major cross-sectional axes. As expected, the resistance
to flow along the major axis is much lower than that along the minor axis.
Results in terms of Kozeny factor are shown in Fig. 6. The shape of the cylin-
der seems to have a significant effect on Kozeny factor. Some limitations of
this analysis are that the parallel case was not considered and that the calcu-
lation of Kozeny factor at a particular combination of porosity and axis ratio
requires a lengthy computer run.

An analysis for perpendicular flow at small Reynolds numbers through a
regular square array of elliptic cylinders was developed by Kuwabara (43) by
solving the two-dimensional equation of Oseen. The creeping flow values can be
approximated by choosing a small Reynolds number (e.g., 0.08). For the limiting
case of a circular cylinder, Kuwabara's resulting Kozeny factors agree fairly
well with those of Hasimoto above a porosity of near 0.93. For example, at a
porosity of 0.95, the Kozeny factors 23.6 and 21.2 were obtained, respectively,
by Kuwabara and Hasimoto, while the values in the same order at 0.99 porosity
were 63.1 and 61.6.
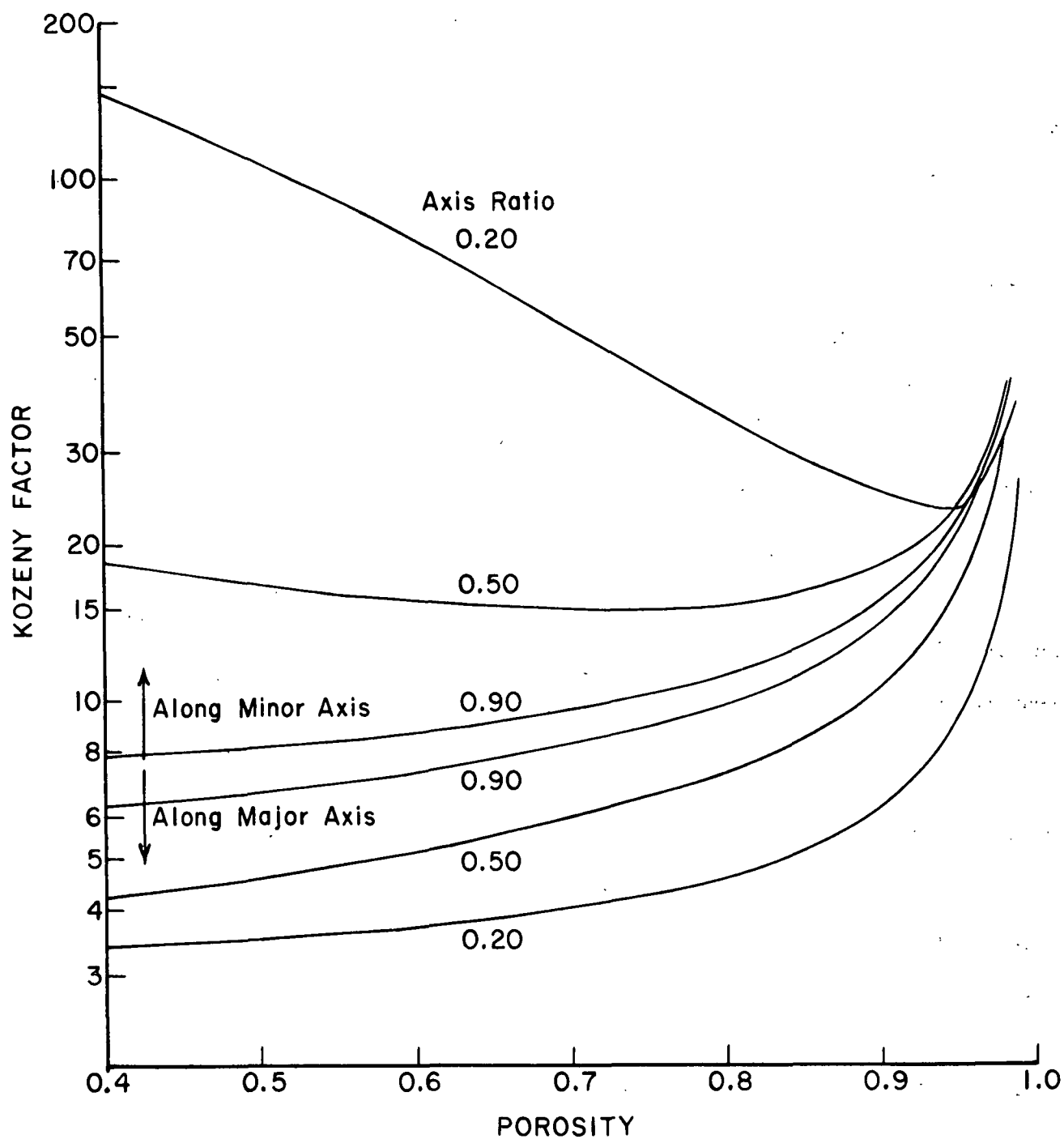
Figure 6. Perpendicular Flow Kozeny Factors from Cell Model
Analysis of Masliyah and Epstein

STATEMENT OF THE PROBLEM

The question of what effect the cross-sectional shape of a fiber has on the resistance to fluid permeation through fiber mats has not yet been satisfactorily answered, despite two experimental approaches to the problem and one theoretical analysis as reviewed in the preceding section. The experimental work of Bliesner (8) indicated the existence of a relationship between Kozeny factor, a measure of relative resistance, and fiber cross-sectional shape, but the study was limited in scope. Also, it suggested the complicating consideration of correcting the surface area because of interfiber contact. Labrecque (39) attempted to clarify the question by further experimental effort, but encountered some difficulties which made his data questionable. The only theoretical study, that of Epstein and Masliyah (40) concerning assemblages of elliptic cylinders, utilized an involved numerical solution procedure so that Kozeny factors are available at only a few elliptic axis ratios and porosities. Consequently these results are not widely applicable to fiber mats where the fibers can possess any axis ratio between 1 and 0.1.

The primary objective of this thesis program is to clarify the effect of fiber cross-sectional shape on the permeability of fiber mats. To do this, a cell model analysis for creeping flow through assemblages of elliptic cylinders will be developed. This is to be similar to the cell model analyses for circular cylinders completed by Happel (20) and Kuwabara (18).

Upon completion of the cell model analysis, the theoretical results will be applied to the permeation of real fiber mats and compared to experimental data in order to ascertain the effect of fiber shape on Kozeny factor. The surface area correction for interfiber contact will be reconsidered to determine if it is valid and significant.

THEORETICAL ANALYSIS OF FLOW THROUGH
ASSEMBLAGES OF ELLIPTIC CYLINDERS

CELL MODEL OF FLOW

The steady, isothermal, creeping flow of fluids relative to assemblages of elliptic cylinders is analyzed by employing a cell model technique similar to that used by both Happel (20) and Kuwabara (18) in their analyses of flow past arrays of circular cylinders. The cell model approach considers the cluster of cylinders to be a collection of individual cells each composed of a solid cylinder segment surrounded by a fluid envelope. The cell which is treated analytically is an "average" of all the individual cells within the array of particles.

Two confocal ellipses serve as the typical cell, the inner one representing the surface of the solid cylinder segment and the outer one a virtual fluid surface. The position of the outer, virtual surface is such that the ratio of fluid volume to cell volume equals the porosity of the assemblage of cylinders. On the solid surface, the no-slip condition is assumed, while on the virtual surface the condition of zero normal velocity and one other condition are assumed. The other condition can be that of zero vorticity, as used by Kuwabara, or that of zero shear stress, as used by Happel. Elliptic cylindrical coordinates $(\xi, \eta, \underline{z})$ are used to simplify the mathematical description of boundaries and boundary conditions. A discussion of these coordinates and their relation to Cartesian coordinates is given in Appendix III. The surfaces of constant ξ are confocal ellipses, while those of constant η are confocal hyperbolas. The cell model is illustrated in Fig. 7. The two ellipses have a focal length of $\underline{c}$. The inner ellipse, the solid cylinder, has major and minor half-axes of $\underline{a}_o$ and $\underline{b}_o$, respectively, and is described by $\xi = \xi_o$. The virtual
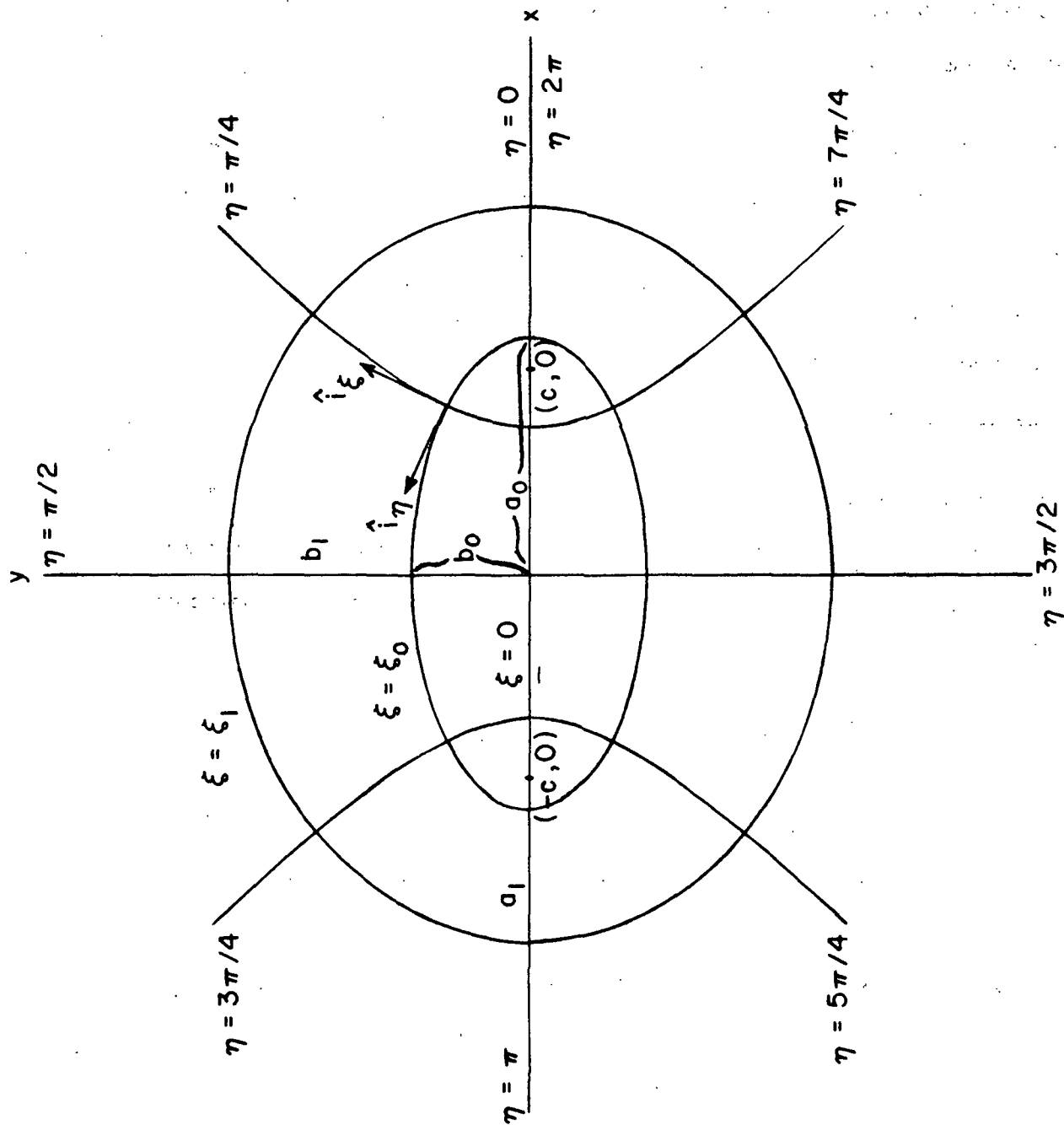
Figure 7. Cell Flow Model Showing Two Confocal Elliptic Cylinders in Cross Section and Elliptic Coordinates

surface has major and minor half-axes of a_1 and b_1, respectively, and $\xi = \xi_1$. The axis ratios β_o and β_1 are defined as the ratios of minor to major half-axes of the solid and virtual ellipses, respectively.

Three cases of flow relative to the cell are of interest: flow parallel to the central axis of the cylinder; flow perpendicular to the central axis and parallel to the minor cross-sectional axis; and, flow perpendicular to the central axis and parallel to the major cross-sectional axis. Each of these three flow problems is considered individually in the following pages, although the latter two cases are very similar in approach and solution method.

A review of the equations of state for Newtonian fluids in creeping flow in generalized orthogonal curvilinear coordinates is presented in Appendix II. Also listed are some transformations relating the curvilinear and Cartesian coordinate systems.

FLOW PARALLEL TO ELLIPTIC CYLINDER

The analysis of steady creeping flow parallel to the central axis of the elliptic cylinder (z-direction) in the cell requires that only one pressure gradient, dp/dz, and one velocity component, v_z, be accounted for. The equation of continuity, written in full in Equation (205), reduces to

$$\partial(v_z/h^2)/\partial z = 0. \tag{31}$$

The equation of motion has only one component, given by Equation (211), which reduces for this case to

$$- dp/dz + \mu\nabla^2 v_z = 0. \tag{32}$$

The Laplacian operator, Equation (207), has become

$$\nabla^2 = h^2(\partial^2/\partial\xi^2 + \partial^2/\partial\eta^2) \tag{33}$$

with the third term dropped because of the continuity equation. In a re-arranged form, Equation (32) becomes

$$\partial^2 v_z/\partial\xi^2 + \partial^2 v_z/\partial\eta^2 = (dp/dz)(c^2/\mu)(\sinh^2\xi + \sin^2\eta) = f(\xi,\eta). \tag{34}$$

This is the equation to be solved to complete the analysis of flow parallel to the elliptic cylinder in the cell, using the following boundary conditions:

$$v_z = 0 \quad \text{on} \quad \xi = \xi_0, \tag{35}$$

$$\partial v_z/\partial\xi = 0 \quad \text{on} \quad \xi = \xi_1. \tag{36}$$

The first condition is simply the no-slip requirement on the solid surface. The second condition, on the virtual fluid surface, satisfies both Happel's zero shear stress requirement and Kuwabara's zero vorticity condition. Equation (34) is a Poisson equation, or an inhomogeneous Laplace equation, and is not separable.

EXACT SOLUTION

An exact solution to the above boundary value problem using a Green's function method was outlined by Nelson (44). Consider the Poisson equation, Equation (34), to be of the form

$$\partial^2\phi/\partial\xi^2 + \partial^2\phi/\partial\eta^2 = \lambda\phi, \tag{37}$$

where $$\phi = W \cdot V = W(\xi) \cdot V(\eta). \tag{38}$$

The variables can be separated by substituting for ϕ, yielding

$$(1/W) \, d^2W/d\xi^2 + (1/V) \, d^2V/d\eta^2 = \lambda. \tag{39}$$

The symmetry of flow about the cylinder requires that $\underline{V}(\eta) = \underline{V}(-\eta) = \underline{V}(\pi-\eta)$, leading to the choice

$$V(\eta) = \cos j\eta, \quad j = \text{even integer.} \tag{40}$$

The boundary conditions, Equations (35) and (36), provide that $\underline{W}(\xi_0) = 0$ and $\underline{W}'(\xi_1) = 0$, where the prime indicates differentiation with respect to ξ. The function

$$W = \sin[(k\pi/2)(\xi-\xi_0)/\delta], \quad k = \text{odd integer,} \tag{41}$$

satisfies these conditions, with

$$\delta = \xi_1 - \xi_0. \tag{42}$$

The eigenvalues are thus

$$\lambda = -(k\pi/2\delta)^2 - j^2 \tag{43}$$

and the eigenfunctions are

$$\phi_{jk} = (1/N_{jk}) \cos j\eta \, \sin[(k\pi/2\delta)(\xi-\xi_0)], \tag{44}$$

where $\underline{N}_{jk}$ is a normalization factor, defined as

$$N_{jk} = (\pi\delta/2)^{1/2} \tag{45}$$

except for $\underline{j} = 0$, where the factor is

$$N_{0k} = (\pi\delta)^{1/2}. \tag{46}$$

The Green's function, $\underline{G}$, is

$$G = \sum_j \sum_k [\phi_{jk}(\xi,\eta) \, \phi_{jk}(\xi',\eta')]/\lambda_{jk} \tag{47}$$

or, substituting for the eigenfunctions and eigenvalues,

$$G = - \sum_j \sum_k \frac{\cos j\eta \, \sin[(k\pi/2\delta)(\xi-\xi_0)] \, \cos j\eta' \, \sin[(k\pi/2\delta)(\xi'-\xi_0)]}{N_{jk}^2 [(k\pi/2\delta)^2 + j^2]}. \quad (48)$$

The solution, $\underline{v}_z$, is

$$v_z(\xi,\eta) = \int_0^{2\pi} \int_{\xi_0}^{\xi_1} G(\xi,\eta;\xi',\eta') \, f(\xi',\eta') \, d\xi' \, d\eta'. \quad (49)$$

Define

$$\gamma = k\pi/2\delta \quad (50)$$

and substitute for $\underline{G}$ and $\underline{f}$ to obtain

$$v_z = - (c^2/\mu)(dp/dz) \sum_j \sum_k A_{jk} \cos j\eta \{\sin[\gamma(\xi-\xi_0)]\}/[N_{jk}^2(\gamma^2 + j^2)], \quad (51)$$

where $\underline{A_{jk}}$ is the integral

$$A_{jk} = \int_0^{2\pi} \int_{\xi_0}^{\xi_1} \sin[\gamma(\xi'-\xi_0)] \cos j\eta' \, (\sinh^2\xi' + \sin^2\eta') \, d\xi' \, d\eta'. \quad (52)$$

Evaluation of the integrals and rearrangement produces the following expression for the velocity distribution:

$$v_z(\xi,\eta) = - (c^2/\mu)(dp/dz) \, X_E \quad (53)$$

$$X_E = \sum_{\substack{k=1 \\ \text{odd}}}^{\infty} \sin[\gamma(\xi-\xi_0)] \, R_k/[\gamma^2(\gamma^2 + 4)\delta] \quad (54)$$

$$R_k = 2 \, (-1)^{(k-1)/2} \sinh 2\xi_1 + \gamma \cosh 2\xi_0 - \gamma \cos 2\eta. \quad (55)$$

APPROXIMATE SOLUTION

An approximate solution to the boundary value problem for parallel flow has also been completed. This solution, due to Meyer (23), expresses the

velocity distribution as a third degree polynomial. The approximate solution is outlined below.

In addition to the boundary conditions as stated in Equations (35) and (36), an exact solution would also satisfy the conditions

$$\left.\begin{array}{l} \partial v_z/\partial \eta = 0 \\ \partial^2 v_z/\partial \eta^2 = 0 \end{array}\right\} \quad \text{on} \quad \xi = \xi_o \tag{56}$$

producing from Equation (34),

$$\partial^2 v_z/\partial \xi^2 = f(\xi_o, \eta) \quad \text{on} \quad \xi = \xi_o. \tag{57}$$

The integration of Equation (34) over ξ from ξ_o to ξ_1 together with the second boundary condition yields the following:

$$\int_{\xi_o}^{\xi_1} f(\xi,\eta) \, d\xi - \int_{\xi_o}^{\xi_1} (\partial^2 v_z/\partial \eta^2) \, d\xi + g_{(z)}(\eta) = 0, \tag{58}$$

where the function $g_{(z)}(\eta)$ is

$$g_{(z)}(\eta) = (\partial v_z/\partial \xi)_{\xi=\xi_o}. \tag{59}$$

Since both ξ_o and ξ_1 are independent of η, Equation (58) becomes the ordinary differential equation

$$\frac{d^2}{d\eta^2} \int_{\xi_o}^{\xi_1} v_z \, d\xi - g_{(z)}(\eta) - \int_{\xi_o}^{\xi_1} f(\xi,\eta) \, d\xi = 0, \tag{60}$$

which is a fourth condition in addition to those of Equations (35), (36), and (57). The velocity, v_z, is expressed as a third degree polynomial,

$$v_z = \alpha_1(\xi-\xi_o)/\delta + \alpha_2(\xi-\xi_o)^2/\delta^2 + \alpha_3(\xi-\xi_o)^3/\delta^3, \tag{61}$$

where the factors α_1, α_2, and α_3 are functions of η determined from the above conditions. They are found to be

$$\alpha_1 = \delta \, g_{(z)}(\eta) \tag{62}$$

$$\alpha_2 = \delta^2 \, f(\xi_0,\eta)/2 \tag{63}$$

$$\alpha_3 = - [\delta \, g_{(z)}(\eta) + \delta^2 \, f(\xi_0,\eta)]/3. \tag{64}$$

The velocity distribution is thus

$$v_z = f(\xi_0,\eta)[(\xi-\xi_0)^2/2 - (\xi-\xi_0)^3/(3\delta)]$$
$$+ g_{(z)}(\eta)[(\xi-\xi_0) - (\xi-\xi_0)^3/(3\delta^2)]. \tag{65}$$

The function $g_{(z)}(\eta)$ is unknown but can be determined by introducing Equation (65) into Equation (60) and seeking a solution that is periodic with π because of the symmetry in the flow model. Upon defining

$$1/n^2 = 5 \, \delta^2/12 \tag{66}$$

$$B_1 = (c^2/2\mu)(dp/dz)(\delta^3/3 + \delta) \tag{67}$$

$$B_2 = (c^2/4\mu)(dp/dz)(\sinh 2\xi_1 - \sinh 2\xi_0) \tag{68}$$

the differential equation for $g_{(z)}(\eta)$ becomes

$$(1/n^2) \, g_{(z)}{}'' - g_{(z)} + B_1\cos 2\eta - B_2 = 0, \tag{69}$$

where the prime indicates differentiation with respect to η. The desired particular solution is

$$g_{(z)}(\eta) = - B_2 + B_1 n^2(\cos 2\eta)/(n^2 + 4). \tag{70}$$

The approximate solution for the velocity distribution is as follows:

$$v_z = - (c^2/\mu)(dp/dz) \, X_A \tag{71}$$

$$X_A = (\sinh^2\xi_0 + \sin^2\eta)[- (\xi-\xi_0)^2/2 + (\xi-\xi_0)^3/(3\delta)]$$

$$+ [(\xi-\xi_0) - (\xi-\xi_0)^3/(3\delta^2)][(\sinh 2\xi_1 - \sinh 2\xi_0)/4 \qquad (72)$$

$$- (\delta^3 + 3\delta)(\cos 2\eta)/(10 \delta^2 + 6)].$$

DETERMINATION OF KOZENY FACTOR

The Kozeny factor, $\underline{k}_{(z)}$, for parallel flow through the assemblage of elliptic cylinders is determined from the velocity distribution by using the following two independent equations for the flow rate, $\underline{Q}$:

$$Q = \bar{v}\pi(a_1 b_1 - a_0 b_0) = (U/\varepsilon)\pi(a_1 b_1 - a_0 b_0), \qquad (73)$$

$$Q = \int_0^{2\pi} \int_{\xi_0}^{\xi_1} v_z(\xi,\eta) \frac{\partial(x,y)}{\partial(\xi,\eta)} d\xi\, d\eta. \qquad (74)$$

The first of these states that the flow rate equals the product of the mean velocity, $\bar{v}$, and the cross-sectional area of flow. The second integrates the local velocity over the ranges of ξ and η, using the Jacobian

$$\frac{\partial(x,y)}{\partial(\xi,\eta)} = \left|\frac{\partial x}{\partial\xi}\frac{\partial y}{\partial\eta} - \frac{\partial x}{\partial\eta}\frac{\partial y}{\partial\xi}\right| = c^2(\sinh^2\xi + \sin^2\eta) \qquad (75)$$

because of integration over curvilinear coordinates. By equating the two expressions for the flow rate, an equation for the pressure drop, $d\underline{p}/d\underline{z}$, can be obtained, which is inserted in the Kozeny-Carman equation

$$k = - (\varepsilon m^2/\mu U)\, dp/dz \qquad (76)$$

to determine the Kozeny factor. The hydraulic radius, $\underline{m}$, is defined as

$$m = \pi(a_1 b_1 - a_0 b_0)/C, \qquad (77)$$

where $\underline{C}$ is the circumference of the solid ellipse, which is approximated by

$$C = \pi a_0 H, \tag{78}$$

$$H \approx (3 + 10 \beta_0 + 3 \beta_0^2)/[4(1 + \beta_0)]. \tag{79}$$

The flow rate in Equation (74) is determined by using the velocity distribution, $\underline{v}_z$, and integrating, resulting in the following:

$$Q = - \pi c^4 (dp/dz) P^*/\mu, \tag{80}$$

where $\underline{P^*}$ is dependent on the solution used. For the exact solution, $\underline{P^*}$ equals

$$P_E^* = \sum_{\substack{k=1 \\ odd}}^{\infty} \{4[\alpha_0(-1)^{(k-1)/2} + (\gamma/2)(1+\beta_0^2)/(1-\beta_0^2)]^2 \\ + (\gamma^2+4)/2\}/[\gamma^2(\gamma^2+4)^2], \tag{81}$$

while for the approximate solution, $\underline{P^*}$ is

$$P_A^* = \beta_0^2[\delta/3 - 1/4\delta + (1-\varepsilon)(1/D - 1/\beta_0)/8\delta^2]/[(1-\beta_0^2)^2(1-\varepsilon)^2] \\ + \beta_0(1+\beta_0^2)[- \delta^2/12 + 1/4 - (1-\varepsilon)(1/D - 1/\beta_0)/8\delta]/[(1-\beta_0^2)^2(1-\varepsilon)] \\ + \delta^3/(12 + 20\delta^2), \tag{82}$$

where

$$D = (1-\varepsilon)[(1 + 1/\alpha_0^2)^{1/2} - 1/\alpha_0]. \tag{83}$$

Equation (231) defines α_0. Using the above equations and some of the relationships in Appendix III, the equation for the Kozeny factor becomes

$$k_{(z)} = \beta_0^3 \varepsilon^3/[P^*(1-\beta_0^2)^2 H^2(1-\varepsilon)^3]. \tag{84}$$

The values for the Kozeny factor for parallel flow obtained in this analysis for both solution methods will be presented in a later section.

FLOW PERPENDICULAR TO ELLIPTIC CYLINDER

The steady creeping flow past an elliptic cylinder of a cell in an array and perpendicular to the cylinder's central axis is treated as a two-dimensional symmetric flow problem, with the velocity, $\vec{v}$, as follows:

$$\vec{v} = v_\xi \hat{i}_\xi + v_\eta \hat{i}_\eta. \tag{85}$$

This flow is described by the equation of continuity, which reduces from Equation (205) to

$$\nabla \cdot \vec{v} = h^2[\partial(v_\xi/h)/\partial\xi + \partial(v_\eta/h)/\partial\eta] = 0 \tag{86}$$

and by the ξ and η components of the equation of motion, given in full by Equations (209) and (210). Upon introducing the stream function, ψ, defined by

$$v_\xi/h = \partial\psi/\partial\eta \qquad v_\eta/h = -\partial\psi/\partial\xi \tag{87}$$

the components of the equation of motion become

$$\frac{\partial p}{\partial \xi} = \mu \left\{ h\left[\frac{\partial^2}{\partial\xi^2}\left(h\frac{\partial\psi}{\partial\eta}\right) + \frac{\partial^2}{\partial\eta^2}\left(h\frac{\partial\psi}{\partial\eta}\right)\right] - \frac{\nabla^2 h}{h}\frac{\partial\psi}{\partial\eta} + \frac{\partial h^2}{\partial\eta}\frac{\partial^2\psi}{\partial\xi^2} - \frac{\partial h^2}{\partial\xi}\frac{\partial^2\psi}{\partial\xi\partial\eta} \right\} \tag{88}$$

$$\frac{\partial p}{\partial \eta} = \mu \left\{ -h\left[\frac{\partial^2}{\partial\xi^2}\left(h\frac{\partial\psi}{\partial\xi}\right) + \frac{\partial^2}{\partial\eta^2}\left(h\frac{\partial\psi}{\partial\xi}\right)\right] + \frac{\nabla^2 h}{h}\frac{\partial\psi}{\partial\xi} - \frac{\partial h^2}{\partial\xi}\frac{\partial^2\psi}{\partial\eta^2} + \frac{\partial h^2}{\partial\eta}\frac{\partial^2\psi}{\partial\xi\partial\eta} \right\} \tag{89}$$

where the Laplacian operator is as defined in Equation (33). By cross-differentiation of the two component equations, the pressure is eliminated. The result can be expressed simply by the linear, fourth-order, biharmonic equation

$$\nabla^2(h^2\nabla^2\psi) = 0, \tag{90}$$

where $\qquad \nabla^2 = \partial^2/\partial\xi^2 + \partial^2/\partial\eta^2. \tag{91}$

For statement of the boundary conditions, the perpendicular flow analysis is divided into two problems, one for flow along the minor cross-sectional axis and one along the major cross-sectional axis. The solutions for these two problems follow a method outlined by Meyer (45), and are considered separately.

ALONG MINOR CROSS-SECTIONAL AXIS

Assume the solid cylinder is moving with velocity $\underline{U}$ in the direction of its minor axis ($\underline{y}$-direction) while the surrounding fluid is at rest. The no-slip condition on the solid surface provides that

$$v_y = U, \quad v_x = 0 \quad \text{on} \quad \xi = \xi_0.$$

Transforming these to elliptic cylindrical coordinates by using Equation (216), these conditions become

$$v_\xi = hUc \cosh \xi \sin \eta, \quad v_\eta = hUc \sinh \xi \cos \eta \quad \text{on} \quad \xi = \xi_0$$

or, in terms of the stream function,

$$\partial\psi/\partial\eta = Uc \cosh \xi \sin \eta \quad \text{on} \quad \xi = \xi_0, \tag{92}$$

$$\partial\psi/\partial\xi = - Uc \sinh \xi \cos \eta \quad \text{on} \quad \xi = \xi_0. \tag{93}$$

On the virtual surface, it is assumed that the normal velocity, v_ξ, vanishes,

$$v_\xi = h(\partial\psi/\partial\eta) = 0 \quad \text{on} \quad \xi = \xi_1$$

or, since $\underline{h}$ is nonzero,

$$\partial\psi/\partial\eta = 0 \quad \text{on} \quad \xi = \xi_1. \tag{94}$$

The fourth boundary condition can either be the zero vorticity condition of Kuwabara or the zero shear stress condition of Happel. Only the z-direction component of the vorticity, ω, is nonzero; its magnitude is

$$\omega = - h^2 \nabla^2 \psi. \qquad (95)$$

If the vorticity is zero on the virtual surface, the equation

$$\nabla^2 \psi = 0 \qquad \text{on} \quad \xi = \xi_1 \qquad (96)$$

is the fourth boundary condition. The zero shear stress condition requires that the equation

$$\partial^2 \psi/\partial \xi^2 - 2(\partial \psi/\partial \xi)\sinh \xi \cosh \xi/(\sinh^2 \xi + \sin^2 \eta) = 0 \quad \text{on} \quad \xi = \xi_1 \quad (97)$$

be satisfied. Because of the mathematical difficulty that would be encountered by using the zero shear stress condition relative to the zero vorticity condition, Equation (96) is chosen as the fourth boundary condition.

Solution for the Stream Function

The solution to this boundary value problem can be expressed as

$$\psi = \psi^{(1)} + \psi^{(2)}, \qquad (98)$$

where $\psi^{(1)}$ and $\psi^{(2)}$ are defined by

$$\nabla^2 \psi^{(1)} = 0, \qquad (99)$$
$$h^2 \nabla^2 \psi^{(2)} = - \omega \qquad (100)$$

in which ω also is a solution of the Laplace equation

$$\nabla^2 \omega = 0. \qquad (101)$$

Equation (99) is solved by separation of variables yielding the solution

$$\psi^{(1)} = \sum_{j=0}^{\infty} (a_j \sinh j\xi + b_j \cosh j\xi) \cos j\eta. \qquad (102)$$

Because of the similarity of Equations (101) and (99), the solution for ω is seen to be

$$\omega = \sum_{j=1}^{\infty} (A_j \sinh j\xi + B_j \cosh j\xi) \cos j\eta \qquad (103)$$

The vorticity is a maximum at $\eta = 0$ and is zero at $\eta = \pi/2$, conditions which are satisfied by the cosine function in Equation (103) when $\underline{j} = 1, 3, 5, \ldots$. Considering the boundary conditions, which do not require series expansion, put $\underline{j} = 1$ and omit the series notation. Using the condition of vanishing vorticity on the imaginary surface, the vorticity equation becomes

$$\omega = B_{(y)}(\sinh \xi - \tanh \xi_1 \cosh \xi) \cos \eta, \qquad (104)$$

where $\underline{B}_{(\underline{y})}$ is a parameter that cannot yet be determined. Rewriting the boundary conditions in terms of $\psi^{(1)}$ and $\psi^{(2)}$ produces the following:

$$\partial\psi^{(1)}/\partial\eta + \partial\psi^{(2)}/\partial\eta = Uc \cosh \xi \sin \eta \qquad \text{on} \quad \xi = \xi_0 \qquad (105)$$

$$\partial\psi^{(1)}/\partial\xi + \partial\psi^{(2)}/\partial\xi = - Uc \sinh \xi \cos \eta \qquad \text{on} \quad \xi = \xi_0 \qquad (106)$$

$$\partial\psi^{(1)}/\partial\eta = - \partial\psi^{(2)}/\partial\eta \qquad \text{on} \quad \xi = \xi_1 \qquad (107)$$

$$\nabla^2\psi^{(2)} = 0 \qquad \text{on} \quad \xi = \xi_1. \qquad (108)$$

Assuming that

$$[\partial\psi^{(2)}/\partial\eta]_{\xi=\xi_0} = 0 \qquad (109)$$

and

$$[\partial\psi^{(2)}/\partial\xi]_{\xi=\xi_0} = 0 \qquad (110)$$

and putting $j = 1$, $a_j = 0$, and $b_j = - Uc$ in Equation (102), the conditions in Equations (105) and (106) are satisfied and

$$\psi^{(1)} = - Uc \cosh \xi \cos \eta \qquad (111)$$

is the desired particular solution. Equation (107) now becomes

$$[\partial\psi^{(2)}/\partial\eta]_{\xi=\xi_1} = - Uc \cosh \xi_1 \sin \eta \qquad (112)$$

which on integrating yields

$$[\psi^{(2)}]_{\xi=\xi_1} = Uc \cosh \xi_1 \cos \eta, \qquad (113)$$

where the integration constant is zero so that ψ is zero on $\xi = \xi_1$.

The Poisson equation, Equation (100), remains to be solved subject to the boundary conditions. Because no appropriate Green's function was found, an approximate solution method is used. Rewriting Equation (100),

$$\partial^2\psi^{(2)}/\partial\xi^2 + \partial^2\psi^{(2)}/\partial\eta^2 = - (\omega/h^2) \qquad (114)$$

and integrating between ξ_0 and ξ_1, the following equation results:

$$g_{(y)}(\eta) + \frac{d^2}{d\eta^2} \int_{\xi_0}^{\xi_1} \psi^{(2)} \, d\xi = - \int_{\xi_0}^{\xi_1} (\omega/h^2) \, d\xi. \qquad (115)$$

The function $g_{(y)}(\eta)$ is defined as

$$g_{(y)}(\eta) = [\partial\psi^{(2)}/\partial\xi]_{\xi=\xi_1}. \qquad (116)$$

Before Equation (115) can be solved for $g_{(y)}(\eta)$, a general form of $\psi^{(2)}$ must be assumed. A polynomial in ξ is indicated with the number of terms carried dependent on the number of boundary conditions. Thus far, the available conditions are Equations (113), (116), and (108). Another equation which an exact solution satisfies is

$$[\partial^2\psi^{(2)}/\partial\xi^2]_{\xi=\xi_0} + [\partial^2\psi^{(2)}/\partial\eta^2]_{\xi=\xi_0} = - (\omega/h^2)_{\xi=\xi_0}. \qquad (117)$$

Now that four conditions are available, a fourth degree polynomial for $\psi^{(2)}$ can be written. Equation (110) suggests the form

$$\psi^{(2)} = \alpha_2(\xi-\xi_0)^2 + \alpha_3(\xi-\xi_0)^3 + \alpha_4(\xi-\xi_0)^4 + \alpha_5(\xi-\xi_0)^5, \qquad (118)$$

where the coefficients α_2, α_3, α_4, and α_5 are functions of η. Using the above conditions, four equations result which are solved simultaneously to yield the following:

$$\alpha_2 = - B_{(y)}c^2\cos\eta \ (\sinh^2\xi_0 + \sin^2\eta)(\sinh\xi_0 - \tanh\xi_1\cosh\xi_0)/2 \qquad (119)$$

$$\alpha_3 = Uc\cosh\xi_1\cos\eta \ (10/\delta^2 + 1/2)/\delta - 4g_{(y)}(\eta)/\delta^2 - 3\alpha_2/\delta \qquad (120)$$

$$\alpha_4 = - Uc\cosh\xi_1\cos\eta(1 + 15/\delta^2)/\delta^2 + 7g_{(y)}(\eta)/\delta^3 + 3\alpha_2/\delta^2 \qquad (121)$$

$$\alpha_5 = Uc\cosh\xi_1\cos\eta \ (1/2 + 6/\delta^2)/\delta^3 - 3g_{(y)}(\eta)/\delta^4 - \alpha_2/\delta^3 \qquad (122)$$

where δ is as defined by Equation (42). Now that the expression for $\psi^{(2)}$ is complete, the integrals in Equation (115) are evaluated. The results are as follows:

$$\int_{\xi_0}^{\xi_1} \psi^{(2)}d\xi = Uc\cosh\xi_1\cos\eta \ (\delta/2 + \delta^3/120) - \delta^2 g_{(y)}(\eta)/10$$
$$+ \alpha_2\delta^3/60, \qquad (123)$$

$$\int_{\xi_0}^{\xi_1} (\omega/h^2) \ d\xi = B_{(y)}c^2[t_{(y)}\cos\eta - \lambda\cos^3\eta] \qquad (124)$$

with

$$t_{(y)} = [(\cosh^3\xi_1 - \cosh^3\xi_0) - \tanh\xi_1 (\sinh^3\xi_1 - \sinh^3\xi_0)]/3$$
$$- \tanh\xi_1 (\sinh\xi_1 - \sinh\xi_0), \qquad (125)$$

$$\lambda = (\cosh\xi_1 - \cosh\xi_0) - \tanh\xi_1 (\sinh\xi_1 - \sinh\xi_0). \qquad (126)$$

The introduction of Equations (123) and (124) into Equation (115) provides an equation for $\underline{g}_{(y)}(\eta)$, which simplifies to the following:

$$g_{(y)}''(\eta) - 10\, g_{(y)}(\eta)/\delta^2 = -\Phi_{(y)}(\cos \eta), \tag{127}$$

where

$$\Phi_{(y)}(\cos \eta) = D_{(y)}\cos \eta - E_{(y)}\cos^3\eta \tag{128}$$

$$D_{(y)} = Uc \cosh \xi_1 (5/\delta + \delta/12) - B_{(y)}c^2[10t_{(y)}/\delta^2 + \delta\sigma(\cosh^2\xi_0 + 6)/12] \tag{129}$$

$$E_{(y)} = - B_{(y)}c^2(10\lambda/\delta^2 + 3\delta\sigma/4) \tag{130}$$

$$\sigma = (\sinh \xi_0 - \tanh \xi_1 \cosh \xi_0). \tag{131}$$

Equation (127) is solved for $\underline{g}_{(y)}(\eta)$, yielding

$$g_{(y)}(\eta) = \gamma_1 \cos \eta - \gamma_2 \cos^3\eta, \tag{132}$$

where

$$\gamma_1 = [D_{(y)} - 6\delta^2 E_{(y)}/(9\delta^2 + 10)]\delta^2/(\delta^2 + 10), \tag{133}$$

$$\gamma_2 = \delta^2 E_{(y)}/(9\delta^2 + 10). \tag{134}$$

The only remaining operation necessary for the solution for the stream function to be complete is the determination of the factor $\underline{B}_{(y)}$. An additional condition for this purpose that has not yet been used is obtained from the biharmonic equation, Equation (90), which is valid everywhere in the porous space including the solid surface:

$$[\nabla^2(h^2\nabla^2\psi)]_{\xi=\xi_0} = 0. \tag{135}$$

Expanding this yields the expression

$$6\alpha_4 + \alpha_2{}'' + 4\alpha_2(\sinh^2\xi_0 + \sin^2\eta)^{-2}(\sinh^2\xi_0\cosh^2\xi_0 + \sin^2\eta\,\cos^2\eta)$$

$$- (\sinh^2\xi_0 + \sin^2\eta)^{-1}[\alpha_2(\sinh^2\xi_0 + \cosh^2\xi_0 + \cos^2\eta - \sin^2\eta) \qquad (136)$$

$$+ 6\alpha_3\sinh\xi_0\,\cosh\xi_0 + 2\alpha_2{}'\,\sin\eta\,\cos\eta] = 0.$$

Upon substitution for α_2, α_3, α_4, $\alpha_2{}'$, and $\alpha_2{}''$, an equation results which is integrated over η from 0 to 2π to eliminate the dependence on η. This procedure yields an expression in which $\underline{B}_{(y)}$ is the only unknown quantity. Solving for $\underline{B}_{(y)}$,

$$B_{(y)} = G_{(y)}U/c, \qquad (137)$$

where
$$G_{(y)} = [R/T_{(y)}]\cosh\xi_1, \qquad (138)$$

with

$$R = [\cosh 2\xi_0(5/2 - 60/\delta^2 + 900/\delta^4)$$
$$+ \sinh 2\xi_0(\delta - 30/\delta + 600/\delta^3)]/(\delta^2 + 10) \qquad (139)$$

$$T_{(y)} = \sigma T_1 - 60t_{(y)}\Omega/[\delta^3(\delta^2 + 10)]$$
$$+ 30\lambda[(\Omega - 7/2)/\delta^2 + 12\Omega/(\delta^2 + 10)]/[\delta(9\delta^2 + 10)] \qquad (140)$$

$$T_1 = \Lambda - (1/4)\Omega(\cosh 2\xi_0 + 13)/(\delta^2 + 10)$$
$$+ 27\delta^2\Omega/[(\delta^2 + 10)(9\delta^2 + 10)] + (9/4)(\Omega - 7/2)/(9\delta^2 + 10) \qquad (141)$$

$$\Omega = (7\cosh 2\xi_0 + 4\delta\sinh 2\xi_0) \qquad (142)$$

$$\Lambda = - (1/8 + 9/4\delta^2)\cosh 4\xi_0 - (9/4\delta)\sinh 4\xi_0$$
$$+ (3/2)\cosh 2\xi_0 + 3/4 - 9/2\delta^2. \qquad (143)$$

The solution for ψ for perpendicular flow along the minor axis is now complete.

Stream Function for Stationary Cylinder

The preceding development for the stream function is for the case of a cylinder moving within the fluid along with a moving reference system. For

consideration of the streamlines around the cylinder and for a simpler drag force analysis, the stream function for a fixed reference system with flow past a stationary cylinder is desired; call this ψ_*. The fluid velocity now is given by $\vec{u}$, which is related to $\vec{v}$, the fluid velocity for the moving cylinder case, by

$$\vec{u} = \vec{v} - U\,\hat{j}. \tag{144}$$

The ξ and η components of $\vec{u}$ are found to be

$$u_\xi = v_\xi - Uhc \cosh \xi \sin \eta, \tag{145}$$

$$u_\eta = v_\eta - Uhc \sinh \xi \cos \eta. \tag{146}$$

The stationary cylinder stream function is defined by

$$u_\xi/h = \partial\psi_*/\partial\eta, \qquad u_\eta/h = -\,\partial\psi_*/\partial\xi. \tag{147}$$

An expression for ψ_* is found by integrating either of these two defining equations, substituting for v_ξ and v_η using Equation (87), with the result

$$\psi_* = \int (\partial\psi/\partial\eta - Uc \cosh \xi \sin \eta)\, d\eta. \tag{148}$$

But $\psi = \psi^{(1)} + \psi^{(2)}$, and

$$\partial\psi^{(1)}/\partial\eta = Uc \cosh \xi \sin \eta \tag{149}$$

so that

$$\psi_* = \int \partial\psi^{(2)}/\partial\eta\; d\eta = \psi^{(2)}. \tag{150}$$

The stream function for flow past a stationary cylinder is thus the polynomial $\psi^{(2)}$.

Derivation of Drag Force

The drag force due to flow past a stationary cylinder is determined by integrating the stress over the solid surface ($\underline{15}$), as follows:

$$\vec{F} = \int_s \underset{\sim}{\Pi} \cdot d\vec{s} = \int_s \underset{\sim}{\Pi} \cdot \hat{i}_\xi \, ds. \tag{151}$$

The body surface is represented by $\underline{s}$, while $\underset{\sim}{\Pi}$ is the stress tensor defined as

$$\underset{\sim}{\Pi} = -p \, \underset{\sim}{I} + 2\mu \underset{\sim}{\Delta}, \tag{152}$$

where $\underset{\sim}{I}$ is the idemfactor and $\underset{\sim}{\Delta}$ is the rate of deformation tensor. The drag force is thus

$$\vec{F} = -\int_s p \, \hat{i}_\xi \, ds + 2\mu \int_s \underset{\sim}{\Delta} \cdot \hat{i}_\xi \, ds. \tag{153}$$

Only the y-component of $\vec{F}$ is nonzero; this provides

$$F_{(y)} = -\int_s p(\hat{i}_\xi \cdot \hat{j}) \, ds + 2\mu \int_s (\underset{\sim}{\Delta} \cdot \hat{i}_\xi) \cdot \hat{j} \, ds. \tag{154}$$

The rate of deformation tensor for an incompressible fluid is defined as ($\underline{15}$)

$$\underset{\sim}{\Delta} = [(\nabla\vec{v}) + (\nabla\vec{v})^t]/2, \tag{155}$$

where $\underline{t}$ signifies the transpose. For this problem, $\underset{\sim}{\Delta}$ is

$$\underset{\sim}{\Delta} = \hat{i}_\xi \hat{i}_\xi \, d_{\xi\xi} + \hat{i}_\xi \hat{i}_\eta \, d_{\xi\eta} + \hat{i}_\eta \hat{i}_\xi \, d_{\xi\eta} + \hat{i}_\eta \hat{i}_\eta \, d_{\xi\xi} \tag{156}$$

with

$$d_{\xi\xi} = h[\partial v_\xi/\partial\xi + \partial v_\eta/\partial\eta + hv_\eta \, \partial(1/h)/\partial\eta + hv_\xi \, \partial(1/h)/\partial\xi]/2, \tag{157}$$

$$d_{\xi\eta} = h[\partial v_\eta/\partial\xi + \partial v_\xi/\partial\eta - hv_\xi \, \partial(1/h)/\partial\eta - hv_\eta \, \partial(1/h)/\partial\xi]/2. \tag{158}$$

By the equation of continuity it can be shown that

$$d_{\xi\xi} = 0 \tag{159}$$

so that

$$\underset{\sim}{\Delta} = (\hat{i}_\xi \hat{i}_\eta + \hat{i}_\eta \hat{i}_\xi) \, d_{\xi\eta}. \tag{160}$$

The dot products in Equation (154) are

$$\underset{\sim}{\Delta} \cdot \hat{i}_\xi = d_{\xi\eta} \, \hat{i}_\eta, \tag{161}$$

$$(\underset{\sim}{\Delta} \cdot \hat{i}_\xi) \cdot \hat{j} = d_{\xi\eta}(\hat{i}_\eta \cdot \hat{j}). \tag{162}$$

The dot products of unit vectors are equal to

$$\hat{i}_\xi \cdot \hat{j} = h \, \partial y / \partial \xi = hc \cosh \xi \sin \eta, \tag{163}$$

$$\hat{i}_\eta \cdot \hat{j} = h \, \partial y / \partial \eta = hc \sinh \xi \cos \eta. \tag{164}$$

The drag force becomes

$$F_{(y)} = -c \cosh \xi \int_0^{2\pi} p \sin \eta \, d\eta + 2\mu c \sinh \xi \int_0^{2\pi} d_{\xi\eta} \cos \eta \, d\eta \tag{165}$$

since

$$ds = d\eta / h. \tag{166}$$

The expression for $d_{\xi\eta}$ is transformed to one involving the stream function, $\psi^{(2)}$, and is evaluated at $\xi = \xi_0$, the solid surface, with the result

$$(d_{\xi\eta})_{\xi=\xi_0} = B_{(y)}\sigma(\cos \eta)/2. \tag{167}$$

An expression for the pressure, $\underline{p}$, is developed from the equation of creeping motion, Equation (201), which leads to the equation

$$\partial p / \partial \xi = \mu\{h^3 \, \partial[\nabla^2\psi^{(2)}]/\partial\eta + 2h^2(\partial h/\partial\eta) \, \nabla^2\psi^{(2)}\}/h. \tag{168}$$

The Laplacian of $\psi^{(2)}$ is

$$\nabla^2\psi^{(2)} = -\omega/h^2 = -B_{(y)}(\cos \eta)(\sinh \xi - \tanh \xi_1 \cosh \xi)/h^2. \tag{169}$$

Introducing this into the pressure derivative yields

$$\partial p/\partial \xi = \mu B_{(y)} \sin \eta \ (\sinh \xi - \tanh \xi_1 \cosh \xi) \qquad (170)$$

which, after integration, produces

$$p = p_o + \mu B_{(y)} \sin \eta \ (\cosh \xi - \tanh \xi_1 \sinh \xi), \qquad (171)$$

where $\underline{p}_o$ is a reference point pressure.

Evaluation of the integrals in Equation (165) provides the following equation for the drag force:

$$F_{(y)} = - \pi \mu B_{(y)} \ c \cosh \xi_o (\cosh \xi_o - \tanh \xi_1 \sinh \xi_o)$$
$$+ \pi \mu B_{(y)} \ c \sinh \xi_o (\sinh \xi_o - \tanh \xi_1 \cosh \xi_o). \qquad (172)$$

Recalling

$$B_{(y)} = G_{(y)} U/c, \qquad (173)$$

$\underline{F}_{(y)}$ simplifies to

$$F_{(y)} = - \pi \mu U G_{(y)}. \qquad (174)$$

Determination of Kozeny Factor

The drag force resulting from flow in the cell is related to the pressure drop by

$$F/(\pi a_1 b_1) = dp/dx, \qquad (175)$$

where $\underline{x}$ is the direction of motion. Stated simply, this says that the pressure drop across the cell equals the drag force, the only cause of flow resistance, divided by the cell volume. The Kozeny-Carman equation, Equation (76), relates the pressure drop to the Kozeny factor, $\underline{k}$. Combining these two equations and solving for $\underline{k}$ gives

$$k = - F\acute{\epsilon}m^2/(\pi a_1 b_1 \mu U). \tag{176}$$

Recall Equations (77), (78), (79), and (174), and note that

$$(1-\epsilon) = a_o b_o/(a_1 b_1). \tag{177}$$

The Kozeny factor is thus

$$k_{(y)} = \epsilon^3 \beta_o G_{(y)}/[H^2(1-\epsilon)]. \tag{178}$$

ALONG MAJOR CROSS-SECTIONAL AXIS

The analysis for flow parallel to the major cross-sectional axis of the elliptic cylinder and perpendicular to the long axis is similar to the above analysis for flow along the minor axis. Equation (90) describes this flow situation too. The boundary conditions are fundamentally identical, although their form is different. Again, the cylinder is assumed to be moving in a stationary fluid, in this case in the x-direction with velocity U. The no-slip condition on the solid surface requires that

$$v_x = U, \quad v_y = 0 \quad \text{on} \quad \xi = \xi_o$$

which become, in elliptic coordinates,

$$v_\xi = hUc \sinh \xi \cos \eta, \quad v_\eta = - hUc \cosh \xi \sin \eta \quad \text{on} \quad \xi = \xi_o.$$

In terms of the stream function,

$$\partial\psi/\partial\eta = Uc \sinh \xi \cos \eta \quad \text{on} \quad \xi = \xi_o, \tag{179}$$

$$\partial\psi/\partial\xi = Uc \cosh \xi \sin \eta \quad \text{on} \quad \xi = \xi_o. \tag{180}$$

On the imaginary surface, the conditions are zero normal velocity and zero vorticity, as before, stated by Equations (94) and (96). The solution for ψ

is developed as before; the details are summarized in Appendix IV. For flow

along the major cross-sectional axis, the drag force is

$$F_{(x)} = - \pi \mu U G_{(x)} \tanh \xi_1 \tag{181}$$

and the Kozeny factor is

$$k_{(x)} = \varepsilon^3 \beta_0 G_{(x)} \tanh \xi_1 / [H^2(1-\varepsilon)], \tag{182}$$

where $G_{(x)}$ is defined in Equation (273).

PATTERNS OF FLOW

The three directional analyses presented above for flow within the model

cell provide solutions to the respective boundary·value problems which de-

scribe the flow patterns around the solid cylinder. An investigation of the

resultant flow patterns is useful because it demonstrates the significance of

the boundary conditions and because it produces a means for a subjective check

on the accuracy of the solutions.

The analysis of flow parallel to the central axis of the solid elliptic

cylinder in the cell produces a distribution of velocities in the annular

region between the two cylinders. The velocity is zero at the solid surface

and maximum at the virtual surface. Figure 8 illustrates the velocity

distributions along the x-axis ($\eta = 0$) and along the y-axis ($\eta = \pi/2$) for a

cylinder of $\beta_0 = 0.50$ and a porosity of 0.75. The peak velocity varies as a

function of η between the two values presented in the graph. Both the exact

and approximate solutions are plotted. Near the solid surface the two are

almost identical, with more of a difference emerging as the fluid boundary

is approached.
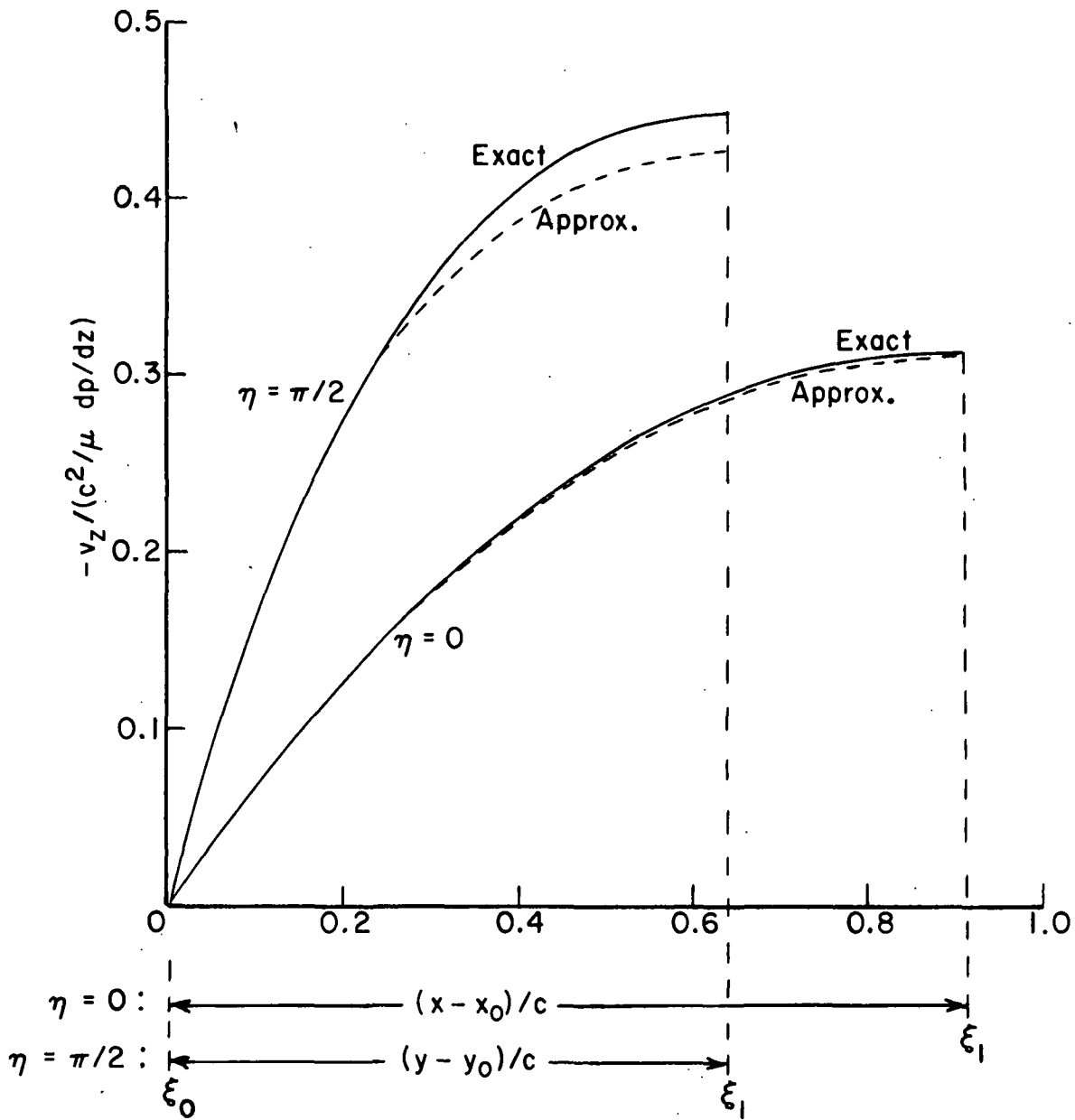
Figure 8. Velocity Distribution in Annulus of Cell Model for
Flow Parallel to Elliptic Cylinder

For flow perpendicular to the elliptic cylinder of the cell, the analysis does not yield velocity distributions but rather stream function distributions. The stream function is related to the two velocity components as previously explained. Curves of constant stream function are streamlines and indicate the direction of flow at a point. For a cylinder of axis ratio 0.20 at porosity 0.75, the pattern for flow past the cylinder along the minor axis is presented in Fig. 9, while Fig. 10 shows the pattern for flow along the major axis. The streamlines are symmetric with respect to both the x and y axes.

RESULTS OF THEORETICAL ANALYSES

The theoretical analyses for flow in the cell result in expressions for directional Kozeny factors, which vary with the porosity and with the axis ratio of the solid cylinder's cross section. Appendix V presents tables of these values for many axis ratios at several porosity points over the range of practical interest. In order to demonstrate the trends, Fig. 11 for parallel flow and Fig. 12 for perpendicular flow show how the Kozeny factor is affected by porosity and axis ratio. An axis ratio of one for a circular cylinder cannot be handled by the analyses, so a value of 0.999 is used instead.

Figure 11 for parallel flow indicates that the porosity has a strong influence on the Kozeny factor, while the effect of the axis ratio is only slight. Only values from the exact solution are used in the graph and in the Appendix. A later section compares the results from the exact and the approximate solutions.
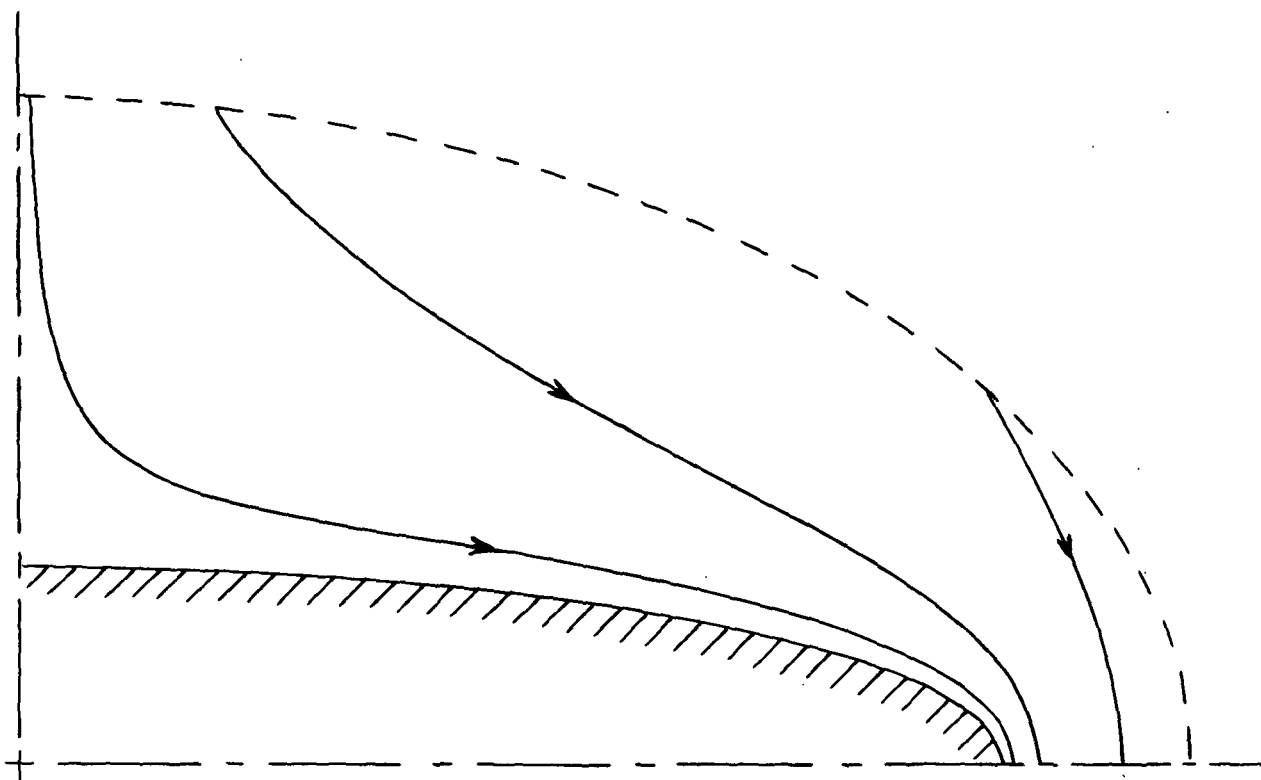
Figure 9. Streamlines in Model Cell for Perpendicular Flow
Along Minor Cross-Sectional Axis.
Porosity = 0.75, Axis Ratio = 0.200
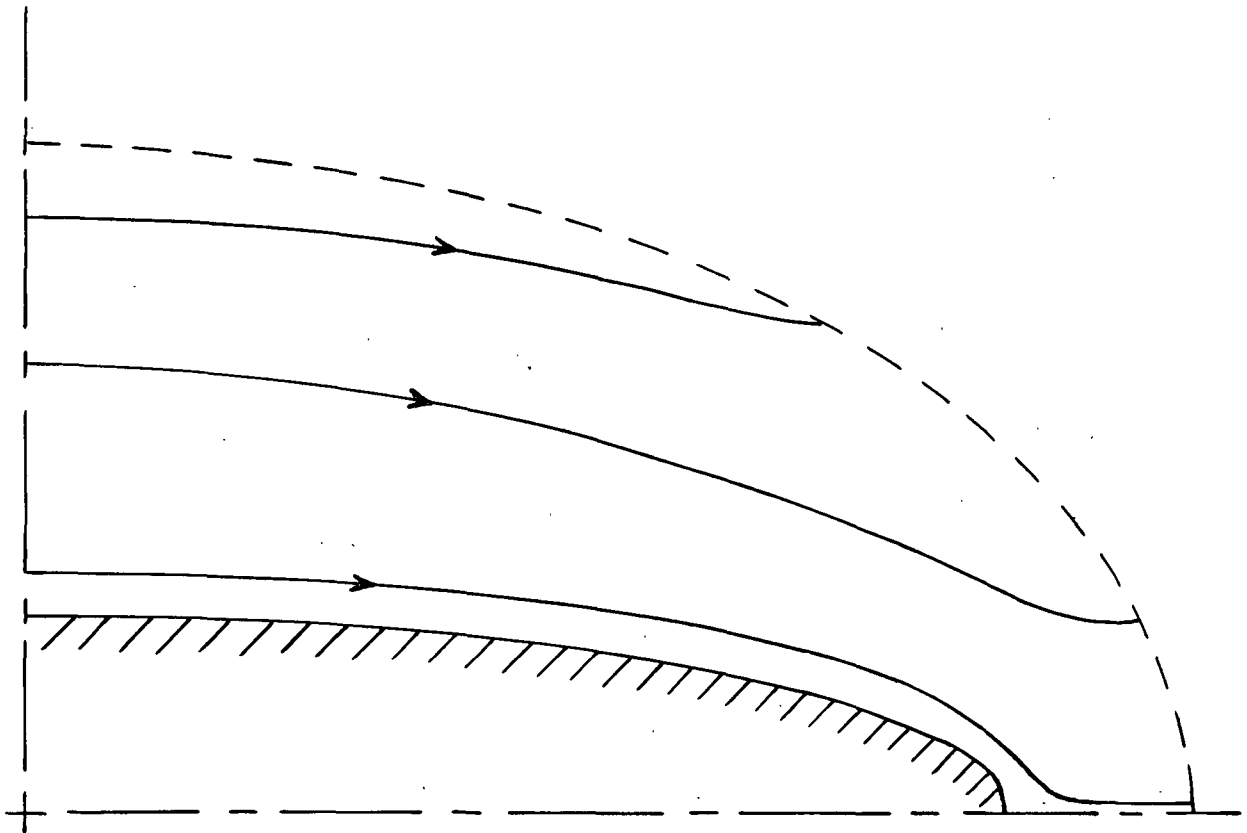
Figure 10. Streamlines in Model Cell for Perpendicular Flow
Along Major Cross-Sectional Axis.
Porosity = 0.75, Axis Ratio = 0.200
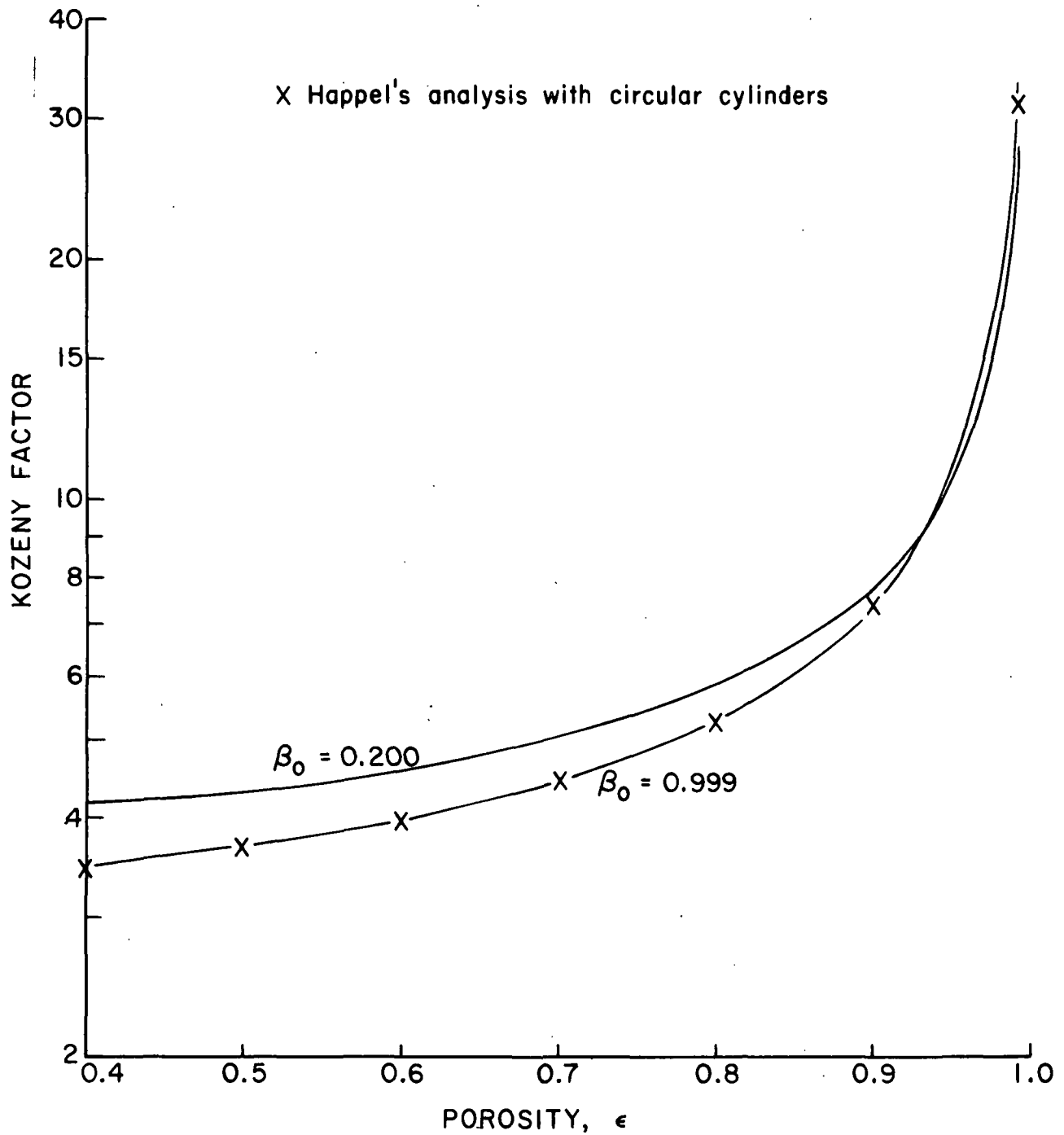
Figure 11. Theoretical Kozeny Factors for Parallel Flow
as a Function of Porosity
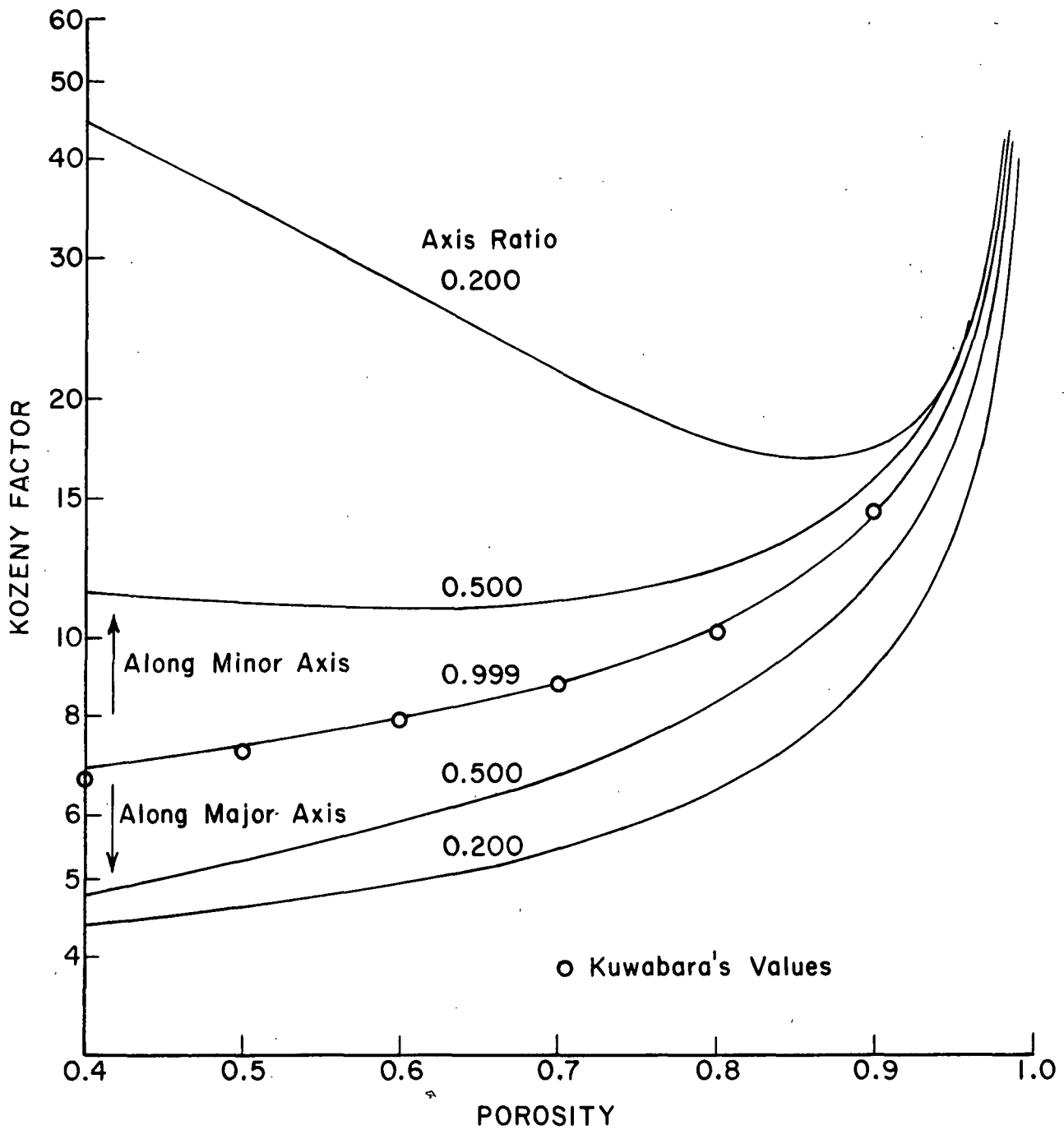
Figure 12. Perpendicular Flow Kozeny Factors from Creeping Flow
Zero Vorticity Cell Model Analysis

The two cases of perpendicular flow are both included in Fig. 12. For a circular cylinder, the two directional perpendicular Kozeny factors are identical; but this is not so for elliptic cylinders where the difference between the two increases as the cylinders become flatter. Again the porosity has a strong impact on the Kozeny factor, but so does the axis ratio.

The computer program which generates the directional Kozeny factors is listed in Appendix VI.

DISCUSSION

The theoretical analyses of the preceding section have been developed in order to study the flow through mats of elliptic fibers. Before real mats of fibers are considered though, some discussion of the validity of the theoretical approach seems appropriate.

VALIDITY OF THEORETICAL ANALYSIS

CELL MODEL APPROACH

The use of a cell containing one fiber segment and its surrounding fluid as a model for treating the flow through a fiber mat may seem to be of questionable value at first glance. Such a cell model approach could be easily rationalized for a regular array of cylinders where all cells within the structure are identical. But for an irregular assemblage like a fiber mat where cells of various shapes and porosities could be identified, the cell model approach presumes that one typical cell can be defined that is descriptive in a statistical sense of all the cells of the assemblage. By analyzing the flow though this typical cell, the properties of the flow through the entire assemblage can be estimated. The interaction of one cell with another is neglected, except as accounted for by the boundary conditions. The effect of two cylinders in close proximity or in contact is overlooked, even though such an arrangement would significantly affect the drag estimate. Assumptions like these are valid at high porosities, since the fibers then would generally be far apart with few contact points. As lower porosities are reached, the validity of applying the cell model to a fiber mat is reduced. Happel (20) suggests for circular cylinders that his analysis is valid ony at porosities

above 0.50. Since fiber mats often are more than 50% porous, such a limitation is not serious from a practical standpoint.

The complex structure of a fiber mat provides a good reason for employing the cell model approach. The boundaries of a porous fiber mat cannot be specified mathematically unless an elaborate, involved procedure is used. Because of this, the solution of a hydrodynamics problem for flow through a mat would be very difficult. The use of a simple model of the porous space helps overcome this problem and enables mathematical analysis of the flow to be accomplished.

The application of the cell model technique to assemblages of elliptic cylinders follows similar studies with spheres and circular cylinders. The success of the cell model approach in these previous studies indicates that the method can be used to obtain reasonable results. A similar analysis with elliptic cylinders should also be expected to yield acceptable results.

The selection of the zero vorticity condition on the virtual surface is arbitrary. This condition was used in Kuwabara's analysis with circular cylinders, which fits experimental observation (21) better than Happel's analysis with the alternate zero shear stress condition. Also, the zero vorticity requirement leads to simpler mathematics. If the shear stress were assumed zero on the virtual boundary, the problem would have been intractable for elliptic cylinders. An argument for one condition or the other using a physical basis is difficult. Happel and Brenner (15) support Happel's choice, reasoning that the zero vorticity cell requires energy exchange with neighboring cells whereas the zero shear stress cell does not interact from an energy standpoint with other cells.

APPROXIMATE SOLUTION PROCEDURE

The solutions to the Poisson equations developed in the two analyses for perpendicular flow are not exact solutions to the boundary value problems, but rather are approximate ones designed to satisfy the boundary conditions. The accuracy of the approximate solutions should be briefly considered.

The parallel flow problem was solved by both an exact method and an approximate method. The velocity distributions from the two solutions are compared in Fig. 8. Near the solid surface both are nearly identical. As the outer, virtual surface is approached, the two diverge slightly with the difference dependent on η. The difference between the two does not seem large for any η. Another comparison between the two can be based on the theoretical Kozeny factors; some values for the two methods are given in Table III. The approximate values are greater than the exact ones but the two become closer at lower porosities. Above 0.90 porosity, the difference is sizeable. The exact values agree well with Happel's results, verifying the exact solution method. The elliptic axis ratio seems to have little effect on the quality of the approximate solution. From these comparisons, the approximate method appears to be sufficiently accurate for the needs of this study.

The approximate method for the perpendicular flow analyses is similar in approach to the parallel flow approximate solution. For perpendicular flow no exact solution was found, so there is no direct way of gauging the reliability of the results. But because of the similarity, the perpendicular results should be reliable since the parallel values are. Perhaps the high porosity values (for $\varepsilon > 0.9$) are somewhat in error, but this is not a serious drawback. The values for all axis ratios should be equally reliable.

TABLE III

COMPARISON OF KOZENY FACTORS FROM EXACT AND
APPROXIMATE SOLUTION METHODS FOR FLOW
PARALLEL TO ELLIPTIC CYLINDERS

Axis Ratio	Porosity	Kozeny Factor		
		Exact	Approximate	Happel ($\beta_0 = 1$)
0.999	0.95	10.79	11.79	10.75
	0.90	7.34	7.79	7.31
	0.80	5.27	5.44	5.23
	0.70	4.42	4.51	4.42
	0.60	3.97	4.01	3.96
	0.50	3.68	3.70	3.67
0.500	0.95	10.76	11.71	
	0.80	5.41	5.57	
	0.60	4.10	4.14	
0.200	0.95	10.49	11.21	
	0.90	7.70	8.00	
	0.80	5.85	5.95	
	0.70	5.03	5.07	
	0.60	4.58	4.60	
	0.50	4.31	4.32	

The streamlines obtained from the approximate perpendicular solutions
appear realistic (see Fig. 9 and 10), indicating that the solutions are sound.
For the limit of the circular cylinder, the elliptic cylinder analysis produces
streamlines that almost coincide with those from Kuwabara's analysis (at
porosity 0.75). For noncircular cylinders there is no basis for a similar
comparison, but the flow patterns for all porosity and axis ratio combina-
tions seem physically reasonable.

The perpendicular flow Kozeny factors for a nearly circular cylinder
are compared to those from the analysis of Kuwabara in Fig. 12. Since the
zero vorticity condition is used in both this analysis and Kuwabara's, the
two should give values that are the same. The actual difference is fairly
small, verifying the analysis for elliptic cylinders in the ciruclar limit.

The small deviation could be due to either the approximate nature of the solution or to computational inaccuracies.

The method used to construct the approximate solutions can be of potential value in many areas wherever a similar boundary value problem is encountered and no exact solution can be found for it.

COMPARISON WITH PREVIOUS ANALYSES

Circular Cylinders

The theoretical analyses for flow through assemblages of elliptic cylinders cannot accommodate cylinders of circular cross section ($\beta_0 = 1$) because a division by zero would be involved. But a very nearly circular cylinder can be considered, such as one with an axis ratio of 0.999. The comparisons between the results of the elliptic cylinder analysis for the nearly circular case and the results of the circular cell model analysis of Kuwabara are discussed above for both parallel and perpendicular flow; the conclusion is that the method of this thesis yields reliable values for the Kozeny factor for circular cylinders. Since the Kuwabara approach is compared with other investigations in a previous section, there is no need to repeat such a comparison for the results from the elliptic analysis with nearly circular cylinders.

Noncircular Cylinders

An analysis similar to the one developed here has been reported recently by Masliyah and Epstein (40,41), who applied the cell model technique to clusters of elliptic cylinders by solving numerically the Navier-Stokes equation. Creeping flow estimates were obtained by assuming a small Reynolds number (0.01). Both the zero vorticity outer boundary condition and the zero

shear stress one were considered, but only the former is of interest presently. Only a few combinations of axis ratio and porosity were used in the calculations. In Fig. 13, some of the Kozeny factors from their analysis are compared with the results from the analysis developed above. The two analyses differ a good bit but give similar trends relative to the effect of axis ratio and porosity. Like results from the two analyses are not necessarily expected because of the fundamentally different approach and solution techniques. The analysis of this thesis is based on the creeping flow equation, whereas Masliyah's work only approximates this case. Also, the mathematical solution of this thesis approximates the exact solution by a power series type of approach, while Masliyah used a finite difference expression and solved it using a relaxation procedure. The difference between the two sets of values may be attributed to inertial forces, which are ignored in the creeping flow analysis.

The results of the analyses for perpendicular flow past clusters of elliptic cylinders can be compared to the values from the study by Kuwabara (43) for flow through a regular square array of elliptic cylinders. The square array analysis is valid only at high porosities; as the cylinders become flatter, the porosity below which the approach is invalid moves closer to 1.0. For flow parallel to the minor cross-sectional axis, Table IV compares the elliptic cell model Kozeny factors to Kozeny factors for the square array and to Kuwabara's circular cell model values. For circular cylinders, the circular cell results are somewhat lower probably because of the approximate solution, which becomes less accurate as the porosity approaches 1.0; this effect was noticed in the similar parallel flow approximate solution. For elliptic cylinders the two approaches give similar trends, and at high porosities the values do not differ greatly.
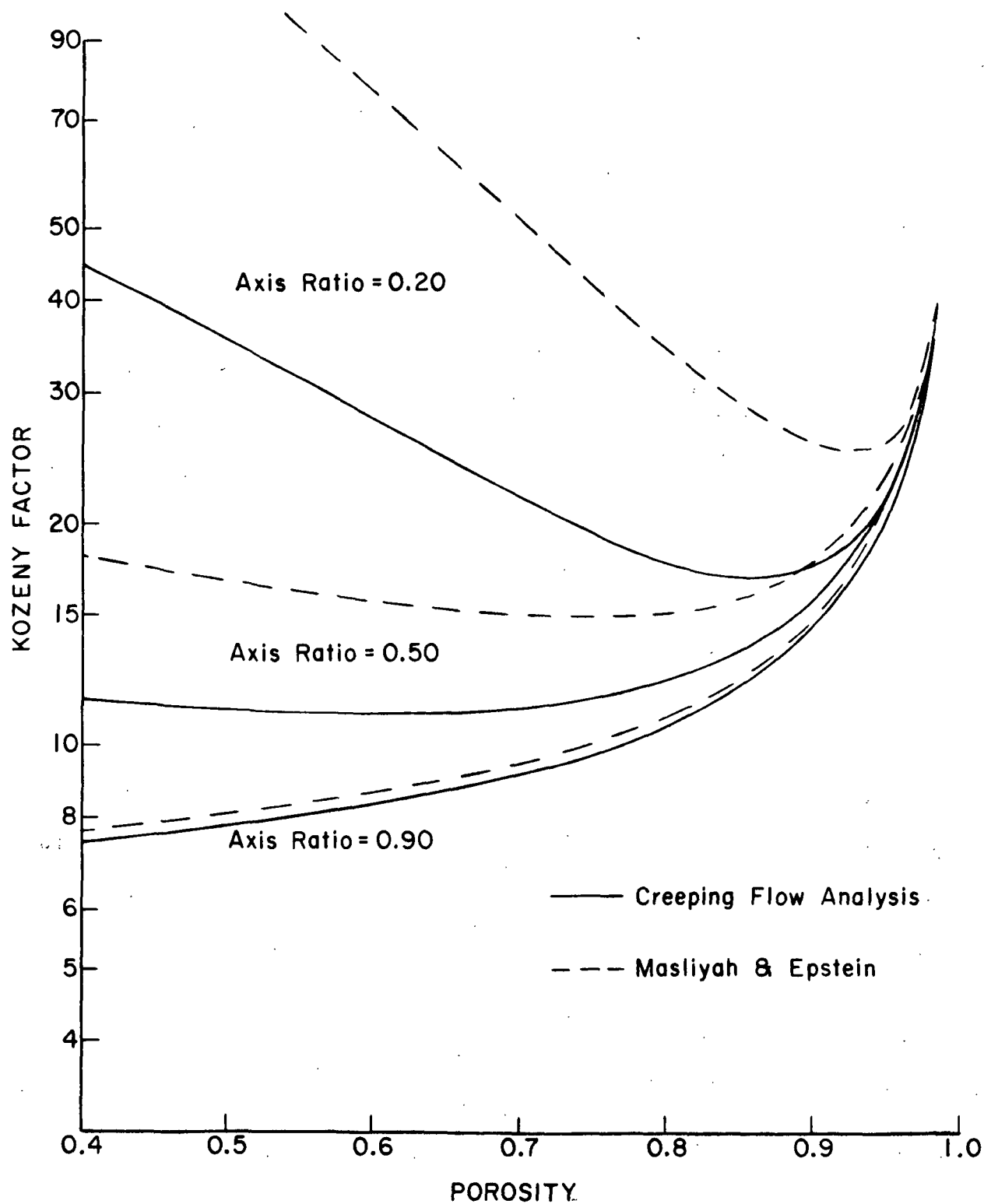
Figure 13. Comparison of Two Zero Vorticity Cell Model Analyses for Perpendicular Flow Along Minor Cross-Sectional Axis

. TABLE IV

COMPARISON OF KOZENY FACTORS FROM CELL MODEL ANALYSIS AND
REGULAR ARRAY ANALYSIS FOR ELLIPTIC CYLINDERS

Axis Ratio	Porosity	Kuwabara Square Array	Elliptic Cell Model	Kuwabara Circular Cell Model
1.00	0.997	154.9	125.2	153.1
	0.99	63.1	54.1	62.1
	0.98	39.6	34.8	38.4
	0.97	30.9	27.3	29.4
	0.96	26.2	23.1	24.6
	0.95	23.6	20.4	21.5
0.50	0.997	162.6	134.3	
	0.99	69.5	58.1	
	0.98	45.9	37.4	
	0.97	37.8	29.4	
	0.96	33.6	25.0	
	0.95	31.8	22.1	
0.10	0.997	138.1	128.2	
	0.99	80.7	49.8	
	0.98	98.3	31.8	
	0.97	566.6	25.8	

APPLICATION TO FIBER MATS

The application of the theoretical analyses for directional Kozeny factors to the permeation of a fluid through a mat of uniform synthetic fibers is of primary interest. The structure of the mat influences the relative contribution of the directional Kozeny factors, and must be considered before applying the cell model analyses to flow through a fiber mat.

STRUCTURE OF FIBER MATS

The orientation of fibers within a mat depends upon how the mat was originally formed as well as the compressive history of the mat. Formation by slow filtration from a dilute fiber suspension produces a mat with the central axes of most fibers lying generally in the plane of the mat; with

elliptic fibers the greater cross-sectional axis is preferentially aligned parallel to the mat plane. This orientation results because the fibers before deposition on the mat become oriented in the fluid so that the drag is maximized. Fibrous mats of practical importance do not usually have as ordered a structure as just described, but tend more toward a random structure. The compression of a mat of fibers can alter the original structure; Elias (46) discusses the causes of this.

The orientation of an elliptic fiber within a mat is discussed in Appendix VII. Two angles are defined as follows: θ is the angle between the fiber's central axis and the normal to the plane of the mat; ϕ is the angle of rotation about the fiber's central axis between the major cross-sectional axis and the plane of the mat, increasing in counterclockwise direction. (See Fig. 20 and 22.)

KOZENY FACTORS FOR FIBER MATS

Composite Kozeny Factor

The Kozeny factor of a fiber mat should be a combination of the three directional Kozeny factors previously determined, with the relative contribution of each dependent on the fiber orientation within the mat. In Appendix VII a composite Kozeny factor for a fiber mat is derived, with the result as follows:

$$k = [k_{(x)} \sin^2 \phi + k_{(y)} \cos^2 \phi] \sin^2 \theta + k_{(z)} \cos^2 \theta. \qquad (183)$$

Special Cases

Several special cases of fiber orientation within the mat are of interest. Using the above equation for a composite Kozeny factor, the resistance to flow through an oriented mat can be predicted for these cases.

Case I: All fiber central axes parallel to flow; $\theta = 0$. The

Kozeny factor is simply $\underline{k}_{(z)}$. This case is not of practical importance

for fiber mats but may be for some flow process.

Case II: All fiber central axes perpendicular to flow; $\theta = \pi/2$.
This case is occasionally of practical interest. Fibrous filters are often

prepared so that as many fibers as possible lie in the plane of the filter

(see Case IV). Three possibilities are considered, as follows:

A: Major cross-sectional axis parallel to flow; $\phi = 0$, $\underline{k} = \underline{k}_{(x)}$.

B: Minor cross-sectional axis parallel to flow; $\phi = \pi/2$, $\underline{k} = \underline{k}_{(y)}$.

C: Cross-sectional axes at angle to flow; $\underline{k} = \underline{k}_{(x)}\sin^2\phi + \underline{k}_{(y)}\cos^2\phi$.

Case III: Distribution of orientations. In a real fiber mat there is

no regular, ordered structure; instead the fibers assume various orientations.

By identifying the orientation distribution, the composite Kozeny factor can

be determined in the following manner:

$$k = \int_0^{\pi/2} [k_{(t)}\sin^2\theta + k_{(z)}\cos^2\theta] \, g(\theta) \, d\theta, \qquad (184)$$

where $\underline{k}_{(t)}$, the transverse flow Kozeny factor, is found in a similar way:

$$k_{(t)} = \int_0^{\pi/2} [k_{(x)}\sin^2\phi + k_{(y)}\cos^2\phi] \, h(\phi) \, d\phi. \qquad (185)$$

The distribution of fiber orientations is expressed by means of the frequency

functions $\underline{g}(\theta)$ and $\underline{h}(\phi)$, which must satisfy the normalization criterion:

$$\int_0^{\pi/2} g(\theta) \, d\theta = 1, \qquad (186)$$

$$\int_0^{\pi/2} h(\phi) \, d\phi = 1. \qquad (187)$$

One particular distribution, that for an isotropic mat, is of interest. The choice of $\underline{g}(\theta) = \sin \theta$ provides such a mat in which the probability of a fiber end falling at any point on a sphere around the fiber center is constant (35). Two possible choices for $\underline{h}(\phi)$ are as follows:

A. By choosing $\underline{h}(\phi) = 2/\pi$, all values of ϕ are equally probable. This choice produces an isotropic mat in which there is no preferred cross-sectional arrangement. The composite Kozeny factor for this mat is

$$k = (1/3)[k_{(x)} + k_{(y)} + k_{(z)}]. \qquad (188)$$

Some Kozeny factors for isotropic mats are presented below.

B. The selection $\underline{h}(\phi) = \cos \phi$ describes a mat in which the probability is greatest that the fiber is oriented with its major cross-sectional axis normal to flow. The composite $\underline{k}$ for this case is

$$k = (2/3) [(1/3)k_{(x)} + (2/3)k_{(y)}] + (1/3)k_{(z)}. \qquad (189)$$

Case IV: A mat formed slowly from a dilute fiber suspension, as discussed above, has the fibers generally in the mat plane. For such a mat, average θ and ϕ values can be chosen to use in Equation (183) for the composite Kozeny factor, since the exact fiber orientation distribution is not known. The choices $\theta = 75°$ and $\phi = 20°$ seem reasonable. The θ estimate follows from Elias' experimental data for fibers of a length/diameter ratio of near 100. Using these values, the $\underline{k}$ value becomes

$$k = 0.067\, k_{(z)} + 0.109\, k_{(x)} + 0.824\, k_{(y)}. \qquad (190)$$

Isotropic Mats

Case III-A above discusses the Kozeny factor for an isotropic mat where all fiber orientations are equally likely to occur. Equation (188) has been used to calculate $\underline{k}$ values for such mats; these Kozeny factors are plotted in Fig. 14 and 15. The effect of porosity at a few axis ratios is seen in Fig. 14, while the effect of axis ratio at several porosities is seen in Fig. 15. The fibers of the mat can be flattened a fair amount, dependent on the porosity, before the fiber cross-sectional shape begins to significantly affect the Kozeny factor. At higher porosities more flattening is permissible before the effect becomes large. For example, at a porosity of 0.90, a mat of fibers of axis ratio 0.10 has a Kozeny factor only slightly different from that for a mat of circular fibers. At 0.75 porosity, the fibers can be flattened to near 0.30 axis ratio before a ten percent change in $\underline{k}$ occurs.

Lord (37) experimentally determined the Kozeny factors for air permeation through a carefully randomized mat in which an effort was made to uniformly distribute the fibers. This mat should closely approximate the isotropic case. The data for silk fibers of nearly circular cross section are seen in Fig. 16 compared to the theoretical results for an isotropic mat of circular fibers. The experimental and theoretical curves are similar, but the former is lower, indicating that there is actually less resistance to flow than the cell model theory predicts. Reasons for this are discussed in the following section.

Real Mats

The slowly formed fiber mat covered by Case IV above is of interest because it approximates the mats formed by Bliesner in his permeation experiments
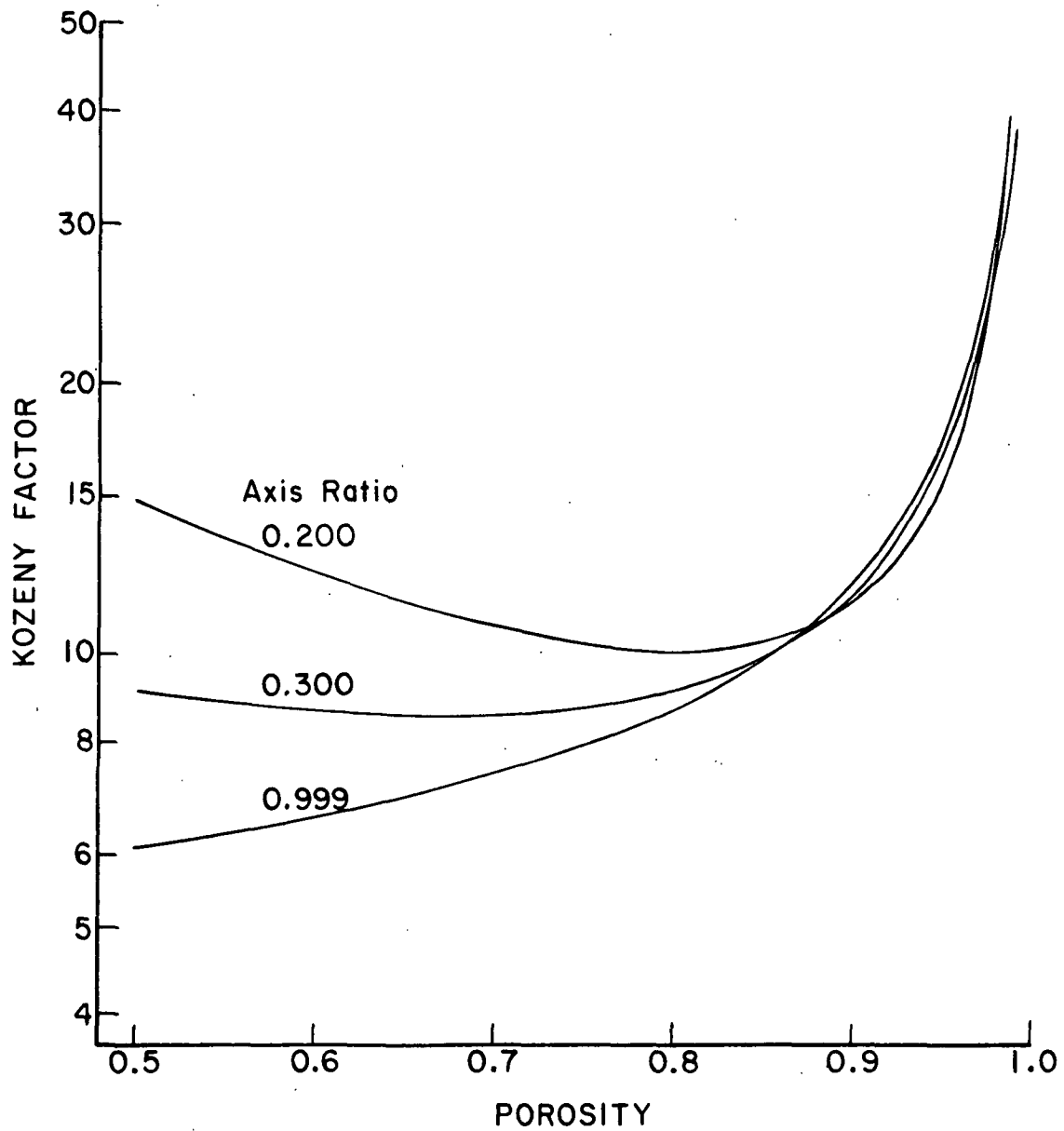
Figure 14.   Isotropic Mat Kozeny Factors as a Function of Porosity
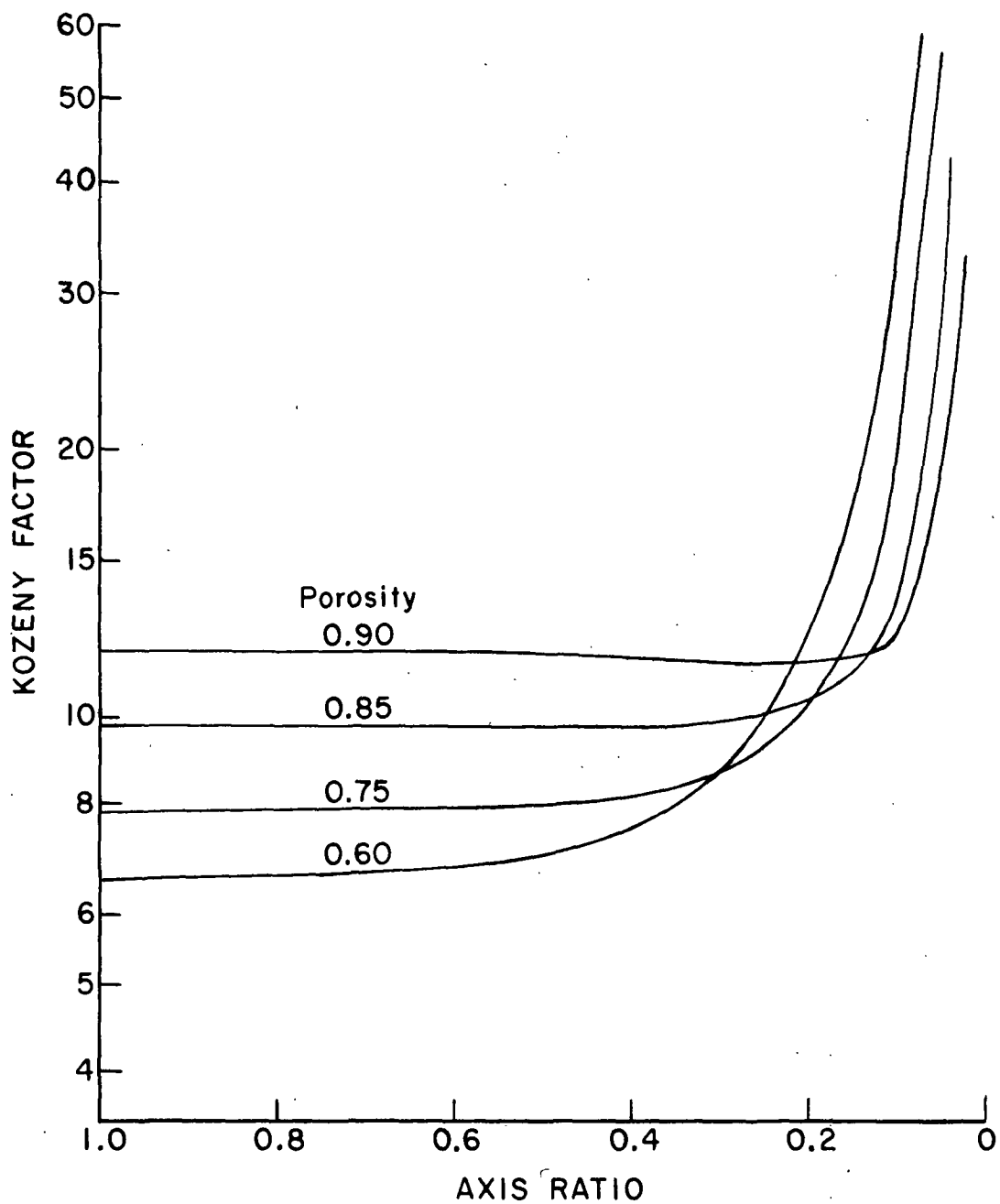
Figure 15. Isotropic Mat Kozeny Factors as a Function of Axis Ratio
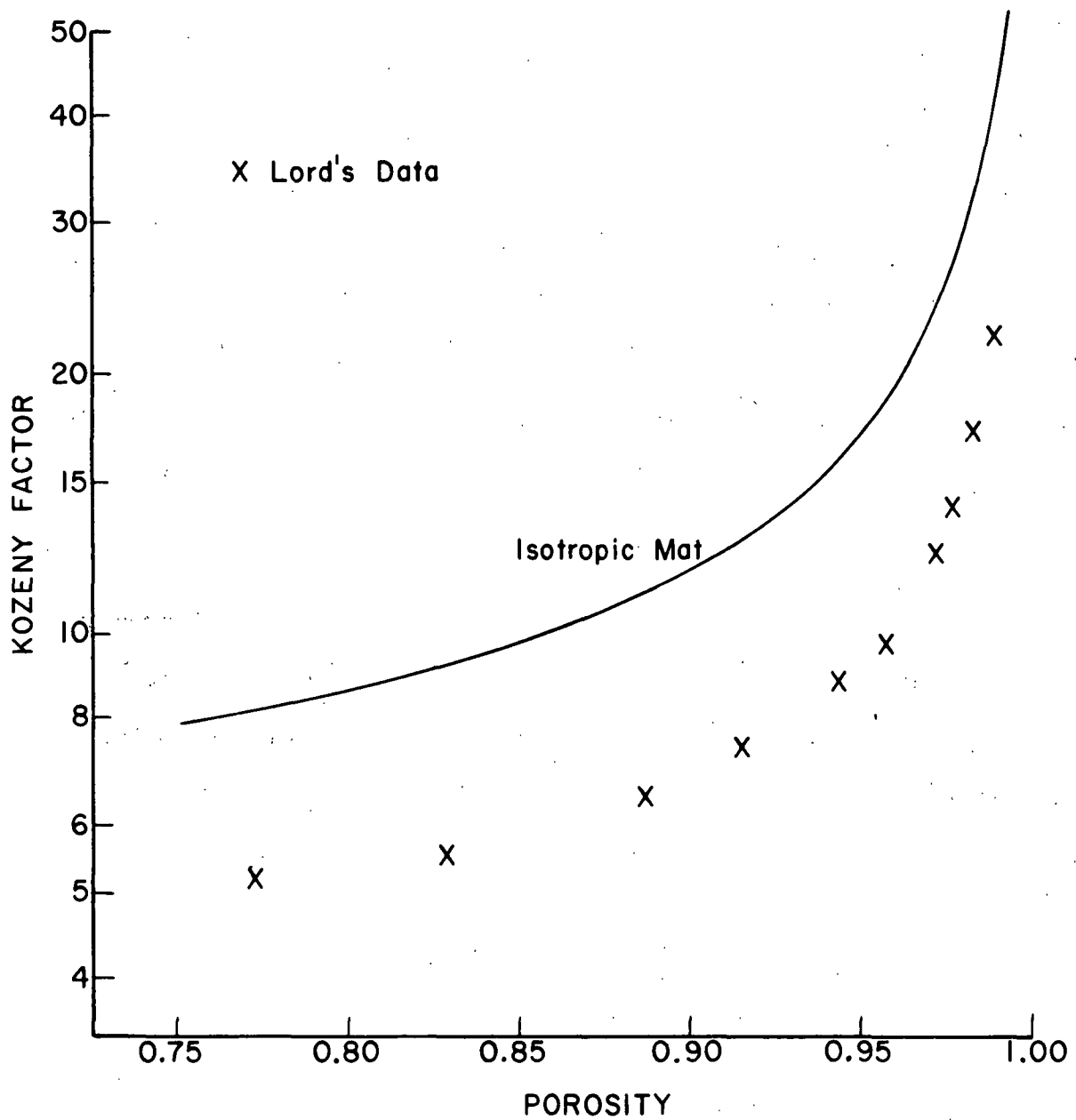
Figure 16. Kozeny Factors for Isotropic Mat and for
Randomized Beds of Silk Fibers

with noncircular fibers, as well as the mats used for the Davies-Ingmanson and Carroll correlations for circular fibers. Because of this, the Kozeny factors computed from Equation (190) are expected to be generally valid for these mats. To test this assumption, the data of Bliesner and the expected k values are compared below. Bliesner's data appear to be sound, at least for circular fibers in the porosity range covered, since his circular fiber mat k's are close to the empirical correlations. Accepting the noncircular data because the circular data appear good may be questionable, although no reason for rejecting the noncircular k's is apparent. The measured Kozeny factors of Bliesner should not necessarily be viewed as the true values because of the limited scope of the experimental program and because of the potential for errors inherent in the experimental procedure.

First consider flow through mats of circular fibers. Figure 17 presents Bliesner's experimental data, the isotropic and oriented k curves based on mat structure, and the two empirical correlations. As with the Lord data, the expected mat Kozeny factors determined from the cell model theory using Equation (190) are greater than the experimental values, although the trend with porosity is the same. While this comparison is disappointing, two reasons may account for the discrepancy, one an experimental problem and one a deficiency in the theory.

Experimentally, a uniform mat cannot be obtained; instead, any real mat contains local regions of resistance lower than the rest of the mat and porosity above the mat average because of pinholes, fiber curling, uneven deposition of fibers, edge effects, etc. These nonuniformities exist to some extent in any real mat regardless of the effort to eliminate the problems. Since the fluid follows the path of least action, the disturbed areas have a
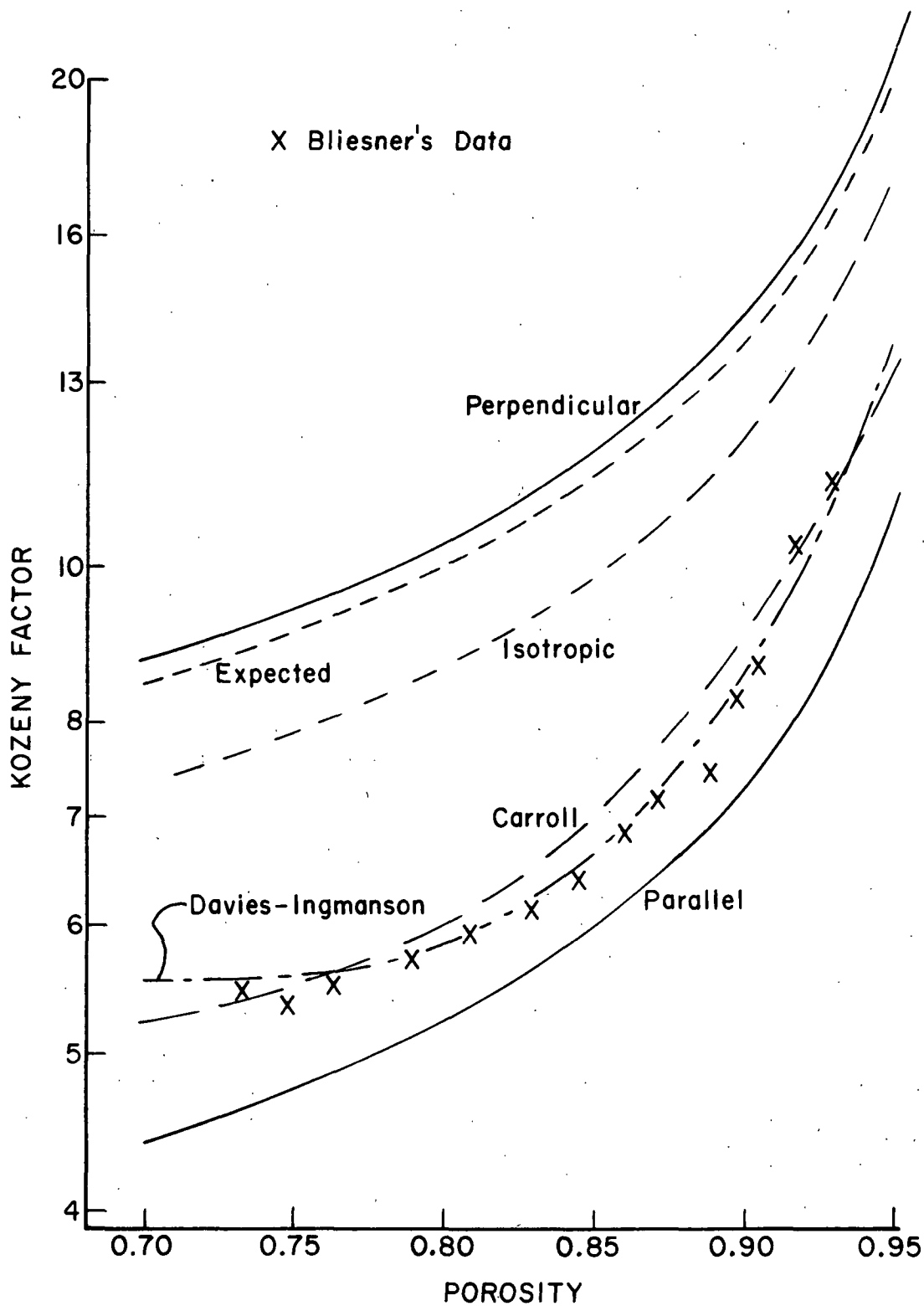
Figure 17. Kozeny Factors for Circular Fibers: Analytical Values and Bliesner's Experimental Data

stronger influence on flow properties than their volume fraction might indicate. A meaningful estimate of the error introduced by mat nonuniformity is very difficult to obtain because of imprecise means of gauging the local porosity. However, the effect of the nonuniformities should be to lower the observed experimental Kozeny factors, thereby explaining partially the discrepancy between theory and experiment.

The second reason for the difference between the expected Kozeny factors and the experimental data concerns the cell model approach where flow past a fiber segment is studied. Areas of fiber contacts are not considered, although two fibers crossing or in close proximity to each other cause less drag than if the two segments were apart. The sum of the drag on two isolated cylinders resulting from perpendicular flow past the cylinders is more than the drag due to flow past two cylinders situated near each other with their cross-sectional centers forming a line parallel to the flow direction. Happel and Brenner (15) discuss such interference effects between particles, summarizing the influence on cylinders as follows:

> "Thus with two cylinders of equal radii with one behind the other, the front cylinder experiences a greater drag than the rear cylinder. ... The drag acting on each of the two cylinders is less than when they are present alone."

Since the drag on two fibers in contact is less than that if the fibers were apart, the overall pressure drop for flow through the mat is below that predicted by the cell model analysis. In other words, the theory is overestimating the pressure drop because the effect of fiber contacts is ignored. This translates into a Kozeny factor that is greater than the true value for the mat considered. The magnitude of this effect cannot be easily estimated. Perhaps the application of the cell technique to the fiber crossing regions

would supply information in this regard, but to do this a quite involved analysis would have to be completed. Concerning elliptic cylinders, the error due to fiber crossings should be larger for flatter fibers, indicating that the discrepancy between theory and experiment may be dependent on the fiber axis ratio.

The data of Bliesner for noncircular fibers are compared to the cell model theoretical estimates in Fig. 18. As for the circular fibers, the empirical Kozeny factors are considerably smaller than the expected values found from Equation (190). The difference between the two seems to increase as the fibers become flatter, which is expected on the basis of the fiber crossing argument above. The experimental k values as a percentage of the theoretical expectations fall approximately as follows: 58% for circular fibers, 44% for axis ratio 0.344, and 40% for axis ratio 0.242; these values are at 0.80 porosity.

The combined effect of the experimental mat nonuniformities and the failure of the theory to consider fiber crossings may be sufficient to account for the discrepancy for both circular and noncircular fibers. Although an analytical estimate of the discrepancy caused by these two effects cannot be determined, perhaps an empirical approach could be used by introducing a parameter, r, into the composite Kozeny factor equation, as follows:

$$k = r \; [k_{(x)}\sin^2 + k_{(y)}\cos^2] \; \sin^2\theta + k_{(z)}\cos^2\theta. \tag{191}$$

The r value could provide for the above effects, but unfortunately would need to be experimentally measured and is probably dependent on both porosity and axis ratio.
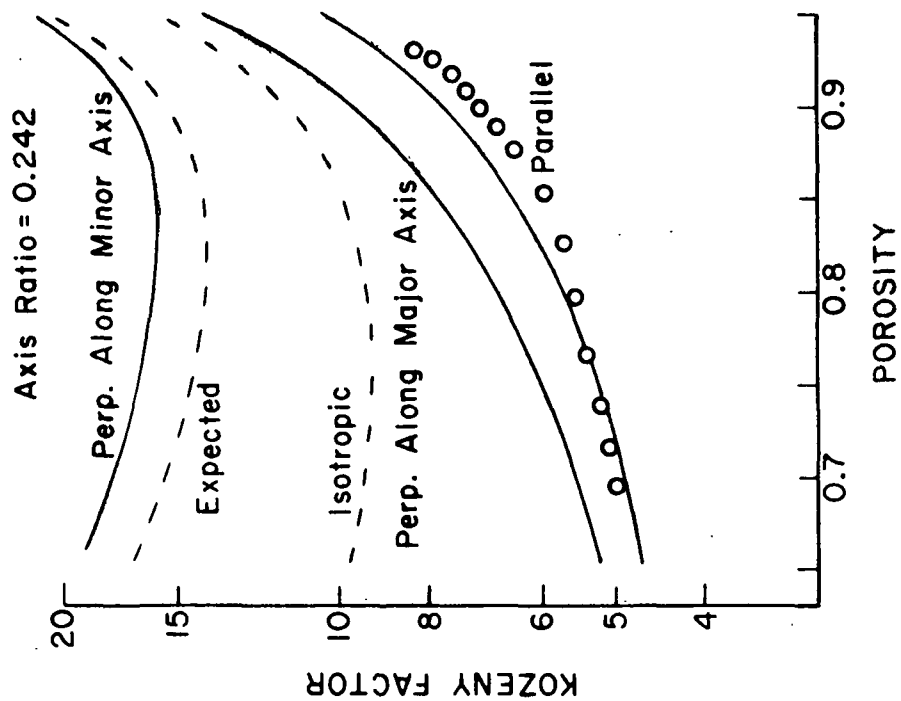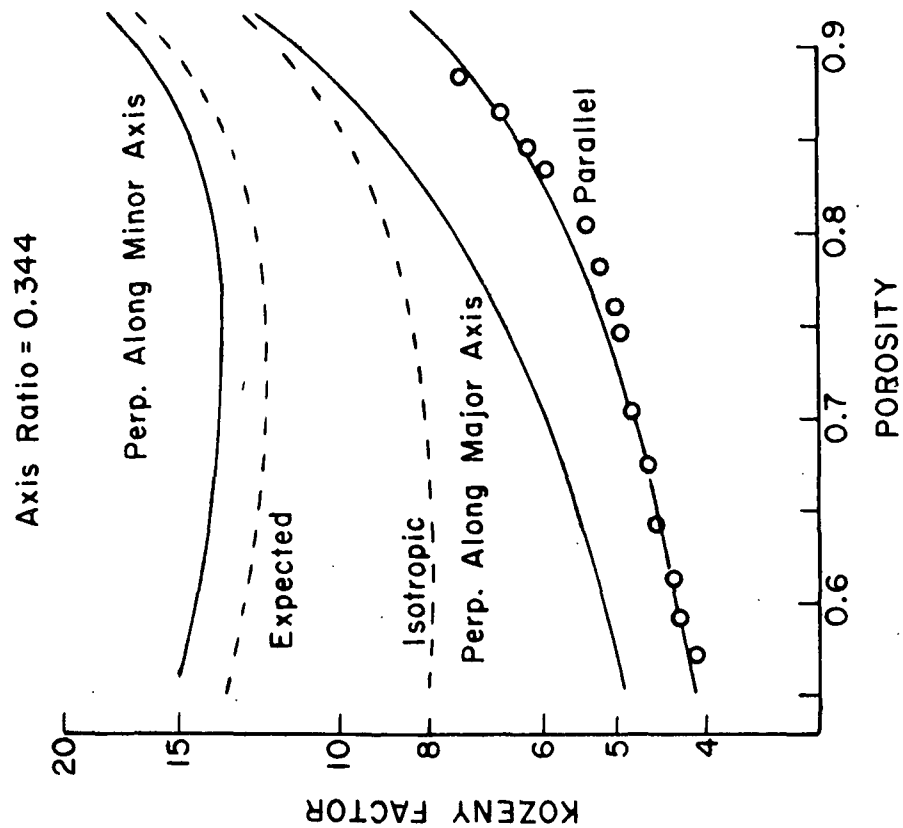
Figure 18. Kozeny Factors for Noncircular Fibers: Analytical Values and Bliesner's Experimental Data

Although not expected because of fiber orientation effects, the isotropic Kozeny factor relationship is a better indicator of real mat behavior than is the expected k value based on mat structure. Fibers of axis ratios 1.00, 0.344, and 0.242 produce experimental data at 0.80 porosity which are 66, 61, and 60%, respectively, of the isotropic k values.

Another way to look at the data is given by Fig. 19. Here the effect of axis ratio on Kozeny factor is more obvious. While this graph represents a porosity of 0.75, other porosities show similar results. The composite Kozeny factor for an isotropic fiber mat is not greatly affected by the cross-sectional axis ratio until a fairly flat fiber is used; for this porosity the change exceeds ten percent below an axis ratio of 0.30. The experimental data follow the same pattern; for the range covered by the tests, the fiber axis ratio seems to have little effect on k. The behavior of k for a real mat as the axis ratio approaches zero is not known from experimental studies, but from the theoretical analysis the conclusion that the Kozeny factor would begin to increase rapidly seems valid. From this discussion, the assumption that a real mat Kozeny factor is independent of fiber cross-sectional shape, at least for axis ratios more circular than 0.2, should introduce only slight errors into the permeation analysis.

One pertinent factor has not yet been discussed, that is, the question of the importance of the surface area correction for interfiber contact. Both Bliesner and Labrecque made such a correction, but a fresh look at this question seems in order.
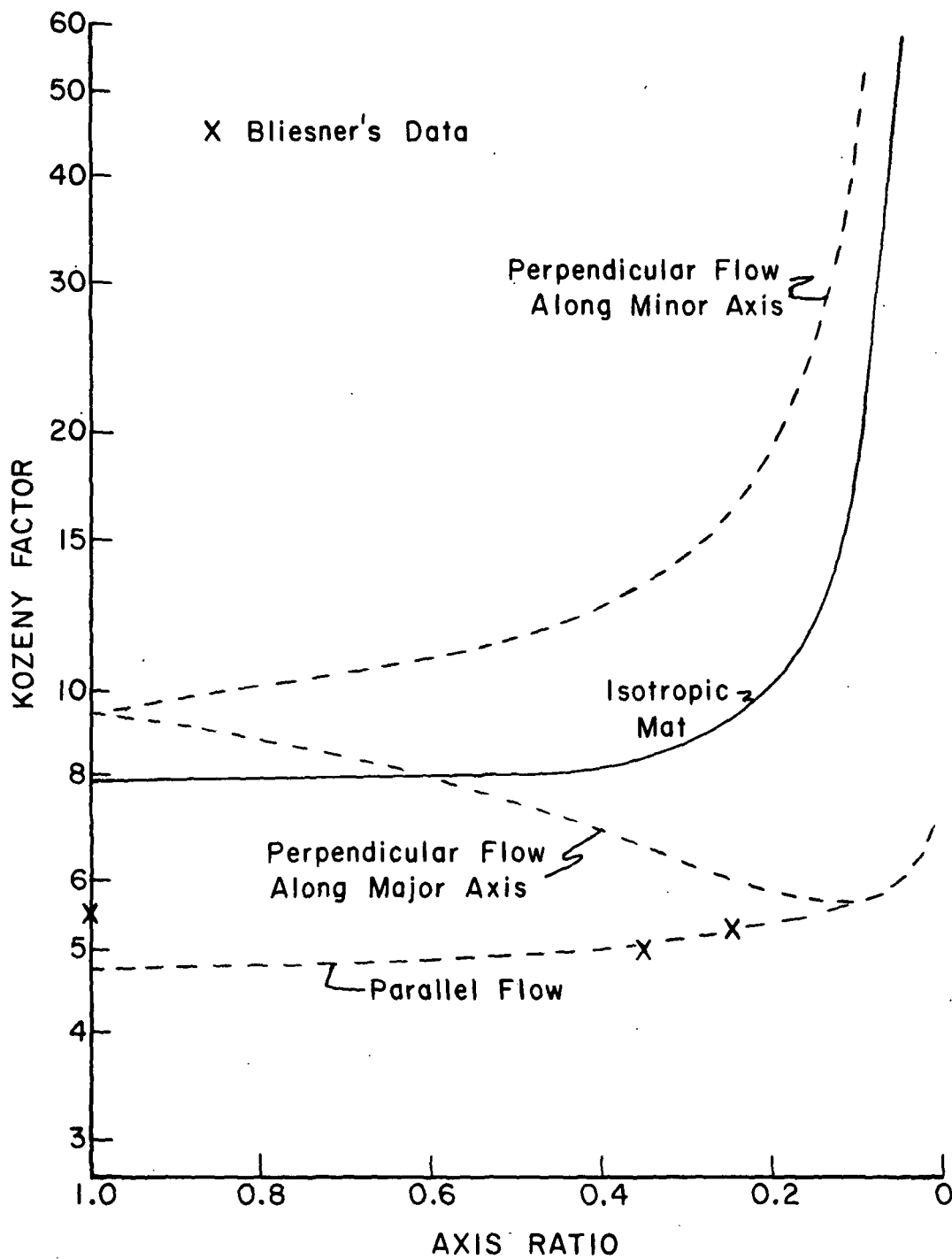
Figure 19. Analytical and Experimental Kozeny Factor as a
Function of Fiber Shape at Porosity 0.75

INTERFIBER CONTACT AREA

The fiber surface area excluded from the permeating fluid because of interfiber contact has been estimated by Bliesner ($\underline{8}$) using as a basis the fiber network analysis of Onogi and Sasaguri ($\underline{38}$). His result for the specific surface corrected for this effect is as follows:

$$S_v = P_f/A_f - 4(1-\epsilon)w^2/(\pi^2 d_e A_f), \qquad (192)$$

where $\underline{P_f}$ = fiber perimeter

$\underline{A_f}$ = fiber cross-sectional area

$\underline{w}$ = projected fiber width

$\underline{d_e}$ = effective fiber diameter

Labrecque ($\underline{39}$) criticized the Bliesner approach because the number of interfiber contacts was assumed independent of fiber shape and because only a fraction, $\underline{F}$, of the fiber width was actually in contact. Developing a similar analysis but accounting for these effects, Labrecque obtained the equation for corrected specific surface

$$S_v = P_f/A_f - 2(1-\epsilon)tw^2F^2/(\pi A_f^2), \qquad (193)$$

where $\underline{t}$ is the fiber thickness. Where Bliesner's method estimates 23% contact area for a mat of fibers of axis ratio 0.242 and porosity 0.70, Labrecque's approach gives 9%, which is much more realistic.

Several criticisms of the Labrecque analysis can be presented regarding the determination of the mean contact area per crossing per fiber, $\underline{A_c'}$. First, the fraction of the fiber width in contact, $\underline{F}$, should be dependent on the stress on the mat; as the pressure increases the contact area at the crossing should too. Second, the $\underline{F}$ factor needs to be empirically determined. Third,

the mean contact area should be dependent on the elastic properties of the fibers, such as Young's modulus and Poisson's ratio. All of these criticisms are nonexistent in the analysis by Finch (47) of the contact area between two isotropic elastic fibers, who applied the equations of Hertz (48) to develop a theoretical relationship and verified the result experimentally with nylon fibers. Using the Finch equation for contact area per crossing, a mean contact area can be determined by specifying an appropriate frequency function for the angle between the axes of the fibers in contact and integrating. The mean contact area per crossing times the number of contacts found from the Onogi and Sasaguri theory equals the surface area in contact. In Appendix VIII, the interfiber contact area estimate for elliptic fiber mats based on the Finch method is developed, and estimates for the fibers used by Bliesner and Labrecque are calculated. The relationship found for fibers of elliptic cross section with half-axes a_o and b_o is as follows:

$$S_v = S_{vo}[1 - 8A_c'(1-\varepsilon)/(\pi^4 a_o^2 H)]. \qquad (194)$$

In this equation, S_{vo} is the specific surface with no interfiber contact, and H is defined by Equation (79). The Bliesner and Labrecque equations converted to apply to fibers of elliptic cross section are, for Labrecque's analysis

$$S_v = S_{vo}[1 - 16(1-\varepsilon)F^2/(\pi^3 H)] \qquad (195)$$

and for that of Bliesner

$$S_v = S_{vo}[1 - 8(1-\varepsilon)a_o/(\pi^3 H b_o)]. \qquad (196)$$

The three are similar in form but different in results. Defining δ_c as the fraction of surface area in contact so that

$$S_v = S_{vo}(1 - \delta_c) \qquad\qquad (197)$$

the contact area fractions for the Labrecque and Finch analyses are compared in Table V.

TABLE V

COMPARISON OF INTERFIBER CONTACT AREA ANALYSES

Axis Ratio	Porosity	Contact Area, %	
		Finch	Labrecque
1.0	0.90	1×10^{-6}	0.075
	0.60	0.045	0.30
	0.40	1.04	0.45
0.242	0.90	2×10^{-6}	1.77
	0.70	0.040	5.3
	0.60	0.53	7.0
	0.50	3.93	8.8
	0.40	20.3	10.6

The calculations using Labrecque's method employed $\underline{F}$ factors determined directly from microphotographs, and are not the same values as reported in his thesis.

The analysis based on the Finch theory seems more fundamentally sound than does the Labrecque analysis. The contact area estimates obtained are negligible for the conditions used in Bliesner's permeation experiments. Consequently the interfiber contact area correction, although valid, is insignificant and will be neglected in comparing the cell model theoretical Kozeny factors to the experimental data.

VALIDITY OF CREEPING FLOW ASSUMPTION

By assuming creeping motion, the cell model analysis is valid only for slow flow rates. But Darcy's law too is applicable only for slow superficial velocities, so the creeping flow assumption does not seem unrealistic.

The relative contributions from viscous and inertial effects for flow through synthetic fiber mats were considered by Ingmanson and Andrews (49). Defining a Reynolds number as

$$Re = \rho U / [\mu S_v (1-\varepsilon)] \tag{198}$$

and considering only mats of porosity below 0.80, they conclude that inertial resistance is only 4% of the total at $\underline{Re}$ = 1, and inertial effects are just becoming significant. At $\underline{Re}$ = 10, the inertial resistance accounted for 30% of the overall pressure drop. For mats of wood pulp fibers, they suggest that a maximum velocity of about 1 cm/sec is the limit for streamline flow with negligible inertial effects.

Spielman and Goren (30) state that the creeping motion assumption is valid near the solid cylinder if the Reynolds number is much less than 1. They define Reynolds number as $\underline{Re}$ = $2a U \rho / \mu$, where $\underline{a}$ is the fiber radius. Far from the cylinder surface inertial effects are more dominant, but in the cell model analysis this effect becomes significant only at very high porosities.

For elliptic cylinders, Epstein and Masliyah (40) define

$$Re = 2a_o U \rho / \mu \tag{199}$$

in which $\underline{a_o}$ is the half-axis perpendicular to flow. To obtain creeping flow results, they simply chose $\underline{Re}$ = 0.01.

The maximum Reynolds number, as defined by Equation (199), for the permeation experiments of Labrecque with elliptic fibers was near 0.2. The values for Bliesner's experiments should be similar. In view of the above comments, the application of a creeping flow model to these permeation results should be reasonable.

APPLICATION TO OTHER SYSTEMS

WOOD FIBER MATS

The results of the cell model analyses for elliptic cylinders hopefully will engender a better understanding of flow through mats of wood pulp fibers. In a wood fiber mat there are many complicating effects, one of which is the variety of cross-sectional shapes. If a mat of never-dried fibers, with axis ratios generally more circular than 0.3, is permeated with a fluid, the results of this study indicate that the Kozeny factor for such flow is probably affected only slightly by the noncircular cross sections. Choosing the Davies-Ingmanson correlation, for example, which applies only to circular fibers, as an expression for the Kozeny factor of a wood fiber mat should not introduce a large error into the study, although this is dependent on the type of fiber and the mat's history.

RELATED AREAS

A number of areas of investigation, such as the theory of particle retention in fibrous filters or mats, the analysis of flocculation of fibers, and zeta-potential studies in fiber slurries, often require a description of flow near the surface of a fiber. The cell model studies for circular cylinders have been applied to these areas (21,35,50,51), but not all fibers

of interest have round cross sections. For these cases the cell model analysis for elliptic cylinders developed herein can be used to advantage in describing the flow around fibers.

Another possible area where the elliptic cylinder cell model flow analysis may be useful is in the flow past banks of tubes of elliptic cross section, such as exist in some heat exchangers. The heat and mass transfer analysis through such arrays may utilize the equations of this thesis, although normally such flow is not occurring in the creeping motion regime.

CONCLUSIONS

The use of the cell model approach to study parallel or perpendicular
flow past arrays of elliptic cylinders provides insight into the effect of
the cross-sectional shape of the cylinders on the drag caused by such flow.
While the drag due to flow past arrays of circular cylinders has been pre-
viously examined by means of the cell model method, the application of this
technique to creeping flow, either parallel or perpendicular to the cylinders'
central axes, past assemblages of elliptic cylinders is greatly expanded in
this work. The results for flow parallel to the cylinders indicate that the
influence of the cross-sectional shape on the drag is significant but not
large, and the effect is porosity dependent. When the flow is perpendicular
to the cylinders, two cases are considered for flow along each of the two
cross-sectional axes. The drag due to perpendicular flow along the major
cross-sectional axis is dependent to a considerable extent on the ratio of
minor to major axes, or the "flatness" of the cylinders. Perpendicular flow
along the minor axis results in drag that is more dependent on the axis ratio
than for the other perpendicular flow direction. This last flow case dis-
plays a very strong dependence on the axis ratio when the cylinder becomes
quite flat, e.g., an axis ratio of 1/3 or less.

The approximate procedure developed to solve the boundary value problems
for both parallel and perpendicular flow cases involving Poisson equations
provides a fairly easy means for obtaining an approximate solution to problems
that may otherwise be intractable or laborious.

The slow permeation of a fluid through a mat of uniform synthetic
fibers can be studied theoretically by combining the results from the
parallel and perpendicular cell model analyses of creeping flow through

arrays in a manner dependent on the mat structure. An elliptic cylinder serves as a useful model of a fiber of oval cross section; by changing the cross-sectional axis ratio, fiber shapes from round to nearly flat can be closely represented by the model. The drag on an individual cylinder can be resolved into force components along each of the three principal axes of the cylinder. In this manner the drag past a particular fiber within the mat can be predicted from the directional cell model analytical results. By determining the distribution of fiber orientations within the mat, the overall mat permeability can be estimated and the effect of changing fiber shape on permeability clarified. The Kozeny factor from the Kozeny-Carman concept of fluid flow through porous media serves as a relative indicator of the resistance to flow through a mat with other parameters constant (porosity and specific surface). For example, an isotropic mat of circular synthetic fibers of porosity 0.75 should theoretically have a Kozeny factor of 7.9, whereas if the fibers have an elliptic cross section of axis ratio 1/3 the Kozeny factor changes to 8.4; with flatter fibers the Kozeny factor increases sharply. Available experimental permeability measurements with synthetic fiber mats indicate that the actual Kozeny factors are much less than the theoretical values derived from the cell model analysis, although their trends of variation with axis ratio and porosity are similar.

The correction of the specific surface of synthetic fiber mats because of interfiber contact excluding surface area from the permeating fluid appears to be negligible if the mat porosity is greater than 0.60, although this is dependent on fiber properties (axis ratio, Young's modulus, and Poisson's ratio).

When a mat of wood pulp fibers is considered, the various fiber cross-sectional shapes should affect the mat Kozeny factor in a similar manner. Based on the theoretical results for isotropic mats of uniform fibers, the fiber shape does not seem to have a strong influence on the mat Kozeny factor until the fibers are flatter than approximately a 1/3 axis ratio. Since never-dried wood pulp fibers in lightly compressed mats are for the most part more circular than this axis ratio, the commonly adopted assumption that the Kozeny factor for circular fiber mats is applicable to wood pulp fiber mats is justifiable. In principle, the specific surface correction for interfiber contact area is appropriate for wood fiber mats, but further refinements in the analysis would be beneficial.

SUGGESTIONS FOR FUTURE WORK

Regarding the application of the elliptic cell model analysis to flow through fibrous mats, few ideas for extending the present work are obvious. One possibility is to consider the effect that a mat containing fibers with a distribution of axis ratios has on Kozeny factor. This could simulate a wood fiber mat where various cross sections are present. Another possible study would involve developing an accurate means for estimating experimentally the interfiber contact area in a fiber mat. The assumption that the contact area is negligible for the ranges covered by Bliesner's permeation tests could use empirical verification. Also the extension of the cell model analysis to include the fiber crossing regions would help make the theory more appropriate for fiber mats.

The utilization of the elliptic cell model analyses in related areas offers much promise for future investigations. The retention of particles in fibrous assemblages made of noncircular fibers could be studied using these flow equations. Perhaps particle retention or aerosol filtration efficiency can be improved by selecting fibers of appropriate cross-sectional shapes. The analysis of zeta-potential around noncircular fibers can be performed using the flow equations developed herein; the circular fiber model of Ciriacks (51) could be extended to elliptic fibers in order to better model wood pulp fibers.

Other possible areas for future work can undoubtedly be identified with effort, but probably the most promising topics would involve applying the results of this study to related areas rather than extending the present work.

ACKNOWLEDGMENTS

Special thanks are offered to Professor Heribert Meyer, Chairman of my Thesis Advisory Committee, who guided and inspired me throughout this thesis program. Dr. Richard W. Nelson and Dr. James Y. Hung, the other members of my Advisory Committee, also deserve acknowledgment and recognition for their frequent assistance and guidance.

Many other members of the Institute community have earned my thanks by aiding me often during my stay in Appleton, but naming specific individuals would certainly omit someone equally as deserving.

The member companies of the Institute and the donors to the scholarship fund receive my sincere appreciation for making my studies here possible.

LIST OF SYMBOLS USED

$\underline{A}$ = cross-sectional area of porous medium presented to flow

$\underline{A}_o$ = geometric surface area of a fiber

$\underline{A}_c$ = contact area on a fiber

$\underline{A}'_c$ = mean contact area per crossing per fiber

$\underline{A}^*_c$ = $\pi \underline{a}_c \underline{b}_c$ = area of contact per crossing

$\underline{A}_f$ = fiber cross-sectional area

$\underline{A}_w$ = wetted surface area of a fiber

$\underline{A}_{\underline{jk}}$ = integral defined by Equation (52)

$\underline{A}, \underline{B}, \underline{C}, \underline{D}$ = constants in Kuwabara's solution for flow past circular cylinders

$\underline{B}_1, \underline{B}_2$ = constants defined by Equations (67) and (68)

$\underline{B}_{(\underline{x})}, \underline{B}_{(\underline{y})}$ = factors in vorticity expressions

$\underline{C}$ = circumference of ellipse

$\underline{C}, \underline{D}, \underline{E}, \underline{F}$ = constants in Happel's solution for perpendicular flow past circular cylinders

$\underline{D}$ = quantity in parallel flow solution defined by Equation (83)

$\underline{D}_{(\underline{x})}, \underline{D}_{(\underline{y})}$ = quantities in perpendicular flow solutions defined by Equations (269) and (129)

$\underline{E}$ = Young's modulus

$\underline{E}_{(\underline{x})}, \underline{E}_{(\underline{y})}$ = quantities in perpendicular flow solutions defined by Equations (270) and (130)

$\vec{\underline{F}}$ = drag force on solid cylinder

$\underline{F}$ = fraction of fiber width in contact with another fiber in Labrecque's analysis

$\underline{F}_{\underline{N}}$ = normal force pressing two fibers together

$\underline{F}_{(\underline{x})}, \underline{F}_{(\underline{y})}$ = drag force for perpendicular flow problems

$\underline{F}_{(\underline{p})}, \underline{F}_{(\underline{t})}$ = parallel and perpendicular (transverse) components of drag

$\underline{G}$ = Green's function

$\underline{G}_{(\underline{x})}$, $\underline{G}_{(\underline{y})}$ = factors related to $\underline{B}_{(\underline{x})}$ and $\underline{B}_{(\underline{y})}$

$\underline{H}$ = parameter relating circumference and axis ratio of ellipse; defined by Equation (79)

$\underset{\sim}{\underline{I}}$ = idemfactor

$\underline{I}_{\underline{j}}$ = integral in contact area analysis defined by Equation (321)

$\underline{K}$ = permeability coefficient

$\underline{K}_{o}$ = proportionality factor in Darcy's law

$\underline{L}$ = thickness of porous bed

$\underline{L}_{\underline{f}}$ = fiber length

$\underline{L}_{\underline{s}}$ = segment length

$\underline{L}_{\underline{so}}$ = segment length in unloaded mat

$\underline{M}$, $\underline{N}$ = mat compressibility constants

$\underline{N}_{\underline{c}}$ = number of fiber-to-fiber contacts per fiber

$\underline{N}_{\underline{jk}}$ = normalization factor

$\underline{P}_{\underline{f}}$ = fiber perimeter

$\underline{P}^{*}$, $\underline{P}^{*}_{\underline{A}}$, $\underline{P}^{*}_{\underline{E}}$ = quantities in parallel flow solution [see Equations (80)-(82)]

$\underline{Q}$ = volumetric flow rate

$\underline{R}$ = quantity in perpendicular flow solutions defined by Equation (139)

$\underline{R}$ = radius of curvature

$\underline{R}_{11}$, $\underline{R}_{12}$, $\underline{R}_{21}$, $\underline{R}_{22}$ = radii of curvature of two bodies in contact

$\underline{R}_{\underline{k}}$ = quantity defined by Equation (55)

$\underline{Re}$ = Reynolds number

$\underline{S}_{o}$ = specific surface = surface area per unit volume of porous medium

$\underline{S}_{\underline{v}}$ = specific surface = surface area per unit volume of solid fraction

$\underline{S}_{\underline{vo}}$ = specific surface for mat with point contact between fibers

$\underline{T}_1$, $\underline{T}_2$ = quantities in perpendicular flow solutions defined by Equations (141) and (275)

$\underline{T}_{(\underline{x})}$, $\underline{T}_{(\underline{y})}$ = quantities in perpendicular flow solutions defined by Equations (274) and (140)

$\underline{U}$ = superficial velocity

$\underline{V}(\eta)$ = function of η

$\underline{V}_{\underline{f}}$ = volume of a fiber

$\underline{W}(\xi)$ = function of ξ

$\underline{X}_{\underline{A}}$, $\underline{X}_{\underline{E}}$ = factors in parallel flow velocity distributions defined by Equations (72) and (54)

$\underline{a}$ = radius of circular cylinder

$\underline{a}_{o}$, $\underline{b}_{o}$ = half-axes of solid elliptic cylinder's cross section

$\underline{a}_1$, $\underline{b}_1$ = half-axes of outer elliptic cylinder's cross section

$\underline{a}_{\underline{c}}$, $\underline{b}_{\underline{c}}$ = half-axes of ellipses describing surface of contact between two fibers

$\underline{b}$ = radius of virtual fluid surface in circular cell model

$\underline{c}$ = focal length of ellipse

$\underline{c}$ = consistency of a fiber mat

$\underline{c}_{o}$ = consistency of fiber mat in unloaded state

$\underline{d}_{\underline{e}}$ = effective fiber diameter

$\underline{d}_{\xi\xi}$, $\underline{d}_{\xi\eta}$ = components of rate of deformation tensor

$\underline{f}(\xi,\eta)$ = function of ξ and η

$\underline{f}$ = $\underline{n}/\underline{m}$ = ratio of transcendental functions in Finch analysis

$\underline{g}(\theta)$, $\underline{g}(\lambda)$ = frequency functions

$\underline{g}_{(\underline{x})}$, $\underline{g}_{(\underline{y})}$, $\underline{g}_{(\underline{z})}$ = functions of η in approximate solutions for the three flow problems

$\underline{h}$ = metric coefficient

$\underline{h}(\phi)$ = frequency function

$\underline{h}_1$, $\underline{h}_2$, $\underline{h}_3$ = metric coefficients for coordinates $\underline{q}_1$, $\underline{q}_2$, $\underline{q}_3$

$\underline{i}$ = $(-1)^{1/2}$ = imaginary factor

$\hat{\underline{i}}, \hat{\underline{j}}, \hat{\underline{k}}$ = unit vectors in directions $\underline{x}$, $\underline{y}$, and $\underline{z}$

$\hat{\underline{i}}_1, \hat{\underline{i}}_2, \hat{\underline{i}}_3$ = unit vectors in directions $\underline{q}_1$, $\underline{q}_2$, $\underline{q}_3$

$\hat{\underline{i}}_\xi, \hat{\underline{i}}_\eta$ = unit vectors in ξ and η directions

$\underline{j}$ = integer index

$\underline{k}$ = integer index

$\underline{k}$ = Kozeny factor

$\underline{k}_1, \underline{k}_2$ = constants in Davies and Ingmanson empirical correlations for Kozeny factor

$\underline{k}_{(\underline{p})}, \underline{k}_{(\underline{t})}$ = Kozeny factors for parallel and perpendicular (transverse) flow past cylinder

$\underline{k}_{(\underline{x})}, \underline{k}_{(\underline{y})}, \underline{k}_{(\underline{z})}$ = Kozeny factors for directional flow past elliptic cylinders

$\underline{k}'$ = quantity in contact area analysis defined by Equation (310)

$\underline{m}$ = hydraulic radius

$\underline{m}, \underline{n}$ = transcendental functions of auxiliary angle τ

$\underline{n}$ = $(5\delta^2/12)^{-1/2}$

$\underline{p}$ = hydrodynamic pressure

$\underline{p}_o$ = reference point pressure

$\underline{p}_f$ = compacting pressure on fiber mat

$\underline{p}_s$ = stress on solid fraction of mat

$\Delta\underline{p}$ = pressure drop

$\underline{q}_1, \underline{q}_2, \underline{q}_3$ = orthogonal curvilinear coordinates

$\underline{r}$ = radial distance coordinate

$\underline{r}$ = ratio of actual to expected Kozeny factor

$\underline{s}$ = distance along a curve

$\underline{s}$ = fiber distortion factor

$\underline{s}_1, \underline{s}_2, \underline{s}_3$ = distances along curves $\underline{q}_1$, $\underline{q}_2$, $\underline{q}_3$

$\underline{t}$ = fiber thickness

$\vec{t}_{(x)}$, $\vec{t}_{(y)}$ = quantities in perpendicular flow solutions defined by Equations (266) and (125)

$\vec{u}$ = velocity for flow past stationary cylinder

u_ξ, u_η = ξ and η components of velocity $\vec{u}$

$\vec{v}$ = fluid velocity for moving cylinder problem

$\bar{v}$ = mean velocity

v_1, v_2, v_3 = velocity components in directions q_1, q_2, q_3

v_r, v_θ = components of fluid velocity for perpendicular flow past circular cylinder

v_x, v_y, v_z = components of fluid velocity in x, y, z directions

v_ξ, v_η = components of fluid velocity for flow perpendicular to elliptic cylinder

w = projected fiber width

$w(\varepsilon)$ = weighting function

x, y, z = Cartesian coordinates

Δ = rate of deformation tensor

Λ = quantity in perpendicular flow solutions defined by Equation (143)

Π = stress tensor

$\Phi_{(x)}$, $\Phi_{(y)}$ = functions of η in perpendicular flow solutions

Ω = factor in perpendicular flow solutions defined by Equation (142)

α_0 = quantity defined by Equation (231)

α_1, α_2, α_3 = factors dependent on η in parallel flow approximate solution polynomial

α_2, α_3, α_4, α_5 = factors dependent on η in solution polynomial for flow perpendicular to elliptic cylinder along minor half-axis

β_0 = b_0/a_0 = axis ratio of solid ellipse

β_1 = b_1/a_1 = axis ratio of virtual ellipse in cell model

γ	$= \underline{k}\pi/(2\delta)$
γ_0	= mat compression parameter
γ_1, γ_2	= quantities in perpendicular flow solution defined by Equations (133) and (134)
δ	$= \xi_1 - \xi_0$
$\delta_{\underline{c}}$	= fraction of fiber surface area in contact with other fibers
ϵ	= porosity or void fraction
$\zeta_2, \zeta_3, \zeta_4, \zeta_5$	= factors dependent on η in solution polynomial for flow perpendicular to elliptic cylinder along major axis
θ	= angular cylindrical coordinate
θ	= angle between a fiber's central axis and the normal to the plane of the mat
κ	= quantity in contact area analysis defined by Equation (309)
λ	= eigenvalue
λ	= quantity in perpendicular flow solutions defined by Equation (126)
λ	= angle between central axes of two fibers in contact
μ	= dynamic viscosity of fluid
ν	$= (1-\epsilon)$ = solid fraction of a porous medium
ν	= Poisson's ratio
ξ, η	= confocal elliptic coordinates
ξ_0	= elliptic coordinate representing solid cylinder
ξ_1	= elliptic coordinate representing virtual fluid boundary
ρ	= fluid density
$\rho_{\underline{f}}$	= fiber density
σ	$= (\sinh \xi_0 - \tanh \xi_1 \cosh \xi_0)$
τ	= auxiliary angle
ϕ	= eigenfunction
ϕ	= angle between a fiber's major cross-sectional axis and plane of mat

ψ = stream function for flow past moving cylinder

$\psi^{(1)}$ = part of stream function that satisfies Laplace equation

$\psi^{(2)}$ = part of stream function from particular solution to Poisson equation

ψ_* = stream function for flow past stationary cylinder

ω = vorticity

$d/d\underline{x}$ = ordinary derivative

$\partial/\partial\underline{x}$ = partial derivative

∇ = nabla operator

∇^2 = Laplacian operator

∇^4 = biharmonic operator

LITERATURE CITED

1. Darcy, H. P. G. Les fontaines publiques de la ville de Dijon. Paris, Victor Dalamont, 1856.

2. Scheidegger, A. E. The physics of flow through porous media. Rev. ed. Toronto, University of Toronto Press, 1960.

3. Irmay, S., Trans. Am. Geophys. Union 39(4):702(1958).

4. Whittaker, S., Chem. Eng. Sci. 21(3):291-300(1966).

5. Carman, P. C., Trans. Inst. Chem. Engrs. (London) 15:150-66(1937).

6. Davies, C. N. Air filtration. New York, Academic Press, 1973.

7. Carman, P. C. Flow of gases through porous media. New York, Academic Press, 1956.

8. Bliesner, W. C. A study of the porous structure of fibrous sheets using permeability techniques. Doctor's Dissertation. Appleton, Wisconsin, The Institute of Paper Chemistry, 1963.

9. Han, S. T., Pulp Paper Mag. Can. 70(9):T134-46(1969).

10. Davies, C. N., Proc. Inst. Mech. Engrs. (London) B1:185(1952).

11. Ingmanson, W. L., Andrews, B. D., and Johnson, R. C., Tappi 42(10):840-9 (1959).

12. Carroll, C. W. Unpublished work. Appleton, Wisconsin, The Institute of Paper Chemistry, 1965.

13. Emersleben, O., Phys. Z. 26:601(1925).

14. Sparrow, E. M., and Loeffler, A. L., Jr., A.I.Ch.E. Journal 5(3):325-30 (1959).

15. Happel, J., and Brenner, H. Low Reynolds number hydrodynamics. New York, Prentice-Hall, Inc., 1965.

16. Hasimoto, H., J. Fluid Mech. 5:317-28(1959).

17. Happel, J., A.I.Ch.E. Journal 4(2):197-201(1958).

18. Kuwabara, S., J. Phys. Soc. Japan 14(4):527-32(1959).

19. Marmur, A., and Rubin, E., Ind. Eng. Chem. Fundam. 11(4):497-502(1972).

20. Happel, J., A.I.Ch.E. Journal 5(2):174-7(1959).

21. Kirsch, A. A., and Fuchs, N. A., Ann. Occup. Hyg. 10:23-30(1967).

22. Kirsch, A. A., and Fuchs, N. A., J. Phys. Soc. Japan 22(5):1251-5(1967).

23. Meyer, H. Unpublished work. Appleton, Wisconsin. The Institute of Paper Chemistry, 1969.

24. Fuchs, N. A., and Stechkina, I. B., Dokl. Akad. Nauk SSSR 147:1144-6(1962).

25. Pich, J., Ann. Occup. Hyg. 9:23-7(1966).

26. LeClair, B. P., and Hamielec, A. E., Ind. Eng. Chem. Fundam. 9(4):608-13 (1970).

27. El-Kaissy, M. M., and Homsy, G. M., Ind. Eng. Chem. Fundam. 12(1):82-90 (1973).

28. Iberall, A. S., J. Res. Natl. Bur. Stds. 45:398-406(1950).

29. Lamb, H. Hydrodynamics. 6th ed. London, Cambridge University Press, 1932.

30. Spielman, L., and Goren, S. L., Environ. Sci. Tech. 2(4):279-87(1968).

31. Brinkman, H. C., Appl. Sci. Res. A1:27(1947).

32. Kyan, C. P., Wasan, D. T., and Kintner, R. C., Ind. Eng. Chem. Fundam. 9(4):596-603(1970).

33. Clarenburg, L. A., and Piekaar, H. W., Chem. Eng. Sci. 23(7):765-71(1968).

34. Meyer, H., Tappi 54(9):1426-50(1971).

35. The Institute of Paper Chemistry. The status of the sheet-forming process: a critical review. Appleton, Wisconsin, 1965.

36. Farrar, N. O. Unpublished work. Appleton, Wisconsin. The Institute of Paper Chemistry, 1964.

37. Lord, E., J. Text. Inst. 46:T191-213(1955).

38. Onogi, S., and Sasaguri, K., Tappi 44(12):874-80(1961).

39. Labrecque, R. P. An investigation of the effects of fiber cross-sectional shape on the resistance to the flow of fluids through fiber mats. Doctor's Dissertation. Appleton, Wisconsin. The Institute of Paper Chemistry, 1967.

40. Epstein, N., and Masliyah, J. H., Chem. Eng. J. 3(2):169-75(1972).

41. Masliyah, J. H. Symmetric flow past orthotropic bodies: single and clusters. Doctor's Dissertation. Vancouver, B.C., University of British Columbia, 1970.

42. Masliyah, J. H., and Epstein, N., Ind. Eng. Chem. Fundam. 10(2):293-9 (1972).

43. Kuwabara, S., J. Phys. Soc. Japan 14(4):522-7(1959).

44. Nelson, R. W. Personal communcation, 1973.

45. Meyer, H. Personal communcation, 1973.

46. Elias, T. C. An investigation of the compression response of ideal unbonded fibrous structures by direct observation. Doctor's Dissertation. Appleton, Wisconsin. The Institute of Paper Chemistry, 1965.

47. Finch, R. B., Textile Res. J. 21(6):383-92(1951).

48. Hertz, H. R. "On the contact of rigid elastic solids and on hardness." Miscellaneous papers. p. 163-83. London, Macmillan Co., 1896.

49. Ingmanson, W. L., and Andrews, B. D., Tappi 46(3):150-5(1963).

50. Dyer, D. A. Doctoral thesis in progress. Appleton, Wisconsin. The Institute of Paper Chemistry, 1974.

51. Ciriacks, J. A. An investigation of the streaming current method for determining the zeta potential of fibers. Doctor's Dissertation. Appleton, Wisconsin. The Institute of Paper Chemistry, 1967.

52. Bird, R. B., Stewart, W. E., and Lightfoot, E. N. Transport phenomena. New York, John Wiley and Sons, Inc., 1960.

53. Wilder, H. D. The compression creep properties of wet pulp mats. Doctor's Dissertation. Appleton, Wisconsin. The Institute of Paper Chemistry, 1959.

APPENDIX I

CURVILINEAR REGRESSION OF LABRECQUE'S
EXPERIMENTAL KOZENY FACTORS

The pressure drop and flow rate data obtained by Labrecque (39) in his

permeation experiments through mats of synthetic nylon fibers of several

cross sections were converted into Kozeny factors. For these calculations,

the values for fiber density, specific surface, and cross-sectional area

were corrected for swelling in water, determined by Labrecque to be a 4.3%

diameter increase. Table VI lists the swollen values used to compute the

Kozeny factors.

TABLE VI

PROPERTIES OF LABRECQUE'S NYLON FIBERS

Axis Ratio	Swollen Density, g/cm^3	Swollen Specific Surface, cm^{-1}	Swollen Cross-Sectional Area, μm^2
1.00	1.103	1684	487
0.379	1.095	1944	480
0.243	1.142	2085	544
0.213	1.090	2259	537

A curvilinear regression analysis was performed using the calculated

Kozeny factors. Table VII presents the best-fit regression curves for this

data. Other information relevant to the regression is given in Table VIII.

TABLE VII

REGRESSION CURVES OF LABRECQUE'S EXPERIMENTAL
KOZENY FACTORS

Axis Ratio	Regression Equation
1.00	$k = 3.777 + 14.524(\varepsilon-0.70) - 2.717(\varepsilon-0.70)^2 - 82.248(\varepsilon-0.70)^3$
0.379	$k = 2.475 + 11.034(\varepsilon-0.60) + 2.981(\varepsilon-0.60)^2 - 43.517(\varepsilon-0.60)^3$
0.243	$k = 2.603 + 11.001(\varepsilon-0.60) + 5.356(\varepsilon-0.60)^2 - 21.715(\varepsilon-0.60)^3$
0.213	$k = 3.567 + 9.165(\varepsilon-0.60) - 3.983(\varepsilon-0.60)^2 - 6.074(\varepsilon-0.60)^3$

TABLE VIII

REGRESSION ANALYSIS INFORMATION

Axis Ratio	Porosity Range	R^2	SSW	TSS
1.00	0.498-0.847	0.92	4.87	63.65
0.379	0.344-0.800	0.90	5.28	51.53
0.243	0.364-0.809	0.92	4.74	56.38
0.213	0.274-0.781	0.88	12.10	99.17

Note: R = regression coefficient; SSW = sum of squares within regression; TSS = total sum of squares.

APPENDIX II

EQUATIONS OF CREEPING FLOW IN ORTHOGONAL CURVILINEAR COORDINATES
AND TRANSFORMATION RELATIONSHIPS WITH CARTESIAN COORDINATES

The steady creeping flow of an incompressible Newtonian fluid is described (52) by the equation of continuity

$$\nabla \cdot \vec{v} = 0 \tag{200}$$

and the equation of motion

$$\mu \nabla^2 \vec{v} - \nabla p = 0. \tag{201}$$

The creeping motion equation results from the steady-state Navier-Stokes equation by assuming that the inertial forces are negligible relative to the viscous forces, which is true for very slow flow. The velocity vector is

$$\vec{v} = \hat{i}_1 v_1 + \hat{i}_2 v_2 + \hat{i}_3 v_3 \tag{202}$$

which has components v_1, v_2, and v_3 in the direction of the unit vectors $\hat{i}_1$, $\hat{i}_2$, and $\hat{i}_3$ along the coordinate axes q_1, q_2, and q_3.

Happel and Brenner (15) in the appendix to their book describe in detail the usage of orthogonal curvilinear coordinate systems and the vector algebra associated with such systems. The following discussion presents some of the relationships pertinent to the analyses of this thesis.

The curvilinear coordinates are independent functions of position such that $q_1 = q_1(x,y,z)$, $q_2 = q_2(x,y,z)$, and $q_3 = q_3(x,y,z)$. The use of curvilinear coordinates requires the introduction of metric coefficients h_1, h_2, and h_3, defined as follows:

$$h_1 = \left| dq_1/ds_1 \right|, \qquad h_2 = \left| dq_2/ds_2 \right|, \qquad h_3 = \left| dq_3/ds_3 \right|, \tag{203}$$

where s_k is the distance along the coordinate curve q_k. In an orthogonal system in which x, y, and z are known explicitly in terms of q_1, q_2, and q_3, i.e., $x = x(q_1,q_2,q_3)$, etc., the metric coefficients are readily determined from the equation

$$1/h_k^2 = (\partial x/\partial q_k)^2 + (\partial y/\partial q_k)^2 + (\partial z/\partial q_k)^2, \quad k = 1,2,3. \quad (204)$$

Expressing the divergence of $\vec{v}$ in curvilinear coordinates, the equation of continuity becomes

$$\nabla \cdot \vec{v} = h_1 h_2 h_3 \left[\frac{\partial}{\partial q_1}\left(\frac{v_1}{h_2 h_3}\right) + \frac{\partial}{\partial q_2}\left(\frac{v_2}{h_3 h_1}\right) + \frac{\partial}{\partial q_3}\left(\frac{v_3}{h_1 h_2}\right) \right] = 0. \quad (205)$$

The gradient of a scalar, p, is

$$\nabla p = \hat{i}_1 h_1 (\partial p/\partial q_1) + \hat{i}_2 h_2 (\partial p/\partial q_2) + \hat{i}_3 h_3 (\partial p/\partial q_3). \quad (206)$$

The Laplace operator for a scalar function is

$$\nabla^2 = h_1 h_2 h_3 \left[\frac{\partial}{\partial q_1}\left(\frac{h_1}{h_2 h_3}\frac{\partial}{\partial q_1}\right) + \frac{\partial}{\partial q_2}\left(\frac{h_2}{h_3 h_1}\frac{\partial}{\partial q_2}\right) + \frac{\partial}{\partial q_3}\left(\frac{h_3}{h_1 h_2}\frac{\partial}{\partial q_3}\right) \right]. \quad (207)$$

The Laplacian of a vector function, $\vec{v}$, is

$$
\nabla^2 \vec{v} = \hat{i}_1 \left[\nabla^2 v_1 - (v_1/h_1)\nabla^2 h_1 \right.
$$

$$
+ (v_1/h_1)h_1\frac{\partial}{\partial q_1}(\nabla^2 q_1) + (v_2/h_2)h_1\frac{\partial}{\partial q_1}(\nabla^2 q_2) + (v_3/h_3)h_1\frac{\partial}{\partial q_1}(\nabla^2 q_3)
$$

$$
- 2h_1^2\frac{\partial h_1}{\partial q_1}\frac{\partial}{\partial q_1}(v_1/h_1) - 2h_2^2\frac{\partial h_1}{\partial q_2}\frac{\partial}{\partial q_1}(v_2/h_2) - 2h_3^2\frac{\partial h_1}{\partial q_3}\frac{\partial}{\partial q_1}(v_3/h_3)
$$

$$
\left. + h_1\frac{\partial h_1^2}{\partial q_1}\frac{\partial}{\partial q_1}(v_1/h_1) + h_1\frac{\partial h_2^2}{\partial q_1}\frac{\partial}{\partial q_2}(v_2/h_2) + h_1\frac{\partial h_3^2}{\partial q_1}\frac{\partial}{\partial q_3}(v_3/h_3) \right]
$$

$$+ \ldots \quad (208)$$

continuing in this manner for the components in the direction of $\hat{i}_2$ and $\hat{i}_3$. The equation of motion has three components, as follows:

In $\hat{\underline{i}}_1$ direction:

$$
\begin{aligned}
&- h_1(\partial p/\partial q_1) + \mu\left[\nabla^2 v_1 - (v_1/h_1)\nabla^2 h_1\right.\\
&+ \frac{v_1}{h_1} h_1 \frac{\partial}{\partial q_1}(\nabla^2 q_1) + \frac{v_2}{h_2} h_1 \frac{\partial}{\partial q_1}(\nabla^2 q_2) + \frac{v_3}{h_3} h_1 \frac{\partial}{\partial q_1}(\nabla^2 q_3)\\
&- 2 h_2{}^2 \frac{\partial h_1}{\partial q_2} \frac{\partial}{\partial q_1}\left(\frac{v_2}{h_2}\right) - 2 h_3{}^2 \frac{\partial h_1}{\partial q_3} \frac{\partial}{\partial q_1}\left(\frac{v_3}{h_3}\right)\\
&+ h_1 \frac{\partial h_2{}^2}{\partial q_1} \frac{\partial}{\partial q_2}\left(\frac{v_2}{h_2}\right) + \left. h_1 \frac{\partial h_3{}^2}{\partial q_1} \frac{\partial}{\partial q_3}\left(\frac{v_3}{h_3}\right)\right] = 0.
\end{aligned}
\tag{209}
$$

In $\hat{\underline{i}}_2$ direction:

$$
\begin{aligned}
&- h_2(\partial p/\partial q_2) + \mu\left[\nabla^2 v_2 - (v_2/h_2)\nabla^2 h_2\right.\\
&+ \frac{v_1}{h_1} h_2 \frac{\partial}{\partial q_2}(\nabla^2 q_1) + \frac{v_2}{h_2} h_2 \frac{\partial}{\partial q_2}(\nabla^2 q_2) + \frac{v_3}{h_3} h_2 \frac{\partial}{\partial q_2}(\nabla^2 q_3)\\
&- 2 h_1{}^2 \frac{\partial h_2}{\partial q_1} \frac{\partial}{\partial q_2}\left(\frac{v_1}{h_1}\right) \qquad\qquad - 2 h_3{}^2 \frac{\partial h_2}{\partial q_3} \frac{\partial}{\partial q_2}\left(\frac{v_3}{h_3}\right)\\
&+ h_2 \frac{\partial h_1{}^2}{\partial q_2} \frac{\partial}{\partial q_1}\left(\frac{v_1}{h_1}\right) \qquad\qquad + \left. h_2 \frac{\partial h_3{}^2}{\partial q_2} \frac{\partial}{\partial q_3} \frac{v_3}{h_3}\right] = 0.
\end{aligned}
\tag{210}
$$

In $\hat{\underline{i}}_3$ direction:

$$
\begin{aligned}
&- h_3(\partial p/\partial q_3) + \mu\left[\nabla^2 v_3 - (v_3/h_3)\nabla^2 h_3\right.\\
&+ \frac{v_1}{h_1} h_3 \frac{\partial}{\partial q_3}(\nabla^2 q_1) + \frac{v_2}{h_2} h_3 \frac{\partial}{\partial q_3}(\nabla^2 q_2) + \frac{v_3}{h_3} h_3 \frac{\partial}{\partial q_3}(\nabla^2 q_3)\\
&- 2 h_1{}^2 \frac{\partial h_3}{\partial q_1} \frac{\partial}{\partial q_3}\left(\frac{v_1}{h_1}\right) - 2 h_2{}^2 \frac{\partial h_3}{\partial q_2} \frac{\partial}{\partial q_3}\left(\frac{v_2}{h_2}\right)\\
&+ h_3 \frac{\partial h_1{}^2}{\partial q_3} \frac{\partial}{\partial q_1}\left(\frac{v_1}{h_1}\right) + \left. h_3 \frac{\partial h_2{}^2}{\partial q_3} \frac{\partial}{\partial q_2}\left(\frac{v_2}{h_2}\right)\right] = 0.
\end{aligned}
\tag{211}
$$

The need frequently arises to transform expressions from a curvilinear system to a Cartesian system, or vice versa. For this reason, some transformation relations are presented below. The partial differential operator $\partial/\partial \underline{x}$ equals the following:

$$\partial/\partial x = h_1{}^2(\partial x/\partial q_1)\ \partial/\partial q_1 + h_2{}^2(\partial x/\partial q_2)\ \partial/\partial q_2 + h_3{}^2(\partial x/\partial q_3)\ \partial/\partial q_3. \tag{212}$$

The operators $\partial/\partial \underline{y}$ and $\partial/\partial \underline{z}$ are similar. This expression operating on $\underline{q}_k$ yields

$$\partial q_k/\partial x = h_k{}^2(\partial x/\partial q_k), \quad k = 1,2,3. \tag{213}$$

The partial differential operators $\partial/\partial \underline{q}_k$ are obtained by applying the chain rule for partial differentiation,

$$\partial/\partial q_k = (\partial x/\partial q_k)\ \partial/\partial x + (\partial y/\partial q_k)\ \partial/\partial y + (\partial z/\partial q_k)\ \partial/\partial z,$$
$$k = 1,2,3. \tag{214}$$

The conversion of the components of a vector, $\vec{\underline{v}}$,

$$\vec{v} = \hat{i}v_x + \hat{j}v_y + \hat{k}v_z = \hat{i}_1 v_1 + \hat{i}_2 v_2 + \hat{i}_3 v_3 \tag{215}$$

from one system to another is performed with the aid of the following relationships:

$$v_k = h_k\left[v_x(\partial x/\partial q_k) + v_y(\partial y/\partial q_k) + v_z(\partial z/\partial q_k)\right],$$
$$k = 1,2,3 \tag{216}$$

$$v_x = v_1 h_1(\partial x/\partial q_1) + v_2 h_2(\partial x/\partial q_2) + v_3 h_3(\partial x/\partial q_3), \tag{217}$$

(likewise for v_y and v_z).

APPENDIX III

ELLIPTIC CYLINDRICAL COORDINATES AND RELATED PARAMETERS

The elliptic cylindrical coordinate system $(\xi, \eta, \underline{z})$ is an orthogonal curvilinear system related to the Cartesian coordinates by the transformation

$$x + iy = c \cosh(\xi + i\eta), \quad z = z \tag{218}$$

with $\underline{c}$, the focal length, greater than zero. The relationships

$$x = c \cosh \xi \cos \eta, \tag{219}$$

$$y = c \sinh \xi \sin \eta \tag{220}$$

are obtained by expanding the right side of Equation (218) and equating the real and imaginary parts. The ranges for ξ and η are $0 \leq \xi < \infty$ and $0 \leq \eta < 2\pi$. The metric coefficients $\underline{h}_1$, $\underline{h}_2$, and $\underline{h}_3$ for this coordinate system, determined according to Equation (204), are as follows:

$$h_1 = h_2 = h = \left[c(\sinh^2\xi + \sin^2\eta)^{1/2} \right]^{-1}$$

$$h_3 = 1. \tag{221}$$

Equations (219) and (220), upon elimination of η, yield

$$x^2/(c^2\cosh^2\xi) + y^2/(c^2\sinh^2\xi) = 1 \tag{222}$$

which describes a family of ellipses of $\xi = $ constant. The major and minor half-axes of an ellipse $\xi = \xi_0$ are

$$a_0 = c \cosh \xi_0, \tag{223}$$

$$b_0 = c \sinh \xi_0, \tag{224}$$

where $\underline{a}_0 > \underline{b}_0$. Combining these produces the relationship

$$a_0{}^2 - b_0{}^2 = c^2 \tag{225}$$

which demonstrates that all the ellipses ξ = constant are confocal, with foci at $\underline{x} = \pm \underline{c}$, $\underline{y} = 0$. Likewise the equation

$$x^2/(c^2\cos^2\eta) - y^2/(c^2\sin^2\eta) = 1 \tag{226}$$

describes a family of confocal hyperbolas, η = constant, which have the same foci as the ellipses and are normal to them. Define $\beta_0 = \underline{b}_0/\underline{a}_0$, and eliminate $\underline{c}$ from Equations (223) and (224) to obtain the relationship between ξ_0 and the half-axes

$$\xi_0 = \frac{1}{2} \ln[(1+\beta_0)/(1-\beta_0)]. \tag{227}$$

Turning now to the unit cell model of porous space, the two ellipses of the model defined by $\xi = \xi_0$ and $\xi = \xi_1$ have half-axes $\underline{a}_0$, $\underline{b}_0$, and $\underline{a}_1$, $\underline{b}_1$, respectively. The cell is related to the porosity of the assemblage of cylinders by observing that the ratio of the area of the inner ellipse to the area of the outer ellipse equals the solid fraction, $(1-\epsilon)$. Thus,

$$(a_0 b_0)/(a_1 b_1) = (1-\epsilon). \tag{228}$$

The relationship between porosity and the axis ratios β_0 and β_1, by using Equations (225) and (228), is found to be

$$(1-\beta_1{}^2)/\beta_1 = (1-\epsilon)(1-\beta_0{}^2)/\beta_0. \tag{229}$$

Solving for β_1,

$$\beta_1 = \left(\sqrt{1 + \alpha_0{}^2} - 1\right)/\alpha_0, \tag{230}$$

where

$$1/\alpha_0 = (1-\epsilon)(1-\beta_0{}^2)/(2\beta_0). \tag{231}$$

Expressions for $\sinh \xi_0$ and $\cosh \xi_0$ are obtained from Equations (223), (224), and (225), resulting in the following:

$$\cosh \xi_0 = a_0/c = 1/\sqrt{1-\beta_0^2}, \qquad (232)$$

$$\sinh \xi_0 = b_0/c = \beta_0/\sqrt{1-\beta_0^2}. \qquad (233)$$

From these,

$$\tanh \xi_0 = \sinh \xi_0/\cosh \xi_0 = \beta_0. \qquad (234)$$

Other relationships which are sometimes needed are as follows:

$$\xi_1-\xi_0 = \frac{1}{2} \ln\left(\frac{1+\beta_1}{1-\beta_1}\cdot\frac{1-\beta_0}{1+\beta_0}\right) \qquad (235)$$

$$\cosh 2\xi_0 = (1 + \beta_0^2)/(1 - \beta_0^2) \qquad (236)$$

$$\sinh 2\xi_0 = 2\beta_0/(1 - \beta_0^2) = \alpha_0(1-\varepsilon) \qquad (237)$$

$$\sinh 2\xi_1 = \alpha_0. \qquad (238)$$

The derivations of the above are fairly straightforward.

APPENDIX IV

ANALYSIS FOR PERPENDICULAR FLOW ALONG
THE MAJOR CROSS-SECTIONAL AXIS

The boundary value problem describing flow perpendicular to an elliptic cylinder along the major cross-sectional axis is stated in Equations (90), (94), (96), (179), and (180). The solution is developed in a manner similar to that presented in the text for flow along the minor cross-sectional axis.

The solution for ψ is stated as before:

$$\psi = \psi^{(1)} + \psi^{(2)} \tag{239}$$

$$\nabla^2 \psi^{(1)} = 0 \tag{240}$$

$$\nabla^2 \psi^{(2)} = -\omega/h^2 \tag{241}$$

$$\nabla^2 \omega = 0. \tag{242}$$

A general solution to Equation (240) is

$$\psi^{(1)} = \sum_{j=0}^{\infty} (a_j \sinh j\xi + b_j \cosh j\xi) \sin j\eta \tag{243}$$

while a general solution for ω is

$$\omega = \sum_{j=1}^{\infty} (A_j \sinh j\xi + B_j \cosh j\xi) \sin j\eta. \tag{244}$$

The sine function is chosen because the vorticity is maximum at $\eta = \pi/2$ and zero at $\eta = 0$. Using the zero vorticity condition on $\xi = \xi_1$, the expression becomes

$$\omega = B_{(x)} (\sinh \xi - \tanh \xi_1 \cosh \xi) \sin \eta. \tag{245}$$

The factor $\underline{B}_{(\underline{x})}$ will be determined later. Equation (239) calls for restating the boundary conditions:

$$\partial\psi^{(1)}/\partial\eta + \partial\psi^{(2)}/\partial\eta = Uc \sinh \xi \cos \eta \qquad \text{on } \xi = \xi_0 \qquad (246)$$

$$\partial\psi^{(1)}/\partial\xi + \partial\psi^{(2)}/\partial\xi = Uc \cosh \xi \sin \eta \qquad \text{on } \xi = \xi_0 \qquad (247)$$

$$\partial\psi^{(1)}/\partial\eta + \partial\psi^{(2)}/\partial\eta = 0 \qquad \text{on } \xi = \xi_1 \qquad (248)$$

$$\nabla^2\psi^{(2)} = 0 \qquad \text{on } \xi = \xi_1 \qquad (249)$$

Assume that

$$[\partial\psi^{(2)}/\partial\xi]_{\xi=\xi_0} = 0, \qquad (250)$$

$$[\partial\psi^{(2)}/\partial\eta]_{\xi=\xi_0} = 0. \qquad (251)$$

In Equation (243), the selection of $\underline{j} = 1$, $\underline{a}_{\underline{j}} = \underline{Uc}$, and $\underline{b}_{\underline{j}} = 0$ satisfies Equations (246) and (247), yielding

$$\psi^{(1)} = Uc \sinh \xi \sin \eta \qquad (252)$$

as the desired solution for $\psi^{(1)}$. Equation (248) gives

$$[\partial\psi^{(2)}/\partial\eta]_{\xi=\xi_1} = -Uc \sinh \xi_1 \cos \eta \qquad (253)$$

which, on integrating, becomes

$$[\psi^{(2)}]_{\xi=\xi_1} = -Uc \sinh \xi_1 \sin \eta \qquad (254)$$

where an integration constant of zero is chosen.

An approximate solution will be found for the Poisson equation,

$$\partial^2\psi^{(2)}/\partial\xi^2 + \partial^2\psi^{(2)}/\partial\eta^2 = -\omega/h^2. \qquad (255)$$

Integrating between ξ_0 and ξ_1, the result is

$$g_{(x)}(\eta) + \frac{d^2}{d\eta^2} \int_{\xi_0}^{\xi_1} \psi^{(2)} \, d\xi = - \int_{\xi_0}^{\xi_1} (\omega/h^2) \, d\xi, \tag{256}$$

where

$$g_{(x)}(\eta) = [\partial\psi^{(2)}/\partial\xi]_{\xi=\xi_1}. \tag{257}$$

A polynomial form for $\psi^{(2)}$ is assumed, as follows:

$$\psi^{(2)} = \zeta_2(\xi-\xi_0)^2 + \zeta_3(\xi-\xi_0)^3 + \zeta_4(\xi-\xi_0)^4 + \zeta_5(\xi-\xi_0)^5. \tag{258}$$

The ζ_i factors are functions of η. An additional condition is

$$[\partial^2\psi^{(2)}/\partial\xi^2]_{\xi=\xi_0} + [\partial^2\psi^{(2)}/\partial\eta^2]_{\xi=\xi_0} = - (\omega/h^2)_{\xi=\xi_0} \tag{259}$$

The conditions in Equations (249), (254), (257), and (259) are used to solve for the ζ_i factors, with the following results:

$$\zeta_2 = - B_{(x)}c^2\sin \eta \; (\sinh^2\xi_0 + \sin^2\eta) \; \sigma/2 \tag{260}$$

$$\zeta_3 = - Uc \sinh \xi_1\sin \eta \; (1/2 + 10/\delta^2)/\delta - 4g_{(x)}(\eta)/\delta^2 - 3\zeta_2/\delta \tag{261}$$

$$\zeta_4 = \; Uc \sinh \xi_1\sin \eta \; (1 + 15/\delta^2)/\delta^2 + 7g_{(x)}(\eta)/\delta^3 + 3\zeta_2/\delta^2 \tag{262}$$

$$\zeta_5 = - Uc \sinh \xi_1\sin \eta \; (1/2 + 6/\delta^2)/\delta^3 - 3g_{(x)}(\eta)/\delta^4 - \zeta_2/\delta^3. \tag{263}$$

Yet to be determined is $\underline{g}_{(x)}(\eta)$. The two integrals in Equation (256) are evaluated as follows:

$$\int_{\xi_0}^{\xi_1} \psi^{(2)} \, d\xi = - Uc \sinh \xi_1\sin \eta \; (\delta/2 + \delta^3/120)$$
$$- \delta^2 g_{(x)}(\eta)/10 + \delta^3\zeta_2/60, \tag{264}$$

$$\int_{\xi_0}^{\xi_1} (\omega/h^2) \, d\xi = B_{(x)}c^2[t_{(x)}\sin \eta + \lambda \sin^3\eta], \tag{265}$$

where

$$t_{(x)} = [\cosh^3\xi_1 - \cosh^3\xi_0 - \tanh\xi_1 (\sinh^3\xi_1 - \sinh^3\xi_0)]/3$$
$$- (\cosh\xi_1 - \cosh\xi_0) \qquad (266)$$

and λ is as defined in Equation (126). Introducing these into Equation (256) produces the differential equation

$$g_{(x)}''(\eta) - 10 g_{(x)}(\eta)/\delta^2 = \Phi_{(x)}(\sin\eta), \qquad (267)$$

where

$$\Phi_{(x)}(\sin\eta) = D_{(x)}\sin\eta + E_{(x)}\sin^3\eta \qquad (268)$$

$$D_{(x)} = Uc \sinh\xi_1 (5/\delta + \delta/12) + 10B_{(x)}c^2t_{(x)}/\delta^2$$
$$+ \delta B_{(x)}c^2\sigma(\sinh^2\xi_0-6)/12 \qquad (269)$$

$$E_{(x)} = 10 B_{(x)}c^2\lambda/\delta^2 + 3 \delta B_{(x)}c^2\sigma/4. \qquad (270)$$

The solution is

$$g_{(x)}(\eta) = - \delta^2\left[D_{(x)} + 6\delta^2E_{(x)}/(9\delta^2+10)\right](\sin\eta)/(\delta^2+10)$$
$$- \delta^2E_{(x)}(\sin^3\eta)/(9\delta^2+10). \qquad (271)$$

The parameter $B_{(\underline{x})}$ is determined as before from the biharmonic equation evaluated at $\xi = \xi_0$. After integration over η and solution for $B_{(\underline{x})}$, the result is

$$B_{(x)} = - G_{(x)}U/c \qquad (272)$$

$$G_{(x)} = - [R/T_{(x)}] \sinh\xi_1 \qquad (273)$$

$$T_{(x)} = \sigma T_2 - 60t_{(x)}\Omega/[\delta^3(\delta^2 + 10)]$$

$$+ 30 \lambda[(\Omega + 7/2)/\delta^2 + 12\Omega/(\delta^2 + 10)]/[\delta(9\delta^2 + 10)] \qquad (274)$$

$$T_2 = -\Lambda + 2\cosh 2\xi_0 - 3/4 + (1/4)\Omega(\cosh 2\xi_0 - 13)/(\delta^2 + 10)$$

$$+ 27\delta^2\Omega/[(\delta^2 + 10)(9\delta^2 + 10)] + (9/4)(\Omega + 7/2)/(9\delta^2 + 10) \qquad (275)$$

with $\underline{R}$, Ω, and Λ as previously defined.

The stream function, ψ_*, for the fluid moving past an immobile cylinder with a fixed reference system is determined in the following manner. The flow is described by

$$\vec{u} = \vec{v} - U\hat{i} \qquad (276)$$

where the components are

$$u_\xi = v_\xi - Uhc \sinh \xi \cos \eta, \qquad (277)$$

$$u_\eta = v_\eta + Uhc \cosh \xi \sin \eta. \qquad (278)$$

Define ψ_* in terms of $\underline{u}_\xi$ and $\underline{u}_\eta$:

$$u_\xi/h = \partial\psi_*/\partial\eta, \qquad u_\eta/h = -\partial\psi_*/\partial\xi. \qquad (279)$$

Solving for ψ_* yields

$$\psi_* = \int \partial\psi^{(2)}/\partial\eta \, d\eta = \psi^{(2)}. \qquad (280)$$

The drag force due to flow past the stationary cylinder is given by Equation (151). Using Equation (152) for the stress tensor, $\underset{\sim}{\Pi}$, and seeking only the x-component because it alone is nonzero, the drag force becomes

$$F_{(x)} = -\int_s p(\hat{i}_\xi \cdot \hat{i}) \, ds + 2\mu \int_s (\underset{\sim}{\Delta} \cdot \hat{i}_\xi) \cdot \hat{i} \, ds. \qquad (281)$$

As in the case of flow along the minor axis:

$$\mathbf{\Delta} \cdot \hat{i}_{\xi} = d_{\xi\eta} \hat{i}_{\eta}. \tag{282}$$

The unit vector dot products are

$$\hat{i}_{\xi} \cdot \hat{i} = hc \sinh \xi \cos \eta, \tag{283}$$

$$\hat{i}_{\eta} \cdot \hat{i} = - hc \cosh \xi \sin \eta. \tag{284}$$

The drag force now is

$$F_{(x)} = - c \sinh \xi \int_0^{2\pi} p \cos \eta \, d\eta - 2\mu c \cosh \xi \int_0^{2\pi} d_{\xi\eta} \sin \eta \, d\eta. \tag{285}$$

The pressure expression for this problem is developed from Equation (168) as before, but now the Laplacian of $\psi^{(2)}$ is

$$\nabla^2 \psi^{(2)} = - B_{(x)} \sin \eta \, (\sinh \xi - \tanh \xi_1 \cosh \xi)/h^2. \tag{286}$$

The pressure derivative is

$$\partial p / \partial \xi = - \mu B_{(x)} \cos \eta \, (\sinh \xi - \tanh \xi_1 \cosh \xi) \tag{287}$$

which is integrated to give

$$p = p_0 - \mu B_{(x)} \cos \eta \, (\cosh \xi - \tanh \xi_1 \sinh \xi). \tag{288}$$

Evaluation of $d_{\xi\eta}$ at $\xi = \xi_0$ produces

$$(d_{\xi\eta})_{\xi=\xi_0} = - B_{(x)} \sigma (\sin \eta)/2. \tag{289}$$

Performing the integration in Equation (285) and simplifying provides the drag force expression

$$F_{(x)} = - \pi \mu U G_{(x)} \tanh \xi_1. \tag{290}$$

Using the same method as before, the Kozeny factor for this flow problem is

$$k_{(x)} = \varepsilon^3 \beta_o G_{(x)} \tanh \xi_1 / [H^2(1-\varepsilon)]. \tag{291}$$

APPENDIX V

KOZENY FACTORS FROM THEORETICAL ANALYSES

TABLE IX

THEORETICAL KOZENY FACTORS FOR PARALLEL FLOW (EXACT SOLUTION)

Porosity	Axis Ratio				
	0.999	0.900	0.800	0.700	0.600
0.99	31.056	31.039	30.981	30.863	30.654
0.95	10.760	10.761	10.761	10.763	10.763
0.90	7.313	7.316	7.326	7.347	7.381
0.85	5.974	5.978	5.992	6.019	6.065
0.80	5.234	5.239	5.254	5.284	5.334
0.75	4.756	4.761	4.776	4.806	4.856
0.70	4.418	4.422	4.437	4.466	4.513
0.65	4.164	4.168	4.181	4.208	4.251
0.60	3.964	3.968	3.980	4.004	4.043
0.55	3.803	3.806	3.817	3.837	3.971
0.50	3.670	3.673	3.681	3.697	3.726

Porosity	Axis Ratio				
	0.500	0.400	0.300	0.200	0.100
0.99	30.300	29.697	28.625	26.573	22.084
0.95	10.757	10.737	10.674	10.490	9.886
0.90	7.433	7.507	7.605	7.700	7.579
0.85	6.136	6.240	6.382	6.543	6.562
0.80	5.411	5.523	5.675	5.851	5.994
0.75	4.933	5.043	5.192	5.377	5.651
0.70	4.586	4.690	4.833	5.032	5.433
0.65	4.318	4.415	4.553	4.774	5.288
0.60	4.102	4.192	4.329	4.578	5.188
0.55	3.924	4.007	4.147	4.426	5.117
0.50	3.772	3.851	3.998	4.307	5.064

TABLE X

THEORETICAL KOZENY FACTORS FOR PERPENDICULAR FLOW
ALONG MINOR AXIS

Porosity	Axis Ratio				
	0.999	0.900	0.800	0.700	0.600
0.99	54.141	54.830	55.569	56.361	57.215
0.95	20.377	20.717	21.073	21.437	21.801
0.90	14.202	14.500	14.813	15.138	15.473
0.85	11.731	12.025	12.340	12.675	13.038
0.80	10.342	10.644	10.974	11.336	11.747
0.75	9.434	9.749	10.101	10.497	10.967
0.70	8.785	9.117	9.494	9.931	10.469
0.65	8.294	8.645	9.051	9.533	10.147
0.60	7.907	8.279	8.716	9.248	9.944
0.55	7.593	7.987	8.458	9.043	9.828
0.50	7.332	7.749	8.256	8.897	9.778

Porosity	Axis Ratio				
	0.500	0.400	0.300	0.200	0.100
0.99	58.124	59.014	59.556	58.392	49.760
0.95	22.144	22.417	22.502	22.171	21.708
0.90	15.816	16.173	16.601	17.462	22.241
0.85	13.449	13.969	14.809	16.885	27.620
0.80	12.250	12.967	14.271	17.706	35.876
0.75	11.580	12.520	14.343	19.335	46.657
0.70	11.206	12.395	14.796	21.568	59.861
0.65	11.020	12.483	15.526	24.320	75.453
0.60	10.966	12.728	16.479	27.548	93.417
0.55	11.011	13.097	17.626	31.232	113.746
0.50	11.134	13.571	18.947	35.357	136.435

TABLE XI

THEORETICAL KOZENY FACTORS FOR PERPENDICULAR FLOW
ALONG MAJOR AXIS

	Axis Ratio				
Porosity	0.999	0.900	0.800	0.700	0.600
0.99	54.130	53.699	53.133	52.384	51.371
0.95	20.371	20.088	19.732	19.285	18.715
0.90	14.197	13.924	13.592	13.188	12.694
0.85	11.725	11.445	11.113	10.718	10.249
0.80	10.336	10.045	9.705	9.310	8.853
0.75	9.428	9.122	8.772	8.373	7.922
0.70	8.779	8.458	8.096	7.691	7.243
0.65	8.287	7.950	7.576	7.165	6.719
0.60	7.900	7.546	7.159	6.742	6.297
0.55	7.586	7.215	6.815	6.390	5.948
0.50	7.324	6.936	6.522	6.092	5.652

	Axis Ratio				
Porosity	0.500	0.400	0.300	0.200	0.100
0.99	49.954	47.889	44.696	39.359	29.367
0.95	17.976	16.991	15.635	13.678	10.656
0.90	12.083	11.322	10.361	9.133	7.585
0.85	9.692	9.031	8.255	7.371	6.505
0.80	8.326	7.730	7.076	6.416	5.976
0.75	7.417	6.870	6.308	5.816	5.672
0.70	6.756	6.249	5.765	5.407	5.480
0.65	6.248	5.777	5.359	5.111	5.350
0.60	5.841	5.403	5.043	4.888	5.258
0.55	5.505	5.098	4.791	4.716	5.189
0.50	5.223	4.844	4.585	4.580	5.136

APPENDIX VI

COMPUTER PROGRAM FOR CALCULATION OF DIRECTIONAL KOZENY FACTORS


```
C       KOZENY FACTOR CALCULATION -- ZERO VORTICITY MODEL
C       COMPOSITE KOZENY FACTORS--ELLIPTIC CYLINDERS
        DOUBLE PRECISION POR,BO,ALPHA,B1,DX,X,H,FK,P(501),SIGMA,AL,PIKSQ,
     1  COSHX1,COSHXO,SINHX1,SINHXO,SH2XO,CH2XO,XO,X1,TANHX1,DX1,DX9,
     2  SIG,ZLAM,TL,R,T1A,T1B,T1C,T1D,T1,T2,T3,T,   FAC1,FAC2,BRK,BR,
     3  TM,TA,TB,TC,TD,G1,G2,FK1,FK2,FKPAR,FKISO,FKCOS,FKEXP,FKAVG
        WRITE(6,101)
  101   FORMAT('OCOMPOSITE KOZENY FACTORS FOR CREEPING FLOW THROUGH   ')
        WRITE(6,102)
  102   FORMAT(' ', 9X,'ASSEMBLAGES OF ELLIPTIC CYLINDERS')
    5   READ(5,105)BO,POR1,NPORDL
  105   FORMAT(2F10.0,I3)
C       NPORDL = 1 FOR 0.001,10 FOR 0.01, 50 FOR 0.05, ETC.
        IF( BO )15,15,25
   25   WRITE(6,115)BO
  115   FORMAT('OBO = ',F6.3)
        WRITE(6,117)
  117   FORMAT('O  POR      K-PARL     K-PER1     K-PER2      K-ISO      K
     1-COS      K-EXP      K-AVG')
        NOPOR = (1 - POR1)*1000
        DO 10 L=1,NOPOR,NPORDL
        POR= POR1 + (L-1)*0.001
        ALPHA=2.0*BO/((1.-BO**2)*(1.-POR))
        B1=(DSQRT(1.+ALPHA**2)-1)/ALPHA
        DX=DLOG((1.+B1)*(1.-BO)/((1.-B1)*(1.+BO)))/2.0
        COSHX1=1/DSQRT(1.-B1**2)
        COSHXO=1/DSQRT(1.-BO**2)
        SINHXO=BO/DSQRT(1.-BO**2)
        SINHX1=B1/DSQRT(1.-B1**2)
        XO=0.5*DLOG((1+BO)/(1-BO))
        X1=0.5*DLOG((1+B1)/(1-B1))
        SH2XO= 2.*SINHXO*COSHXO
        CH2XO= 2.*SINHXO**2 + 1.
        TANHX1=B1
        PI = 3.1415926536
C       PARALLEL FLOW--ELLIPTIC CYLINDERS--EXACT SOLUTION
        SIGMA=0.0
        AL= 2.*DX
        KSIGN=1
        H=(3.+10.*BO+3.*BO**2)/(4.*(1+BO))
        DO 50 K=1,501,2
        PIKSQ=(PI*K)**2
        BRK= KSIGN*ALPHA+(K* PI  /(2.*AL))*((1+BO**2)/(1-BO**2))
        BR=0.500+(4.*AL**2/(PIKSQ+4.*AL**2))*BRK**2
        P(K)=2.*AL**3*BR/(PIKSQ*(PIKSQ+4.*AL**2))
        SIGMA=P(K)+SIGMA
        KSIGN=-1
        IF(P(K)-.000001)55,55,50
   55   MAXK=K
        GO TO 60
```

```
   50  CONTINUE
   60  FKPAR= (BO*POR  /(1-POR   ))**3/(H**2*SIGMA*(1-BO**2)**2)
C      PERPENDICULAR FLOW ALONG MAJOR AXIS OF ELLIPTIC CYLINDER
       DX1=DX**2+10.0
       DX9=9.0*DX**2+10.0
       SIG=SINHX0-TANHX1*COSHX0
       ZLAM= COSHX1-COSHX0-TANHX1*(SINHX1-SINHX0)
       TL= (COSHX1**3-COSHX0**3-TANHX1*(SINHX1**3-SINHX0**3))/3.
      1    - (COSHX1-COSHX0)
       R= CH2X0*(2.5*DX**4-60.*DX**2+900.)/(DX**4*DX1)
      1    + SH2X0*(DX**4-30.*DX**2+600.)/(DX**3*DX1)
       FAC1= 7.*CH2X0/DX + 4.*SH2X0
       FAC2= 10.*ZLAM + 0.75*SIG*DX**3
       T1= FAC1*(10.*TL+DX**3*SIG*(SINHX0**2-6.)/12.+6.*DX**2*FAC2/DX9)
       T2= (FAC1/2. + 1.75/DX)*FAC2
       T3= -(1.+18./DX**2)*SINHX0**4 - 18.*SINHX0**3*COSHX0/DX + 0.875
      1    - (2.+18./DX**2)*SINHX0**2 - 9.*SINHX0*COSHX0/DX - 6.75/DX**2
       T= 6.*T1/(DX**2*DX1) +6.*T2/(DX**2*DX9) - SIG*T3
       G1=SINHX1*R/T
       FK1 = -B1*POR**3*BO*G1/(H**2*(1.-POR))
C      PERPENDICULAR FLOW ALONG MINOR AXIS OF ELLIPTIC CYLINDER
       TM= (COSHX1**3-COSHX0**3-TANHX1*(SINHX1**3-SINHX0**3))/3.
      1    -TANHX1*(SINHX1-SINHX0)
       T1A= (3.-18./DX**2)*SINHXC**4 - 18.*SINHX0**3*COSHX0/DX -SH2X0**2
      1    + (6.-18./DX**2)*SINHX0**2 - 4.5*SH2X0/DX - 6.75/DX**2 + 3.125
       T1B= -1.75*SH2X0**2 - 45.5*SINHX0**2 - 24.5
      1    - 4.*DX*COSHX0**3*SINHX0 - 12.*DX*SH2X0
       T1C= 189.*DX**2*CH2X0 + 108.*DX**3*SH2X0
       T1D= 31.5*COSHX0**2 - 23.625 + 9.*DX*SH2X0
       TA= T1A + T1B/DX1 + T1C/(DX1*DX9) + T1D/DX9
       TB= -(240.*DX*SH2X0 +420.*CH2X0)/(DX**3*DX1)
       TC= (210.*CH2X0 + 120.*DX*SH2X0 - 105.)/(DX**3*DX9)
      1    + (2520.*CH2X0 + 1440.*DX*SH2X0)/(DX*DX1*DX9)
       TD=SIG*TA + TM*TB + ZLAM*TC
       G2=COSHX1*R/TD
       FK2 = POR**3*BO*G2/(H**2*(1.-POR))
C      COMPOSITE KOZENY FACTORS
       FKISO = 0.50*FKPAR + 0.25*(FK1 + FK2)
       FKCOS = FKPAR/3. + (FK1 + 2.*FK2)*2./9.
       FKEXP = 0.067*FKPAR + 0.109*FK1 + 0.824*FK2
       FKAVG = (FKPAR + FK1 + FK2)/3.
   10  WRITE(6,500)POR,FKPAR,FK1,FK2,FKISO,FKCOS,FKEXP,FKAVG
  500  FORMAT(' ',F6.3,7F11.3)
       GO TO 5
   15  STOP
       END
```

APPENDIX VII

DERIVATION OF COMPOSITE KOZENY FACTOR

Consider the flow past a fiber whose central axis makes an angle θ with the flow direction or the normal to the mat plane (see Fig. 20). The drag force, $\vec{F}$, is in the direction of $-\vec{U}$. The magnitude F is seen from Fig. 21 to be related to the components parallel to and perpendicular to the fiber's central axis, $F_{(z)}$ and $F_{(t)}$, respectively, by

$$F_{(z)} = F \cos \theta, \tag{292}$$

$$F_{(t)} = F \sin \theta. \tag{293}$$

Also, F is the sum of two parts, as follows:

$$F = F_{(t)} \sin \theta + F_{(z)} \cos \theta. \tag{294}$$

The drag force is proportional to the pressure drop, which in turn by the Kozeny-Carman equation at constant μ, ε, and m is proportional to $k \cdot U$. The drag force becomes

$$F \propto k \cdot U = k_{(t)} U_{(t)} \sin \theta + k_{(z)} U_{(z)} \cos \theta. \tag{295}$$

The velocity components are

$$U_{(t)} = U \sin \theta, \tag{296}$$

$$U_{(z)} = U \cos \theta. \tag{297}$$

The composite Kozeny factor is

$$k = k_{(t)} \sin^2 \theta + k_{(z)} \cos^2 \theta. \tag{298}$$
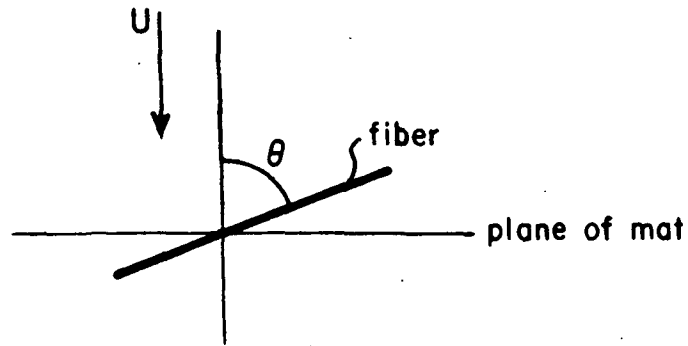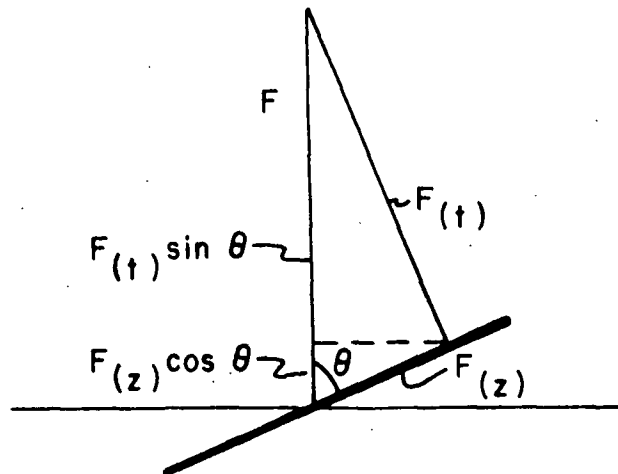
Figure 20. Flow Past a Fiber Within Mat

Figure 21. Resolution of Drag Force Into Parallel and
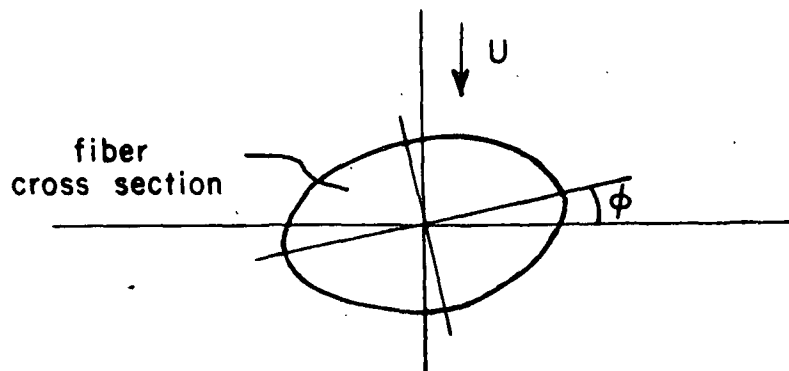Perpendicular Components

Figure 22. Perpendicular Flow Past a Fiber of Elliptic Cross Section

For a fiber of elliptic cross section, the perpendicular flow component depends on the orientation of the cross section relative to the flow direction. Define ϕ as the angle between the major cross-sectional axis of the cylinder and the plane of the mat, as shown in Fig. 22. The perpendicular drag component, as seen in Fig. 23, is equal to

$$F_{(t)} = F_{(x)}\sin\phi + F_{(y)}\cos\phi \qquad (299)$$

which as before yields the combined Kozeny factor expression

$$k_{(t)} = k_{(x)}\sin^2\phi + k_{(y)}\cos^2\phi \qquad (300)$$

The composite Kozeny factor for an elliptic cylindrical fiber mat is

$$k = [k_{(x)}\sin^2\phi + k_{(y)}\cos^2\phi]\sin^2\theta + k_{(z)}\cos^2\theta. \qquad (301)$$
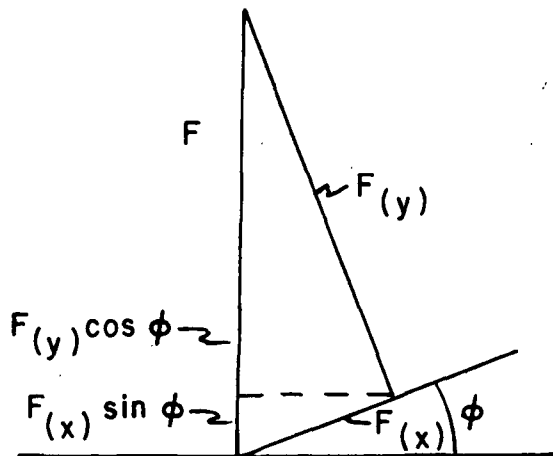

Figure 23. Resolution of Perpendicular Drag Force into Components Along Cross-Sectional Axes

APPENDIX VIII

ESTIMATION OF INTERFIBER CONTACT AREA

Consider a mat of solid fibers of elliptic cross section. An estimate
is desired of the fraction of the total fiber surface area in contact with
other fibers and, therefore, excluded from being passed by a permeating
fluid. The fibers have a cross-sectional area, A_f,

$$A_f = \pi\, a_o\, b_o,\tag{302}$$

where a_o and b_o are the major and minor semiaxes, respectively, of the
elliptic cross section. Assume that A_f and the fiber density, ρ_f, are in-
dependent of stress on the fiber. The fiber perimeter is $\pi a_o H$, where H is
defined by Equation (79). The geometric surface area for a fiber, A_o, is

$$A_o = \pi\, a_o\, H\, L_f\tag{303}$$

in which L_f is the fiber length. The fiber specific surface, S_v, as used in
the Kozeny-Carman equation is the ratio of wetted surface area, A_w, to
fiber volume, V_f:

$$S_v = A_w/V_f.\tag{304}$$

For a rigid fiber with true point contact with other fibers, the wetted area
and the geometric area are equal. But this is not so for a deformable fiber
since the fiber crossing points exclude some surface area from the fluid.
The wetted area is simply the geometric area minus the contact area, A_c:

$$A_w = A_o - A_c.\tag{305}$$

If the mat is under zero stress, there will be no deformation at the contacts, and $A_c = 0$; but this is not the practical case. The contact area for a fiber is

$$A_c = A_c' N_c \tag{306}$$

in which A_c' is the mean contact area per contact per fiber and N_c is the number of fiber-fiber contacts per fiber.

The mean contact area, A_c', can be predicted by means of an analysis by Finch (47). For the case of two curved isotropic elastic solids in contact, Finch derived expressions for the pressure distribution and the shape of the contact interface using as a theoretical basis the work of Hertz (48). The surface of pressure between the two solids is bounded by an ellipse of semiaxes a_c and b_c ($a_c > b_c$) defined by

$$a_c = m\kappa \tag{307}$$

$$b_c = n\kappa \tag{308}$$

$$\kappa = [(3/2)\pi F_N (k_1' + k_2')/(1/R_{11} + 1/R_{12} + 1/R_{21} + 1/R_{22})]^{1/3}. \tag{309}$$

In this expression F_N is the normal force pressing the two bodies together; k_1' and k_2' for each of the two solids are defined by

$$k' = (1 - \nu^2)/(2E), \tag{310}$$

where ν = Poisson's ratio and E = Young's modulus; R_{11} and R_{12} are the radii of curvature of one solid and R_{21} and R_{22} are for the other. The concern here is with two identical fibers in contact, for which $R_{11} = R_{21} = R$ and $R_{12} = R_{22} = \infty$. The expression for κ reduces to

$$\kappa = (3\pi F_N R k'/2)^{1/3}. \tag{311}$$

The factors $\underline{m}$ and $\underline{n}$ are transcendental functions of an auxiliary angle, τ, and are defined by

$$m^3 = 2/[\pi \sin^2(\tau/2)] \int_0^\infty [(1 + f^2 z^2)^3 (1 + z^2)]^{-1/2} \, dz \qquad (312)$$

$$n^3 = 2/[\pi \cos^2(\tau/2)] \int_0^\infty [(1 + z^2/f^2)^3 (1 + z^2)]^{-1/2} \, dz \qquad (313)$$

The parameter $\underline{f}$ is such that

$$f = b_c/a_c = n/m \qquad (314)$$

and is determined implicitly as a function of τ from

$$f^3 \cdot \frac{\displaystyle\int_0^\infty [(1 + f^2 z^2)^3 (1 + z^2)]^{-1/2} \, dz}{\displaystyle\int_0^\infty [(1 + z^2/f^2)^3 (1 + z^2)]^{-1/2} \, dz} = \tan^2(\tau/2). \qquad (315)$$

The area of contact, $\underline{A_c^*}$, is

$$A_c^* = \pi \, a_c \, b_c = \pi \, m \, n \, \kappa^2. \qquad (316)$$

The mean contact area, $\underline{A_c'}$, for two fibers crossing at an angle λ between their central axes is determined from the equation

$$A_c' = \int_0^{\pi/2} A_c^* \, g(\lambda) \, d\lambda. \qquad (317)$$

$\underline{A_c^*}$ of course is a function of λ. The frequency function $\underline{g}(\lambda)$ must be specified before $\underline{A_c'}$ can be calculated, and must satisfy

$$\int_0^{\pi/2} g(\lambda) \, d\lambda = 1. \qquad (318)$$

At $\lambda = 0$ the analysis breaks down, so the chosen $g(\lambda)$ must exclude $\lambda = 0$ as a possible crossing angle. The form

$$g(\lambda) = c_j \sin^j\lambda \qquad (319)$$

can be used, yielding for A_c',

$$A_c' = c_j \pi \kappa^2 I_j, \qquad (320)$$

$$I_j = \int_0^{\pi/2} m\, n\, \sin^j\lambda\, d\lambda. \qquad (321)$$

The integral I_j must be evaluated numerically. The frequency function

$$g(\lambda) = \sin \lambda \qquad (322)$$

seems like a reasonable choice. On calculation of the integral, the mean contact area becomes

$$A_c' = 1.159 \pi \kappa^2. \qquad (323)$$

The number of contacts per fiber is

$$N_c = L_f/L_s, \qquad (324)$$

where L_s is the segment length, or mean distance between contacts. The assumption that L_s is much less than L_f is made so that the fiber ends are neglected. The wetted surface area is

$$A_w = A_o - A_c = \pi a_o H L_f [1 - A_c'/(\pi a_o H L_s)]. \qquad (325)$$

Wilder (53) has correlated segment length and consistency, c, by assuming the relationship

$$L_s/L_{so} = (c_o/c)^{\gamma_o}, \qquad (326)$$

where L_{so} and c_o represent values for the unloaded mat. The theoretical analysis of Onogi and Sasaguri (38) provides the equation

$$c_o = \pi^2 A_f \rho_f/(4 L_{so} t),\tag{327}$$

where t is the fiber thickness. Since here the concern is with elliptic fibers assumed to be in contact with their major axes in the plane of the mat, $t = 2b_o$. This last equation is rewritten to give

$$L_{so} = \pi^3 a_o \rho_f/(8 c_o).\tag{328}$$

Using this and the Wilder equation,

$$L_s = \pi^3 a_o \rho_f (c_o/c)^{\gamma_o}/(8 c_o).\tag{329}$$

Inserting this into the equation for A_w yields

$$A_w = \pi a_o H L_f [1 - c_o(c/c_o)^{\gamma_o} A_c'/(H a_o^2 \pi^4 \rho_f)].\tag{330}$$

Convert to specific surface by dividing by $V_f = \pi a_o b_o L_f$:

$$S_v = S_{vo}[1 - (c/c_o)^{\gamma_o} A_c' (8 c_o)/(a_o^2 \pi^4 H \rho_f)],\tag{331}$$

where S_{vo} is the specific surface for zero contacts,

$$S_{vo} = H/b_o.\tag{332}$$

Introduce the porosity, ϵ,

$$c = \rho_f(1-\epsilon)\tag{333}$$

and assume that $\gamma_o = 1$. The specific surface becomes

$$S_v = S_{vo}[1 - 8 A_c' (1-\epsilon)/(\pi^4 a_o^2 H)].\tag{334}$$

Define δ_c as the fraction of S_{vo} lost due to interfiber contact:

$$S_v = S_{vo}(1 - \delta_c), \tag{335}$$

$$\delta_c = 8\,(1.159)\,\kappa^2\,(1-\varepsilon)/(\pi^3\,a_o^2\,H). \tag{336}$$

In Equation (311), expressions for F_N and R are needed. R is the radius of curvature at the point of contact, which for an ellipse is

$$R = a_o^2/b_o . \tag{337}$$

Real fibers do not have truly elliptic cross sections but oval ones instead whose R at the contact point is greater than that defined by Equation (337). Therefore, a distortion factor, s, is introduced:

$$R = s\,a_o^2/b_o. \tag{338}$$

The values for s for the fibers of Bliesner and Labrecque were estimated from the microphotographs of the fiber cross sections. Bliesner's fibers of axis ratios 1.00, 0.344, and 0.242 have s values of 1.0, 1.7, and 1.5, respectively; and s value of 1.0 was found for Labrecque's circular fibers and 1.2 for his noncircular fibers.

The normal force on a contact point, F_N, divided by the mean contact area equals the stress on the solid fraction of the mat, p_s:

$$p_s = F_N/A_c'. \tag{339}$$

The compacting pressure on the mat, p_f, is related to p_s by

$$p_s = p_f/(1-\varepsilon). \tag{340}$$

To eliminate p_f, introduce the Campbell equation for mat compressibility (35),

$$c = \rho_f(1-\epsilon) = M\, p_f^{\,N} \tag{341}$$

in which M and N are constants dependent on the mat. Thus,

$$F_N = A_c'\,(1-\epsilon)^{-1}\,[\rho_f(1-\epsilon)/M]^{1/N}. \tag{342}$$

For the choice $g(\lambda) = \sin\lambda$, $A_c' = 1.159\,\pi\,\kappa^2$, and

$$F_N = 1.159\,\pi\,\kappa^2\,(1-\epsilon)^{-1}\,[\rho_f(1-\epsilon)/M]^{1/N}. \tag{343}$$

Inserting these relationships for F_N and R into the κ equation, and then using it in the expression for δ_c produces the following:

$$\delta_c = 88.0\,k'^2\,s^2\,[\rho_f(1-\epsilon)/M]^{2/N}/[\beta_0^{\,2}H(1-\epsilon)]. \tag{344}$$

Replacing k' with Equation (310) yields

$$\delta_c = 22.0\,(1-\nu^2)^2\,s^2[\rho_f(1-\epsilon)/M]^{2/N}/[\beta_0^{\,2}E^2H(1-\epsilon)]. \tag{345}$$

This estimates the fraction of surface area excluded from the fluid due to interfiber contact, using as parameters the fiber properties (ν, E, ρ_f, s, β_0) as well as mat properties (ϵ, M, N).

The properties for Bliesner's experiments are summarized in Table XII. The calculated estimates of percentage contact area in Bliesner's mats are given in Table XIII. All properties except E and ν were determined from experimental data. The values of E were obtained from data for similar fibers (35), and the ν value was a guess.

TABLE XII

PROPERTIES OF BLIESNER'S FIBER MATS

Fiber	β_0	s	ρ_f, g/cm^3	M	N	E, dynes/cm^2	ν
Nylon	1.00	1.0	1.112	0.0103	0.229	3×10^9	0.35
Nylon	0.344	1.7	1.108	0.0140	0.247	3×10^9	0.35
Orlon	0.242	1.5	1.158	0.0130	0.200	3×10^{10}	0.35

TABLE XIII

ESTIMATES OF PERCENTAGE CONTACT AREA IN BLIESNER'S FIBER MATS

Porosity	Axis Ratio		
	1.00	0.344	0.242
0.90	1.0×10^{-6}	6.8×10^{-7}	2.0×10^{-6}
0.70	4.9×10^{-3}	1.7×10^{-3}	0.040
0.60	0.05	1.3×10^{-3}	0.53
0.50	0.25	0.06	3.93
0.40	1.04	0.23	20.3

For the nylon fibers used by Labrecque, β_0, ρ_f, and E were found from experimental data. The value of ν was assumed to be 0.35. The compressibility constant M for the circular fiber was estimated from the relationship (35)

$$M \propto E^{-0.24} \qquad (346)$$

which yields for two fibers

$$M_2 = M_1 \, (E_1/E_2)^{0.24}. \qquad (347)$$

Past work for a fiber with $E = 3 \times 10^9$ dynes/cm^2 has found that $M = 0.0104$; since Labrecque's fibers have $E = 2.7 \times 10^8$ dynes/cm^2, M is calculated to be

0.0185. But this is not valid for noncircular fibers. Assume $\underline{M}$ is inversely related to β_o by

$$M_2/M_1 = (\beta_{o1}/\beta_{o2})^\gamma. \tag{348}$$

From Bliesner's data, γ is approximately 0.287 and the oval fiber $\underline{M}$ values can be estimated. $\underline{N}$ is assumed independent of the axis ratio. Table XIV presents the values for the properties of Labrecque's fiber mats. Contact area estimates are given in Table XV.

TABLE XIV

PROPERTIES OF LABRECQUE'S FIBER MATS

Axis Ratio	$\underline{s}$	ρ_f, g/cm^3	$\underline{M}$	$\underline{N}$	$\underline{E}$, dynes/cm^2	ν
1.00	1.0	1.103	0.0185	0.225	2.7×10^8	0.35
0.379	1.2	1.095	0.0244	0.225	2.7×10^8	0.35
0.243	1.2	1.142	0.0278	0.225	2.7×10^8	0.35
0.213	1.2	1.091	0.0288	0.225	2.7×10^8	0.35

TABLE XV

ESTIMATES OF PERCENTAGE CONTACT AREA IN LABRECQUE'S FIBER MATS

Porosity	Axis Ratio			
	1.00	0.379	0.243	0.213
0.90	9.1×10^{-7}	1.1×10^{-6}	1.4×10^{-6}	9.4×10^{-7}
0.70	5.3×10^{-3}	6.4×10^{-3}	8.3×10^{-3}	5.5×10^{-3}
0.60	0.051	0.062	0.081	0.053
0.50	0.30	0.36	0.47	0.31
0.40	1.26	1.53	1.98	1.29